STUDY OF ELECTRICAL AND STRUCTURAL PROPERTIES OF METAL AND SEMI-METAL THIN FILMS

by

AJAY KUMAR

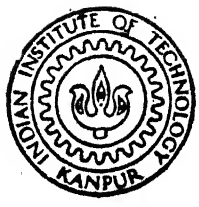

DEPARTMENT OF PHYSICS
INDIAN INSTITUTE OF TECHNOLOGY KANPUR
SEPTEMBER, 1989

STUDY OF ELECTRICAL AND STRUCTURAL PROPERTIES OF METAL AND SEMI-METAL THIN FILMS

A Thesis Submitted
in Partial Fulfilment of the Requirements
for the Degree of

DOCTOR OF PHILOSOPHY

by

AJAY KUMAR

to the

DEPARTMENT OF PHYSICS
INDIAN INSTITUTE OF TECHNOLOGY KANPUR
SEPTEMBER, 1989

CERTIFICATE

This is to certify that work presented in this thesis entitled 'STUDY OF ELECTRICAL AND STRUCTURAL PROPERTIES OF METAL AND SEMIMETAL THIN FILMS' by Ajay Kumar has been carried out under my supervision and it has not been submitted elsewhere for a degree.

O.P. Katyal

O.P. Katyal
Department of Physics
Indian Institute of Technology
Kanpur, India

September 1989.

ACKNOWLEDGEMENTS

It is a great pleasure to express my gratitude to Dr. O.P. Katyal for his guidance, constant help, and encouragement in matters both academic and otherwise, throughout the course of this work.

My sincere thanks are due to Professors Y.R. Waghmare and R.K Ray for their valuable suggestions and keen interest in the progress of my research work.

My thanks are also due to Professors R. M. Singru, R. Ramachandran, S.C. Agarwal, R.C. Srivastava, Jitendra Kumar, and V. A. Singh for encouraging me and taking interest in the progress of my research work.

I am also thankful to Dr. P.T. Rajagopalan, DMSRDE-Kanpur and Dr. C. Suryanarayana, Dept. of Metallurgical Engineering, B.H.U. Varanasi, for the work of electron microscopy of samples.

My sincere thanks are due to Drs. D.S. Misra, Shailendra Kumar, and Gyanesh Chandra for various helpful discussions and suggestions at different stages of this work.

I am also thankful to my friends Drs. J. Govind Rajan, D.S. Pandey, and Messrs Ramesh, Ranjit, Amit, U.V. Singh, Sanjay Gupta, Umesh, R.K. Pandey and many

others who helped in more than one ways and made my stay at I.I.T. Kanpur a memorable pleasure.

I thank Mr. H.N. Nigam and his associates of Physics Department, Mr. J.S. Sharma and his associates of Physics Workshop, and Mr. Sampat Singh and his associates of Liquid Nitrogen Plant for being helpful throughout the course of this work.

I thank Mr. Ghanshyam Rao Hoshing for his excellent typing and Mr. J.C. Verma for tracing the figures.

The work carried out here would not have been possible without the emotional support and constant encouragement from my family. I wish to expres my profound regards to my parents.

Ajay Kumar

TABLE OF CONTENTS

LIST OF FIGURES

Figure Page

Figure Page

LIST OF TABLES

SYNOPSIS

STUDY OF ELECTRICAL AND STRUCTURAL PROPERTIES OF METAL AND SEMIMETAL THIN FILMS

Ajay Kumar
Department of Physics
Indian Institute of Technology, Kanpur

August 1989

When thickness of a metal film becomes comparable to the mean free path of conduction electrons, due to the surface scattering of electrons the electrical transport properties of the metal are modified. This modification is called the size effect. The size effect studies of metal films have been the subject of many research because these studies provide the tests for the transport theories and also offer the convenient methods of determining bulk fundamental parameters such as mean free path, concentration and mobility of the carriers etc. Due to size effect and high concentration of lattice defects in a thin metal film, the resistivity of the film becomes higher than that of the bulk metal. The theory of electrical conductivity of a film developed by Fuchs and extended by Sondheimer deals with the phenomena of isotropic background scattering and surface scattering of charge carriers. Mayadas and Shatzkes (MS) developed a theory of electrical resistivity of polycrystalline metal film which also takes

into account the effect of grain boundary scattering on the film resistivity. Another model which considers the effect of grain boundary scattering on the film resistivity was proposed by Pichard, Tellier and Tosser (PTT model). In this PTT model the electrical resistivity has been calculated for a polycrystalline film when three types of electron scatterings i.e. background, grain boundary and external surface scattering, are simultaneously operative. The electrical resistivity of polyvalent metal films has been the subject of many investigations. In the present study the effect of grain boundary scattering on the film resistivity has been studied in tin (Sn), lead (Pb) and tin-lead (SnPb) alloy films. The size effect in temperature coefficient of resistivity (TCR) has been studied for polycrystalline Sn and Pb films at room temperature. In semimetals (antimony and bismuth) mean free path is large, therefore, these materials are appropriate to judge the adequation of various conduction models. In the present work, the structural and electrical properties of antimony (Sb) and bismuth (Bi) films have been studied. The applicability of different models such as Mayadas, Pichard et al. etc. has been tested on the experimental results.

The Chapter I reviews the various useful models of electrical resistivity of metal films and the experimental

work reported on the electrical properties of tin, lead, tin-lead alloy, antimony and bismuth films.

The Chapter II gives the details of experimental techniques used in the present work. The Sb and Bi films were thermally evaporated onto the glass substrate in a vacuum better than 10^{-5} torr. For this purpose a vacuum coating unit (Hind Hivac model 12A4) was used. The rate of evaporation was about 1 nm/sec. The deposition of Sb films was carried out at substrate temperature of 350K, while for the deposition of Bi films, the substrate was kept at room temperature. During the deposition the thickness was controlled by a quartz crystal monitor and then it was measured by optical method. The resistivity measurements were made in situ using a four probe method over a temperature range 150 to 350K. The four silver electrodes were used as electrical contacts. Extra care was taken to eliminate any thermoelectric voltage by reversing the direction of current for each measurements. During the measurements, the temperature of the substrate was varied by a cold finger, filled with liquid nitrogen and fitted with a heater at the bottom near the substrate. The temperature was measured by a copper-constantan thermocouple fixed rigidly on the substrate. For the measurement of resistance of the Bi films at 77K, the film was immersed directly in the liquid nitrogen and the resistance was recorded. The structural and grain size

studies of Sb and Bi films were made using Scanning Electron Microscopes (JEOL JSM-35 C.F. and PHILIPS PSEM 500) and X-ray diffractometer (ISO-DEBYEFLEX 2002D).

The Chapter IIIA presents the experimental results and discussion on the grain boundary resistivity of polycrystalline Sn, Pb and SnPb alloy films. Using the Matthiessen's rule the experimental value of grain boundary resistivity ρ_g have been calculated with specularity parameter p = 0 from the experimental results on resistivity of Chandra and Katyal for Sn, Pb and SnPb alloy films. The grain boundary resistivity increases with the decreasing grain size D. At different temperatures (175 and 300 K) the experimental results on ρ_g of Sn and Pb films are found to be consistent with MS model and PTT model. Both grain boundary models (MS and PTT) give almost the same results on ρ_g. In SnPb alloy film total resistivity is the weighted sum of two resistivities of constituents. Using the approximate form of MS resistivity equation, an expression for the grain boundary resistivity has been developed in terms of resistivities of constituent films. At 200 and 300K, the experimental results on ρ_g of SnPb alloy films are found to be consistent with this grain boundary resistivity equation. In polycrystalline Sn, Pb, and SnPb alloy films, the film resistivity is mainly contributed by grain boundary scattering. The Chapter IIIB presents the results on

temperature coeffricient of resistivity (TCR) of Sn and Pb films and discussion of the results. The TCR of Sn and Pb films exhibits the size effect. The thickness dependence of TCR can be successfully explained with the help of TCR model of Pichard et al.

The experimental results of the present study of Sb and Bi films are given and discussed in Chapter IV. Both Sb and Bi films are polycrystalline having grains whose size increases with the thickness. The values of bulk resistivity are found by the application of Fuchs model. In case of Sb films, experimental results on grain boundary resistivity ρ_g are found to be consistent with the MS and PTT grain boundary model at 150, 225 and 300K. The degree of agreement of the experimental results with the theoretical curves i.e. MS and PTT, is satisfactory to the same extent. The experimental results on total resistivity of Sb films agree well with the theoretical curves of three dimensional model of Pichard et al.(PTT) at different temperatures. The reflection coefficient R is about 0.135-0.176 while the transmission coefficient t is about 0.82-0.877 for Sb films. The resistivity of bismuth films decreases with the increasing temperature. This type of behaviour arises as a result of competition between temperature dependences of carrier density and carrier mobility. In Bi films, the charge carrier concentration increases with the decrease of thickness. This variation

of carrier concentration with thickness has been estimated theoretically from the presence of surface states. To include this thickness dependence of carrier densities, the conductivity equations have been modified. The results on ρ_g at different temperatures are found to be consistent with the modified PTT model. Similarly, the experimental results on total film resistivity of Bi films at 77, 150, and 300K agree well with the modified Pichard et al. model (PTT). The values of specularity parameter p for Sb and Bi films are 0.49 and 0.43 respectively. The specularity parameter is temperature independent.

Finally, the conclusion of the present work is given in Chapter V. The electrical resistivity of polycrystalline metal films can be explained completely by three dimensional model of Pichard et al.

INTRODUCTION

Because of their potential technical value and scientific curiosity in the properties of two dimensional solid, thin films have been extensively studied for over a century. Initially sufficient technological progress had not been made to give the reasonable scientific confidence to thin film research. But the developments in the last decade have made, directly or indirectly significant contributions to many areas of basic and applied solid state research. Epitaxial growth, size limited electron and phonon transport processes in metals, semiconductors and insulators, quantum mechanical tunneling through normal metal- insulator junction and micromagnetics are some of the noteworthy contributions of thin film phenomena to solid state physics. The technical interests which stimulated these studies have also been rewarded in form of useful inventions such as active and passive devices, solar cells, radiation sources, detectors, magnetic memory devices, and cryotrons. Evaporation and sputtering are the two physical methods, commonly used for the preparation of thin films.

Thin films are most commonly prepared by the condensation of atoms from the vapour phase of materials. The growth of film at substrate occurs in a sequential way. This growth process may be distinguished by four stages. Randomly distributed three dimensional nuclei are first formed to approach a saturation density with a small amount

of deposite. These nuclei grow to form observable islands. Then these islands increase their size by further deposition and come closer to each other; the larger ones appear to grow by coalescence of smaller ones. This disappearance of small islands is quite rapid. In third stage when the island distribution reaches a critical state, a rapid large scale coalescence of islands results in a connected network structure and the islands are flattened to increase surface coverage. The network contains a large number of empty channels. Finally with further deposition the filling of empty channels occurs due to secondary nucleation and the film becomes continuous. Thus according to the growth stage a film may be island type, porous type, and continuous. Each stage has the influence on the thin film properties. The properties of thin films also depend on preparation methods and conditions.

Thin metal films having small thermal capacity and fast response time are finding increasing application in detection of laser pulses.[1,2] The applications of thin metal and alloy films, particularly in the field of microelectronics, are of great importance. Some suitable metallic alloy films are used as thermogenerators.[3] The electrical and structural properties of metal films and metallic alloy films are the subject of many research. Because of surface scattering of carriers in the film of thickness comparable with the mean free path, the

electrical transport properties of metals are modified.[4] This modification is called the size effect. These size effect studies have provided the tests for transport theories and have also offered convenient methods of determining bulk-fundamental parameters such as the concentration and mobility of the carriers, the mean free paths and their temperature and energy dependence for electron-phonon and electron-electron scattering, surface scattering coefficient and Fermi surface topology. A variety of new phenomena of basic importance has emerged from these studies like size dependent specular scattering of electrons in metal films, thickness dependent oscillatory variation of the transport properties in semimetals due to the size quantization of energy levels etc.

The improvement in the vacuum technology and deposition procedures have led to a good degree of control, due to which fundamental research on metal films is continuing to have a better understanding of the solid state behaviour of thin metals. In the present work, tin (Sn), lead (Pb), tin-lead alloy, antimony (Sb), and bismuth (Bi) films have been studied due to following reasons. The Sn and Pb films are used as corrosion preventing coatings because they are highly resistant to stress corrosion cracking and service failure is rare. The metal film such as Pb, Sn, Bi films etc., can be used for the detonation of

high explosive.[5] The Pb and Sn films are also used in testng the corrosion of rocket propulsion fuels. These Pb and Sn metals are important for basic research. These are polyvalent metals having a complicated Fermi surfaces. The applicability of various conduction models[6-12] can be tested for these metal films. Chaudhuri et al.[13] concluded that experimental results of Pb films were in good agreement with the Lucas model[12] with diffuse scattering. Stolecki et al.[14,15] found that size effect in polycrystalline Sn films was consistent with the Wissmann model.[9]

The tin-lead alloy which generates a moderately low thermo e.m.f. relative to copper is useful in the production assembly of components onto printed circuit boards. The use of SnPb alloy as soldering material has been extended to highly sensitive electronic circuits where large D.C. voltage gain is required. Ghosh et al.[16] have studied the resistivity behaviour of SnPb alloy in the temperature range 70°C to 100°C.

In the present study the effect of grain boundary scattering on the film resistivity has been studied in Sn, Pb and SnPb alloy films. The thickness dependence of temperature coefficient of resistivity (TCR) of Sn and Pb films at room temperature has been described with the help of Pichard et al. model.[11] For this study, the required experimental data has been used from the reference 17.

The electronic properties of semimetals (group V elements such as antimony, bismuth etc) are of particular interest. These materials have high carrier mobilities, small effective masses, and non-parabolic energy-momentum relations. Due to these properties these materials are of great experimental interest both for device applications and for studies of wide range of physical phenomena. In thin film state these materials exhibit anomalous but interesting transport properties. In semimetals (Sb and Bi), mean free path is comparatively large so these materials are appropriate to judge the adequation of various models of electronic conduction in thin films. Semimetal bismuth is the best material to study the quantum size effects, because due to its Low Fermi energy, its deBroglie wavelength is appreciably larger. Furthermore by alloying these materials the energy gap can be varied, thereby making possible the production of materials to desired band gap specifications.[18] Numerous investigations have been carried out on the transport properties of these materials with a number of contradictions. The aim of the present work is to study the electrical conduction phenomena in thin semimetal Sb and Bi films at different temperatures. The applicability of different models has been explored on the experimental results.

REFERENCES

1. G.W. Day, D.L. Gaddy, and R.J. Iverson, Appl. Phys. Lett. 13, 289 (1968).
2. A. Olivei, J. Phys. Appl. D8, 561 (1975).
3. G. Abowitz, V. Klints, M. Levy, E. Lancaster, and A. Mountuala, Semicond. Prod. 8, 18 (1965).
4. K.L. Chopra, Thin Film Phenomena (McGraw Hill, New York, 1969) p.4.
5. L.C. Yang, J. Appl. Phys. 45, 2601 (1974).
6. K. Fuchs, Proc. Cambridge. Philos. Soc. 34, 100 (1938).
7. E.H. Sondheimer, Adv. Phys. 1, 1 (1952).
8. A.F. Mayadas and M. Shatzkes, Phys. Rev. B1, 1382 (1970).
9. P. Wissmann, Thin Solid Films 5, 329 (1970).
10. C.R. Pichard, C.R. Tellier, and A.J. Tosser, Thin Solid Films 62, 189 (1979).
11. C.R. Pichard, C.R. Tellier, and A.J. Tosser, Phys. Status Solidi (a) 65, 327 (1981).
12. M.S.P. Lucas, J. Appl. Phys. 36, 1632 (1965).
13. S. Chaudhuri and Arun K. Pal, J. Phys D 8, 1311 (1975).
14. B. Stolecki, F. Warkusz, A. Borodziuk-Kulpa, and C. Wesolowska, J. Mater. Sci. 14. 1349 (1979).
15. B. Stolecki, A. Borodziuk-Kulpa, and C. Wesolowska, Thin Solid Films 56, 299 (1979).

16. C.K. Ghosh and A.K. Pal, Ind. J. Phys. 55A, 193 (1981).

17. Gyanesh Chandra, Ph.D. Thesis, Indian Institute of Technology, Kanpur (1985).

18. D.L. Carter and R.T. Bate, Phys. of Semimetals and Narrow Gap Semiconductors (Pergamon Press, New York, 1971) p.3.

CHAPTER I

ELECTRICAL RESISTIVITY OF THIN METAL FILMS

The resistivity in metals arises due to the collisions of conduction electrons with vibrating lattice atoms (phonons), impurities and defects.[1] In case of thin metal films when the film thickness becomes comparable to the mean free path of conduction electrons, the film boundaries impose a geometrical limitation on the mean free path of conduction electrons. Therefore, in thin films, due to the additional collisions of the electrons with the film surface, the electrical resistivity becomes high. Thomson[2] was first who postulated the concept of surface scattering. According to Thomson model, the electrical conductivity of a film is written as

$$\frac{\sigma_F}{\sigma_o} = \frac{1}{2} K \left[\ell n \left(\frac{1}{K} \right) + \frac{3}{2} \right] \qquad (1.1)$$

where $K = \frac{d}{\ell_o}$

σ_F = Conductivity of metal film

σ_o = Conductivity of bulk metal

ℓ_o = Mean free path of the conduction electron in bulk

d = Film thickness.

The serious objection to this model is that the film conductivity σ_F does not approach bulk conductivity σ_o in equation (1.1) as $K \longrightarrow \infty$. Thomson had considered the free

path of one electron and integrated to obtain the mean value. However, since all electrons in the film are not identical to one another, all electrons must be considered to calculate the average value. The statistical distribution of ℓ_o in the bulk is necessary to formulate a satisfactory model. Fuchs[3] proposed a theory of electric conduction in thin metal films. In this model a spherical Fermi surface and an isotropic mean free path were considered. The conduction electrons were assumed to be diffusely scattered at the surface and the electrical conductivity expression was given as

$$\frac{\sigma_F}{\sigma_o} = 1 - \frac{3}{2K} \int_1^\infty \left[\frac{1}{t_1^3} - \frac{1}{t_1^5} \right] \left[1 - e^{-Kt_1} \right] dt_1 \quad (1.2)$$

where $t_1 = (\text{Cos}\theta)^{-1}$

Equation (1.2) can be approximated for convenience as

$$\frac{\sigma_F}{\sigma_o} = 1 - \frac{3}{8K} \quad \text{or} \quad \frac{\rho_F}{\rho_o} = 1 + \frac{3}{8K} \quad \text{for } K >> 1 \quad (1.3)$$

$$\frac{\sigma_F}{\sigma_o} = \frac{3}{4} K \left(\ell n \frac{1}{K} \right) \quad \text{for } K << 1 \quad (1.4)$$

where ρ_F = Resistivity of the metal film

ρ_o = Resistivity of the bulk metal.

When scattering is not diffuse, a specularity parameter p was introduced, p gives the fraction of the

electrons which is scattered elastically (specular) from the film surfaces while the remainders are diffusely scattered. A generalized form of conductivity of thin film was given by Sondheimer[4,5] as

$$\frac{\sigma_F}{\sigma_o} = 1 - \frac{3}{2K}(1-p)\int_1^\infty \left(\frac{1}{t_1^3} - \frac{1}{t_1^5}\right)\frac{1-\exp(-Kt_1)}{1-p\exp(-Kt_1)}\,dt_1 \qquad \ldots(1.5)$$

The limiting forms of equation (1.5) for relatively thick and thin films can be written as

$$\frac{\sigma_F}{\sigma_o} = 1 - \frac{3}{8}\frac{(1-p)}{K} \qquad K >> 1 \qquad (1.6)$$

$$\frac{\sigma_F}{\sigma_o} = \frac{3K}{4}\frac{(1+p)}{(1-p)}\ell n\left(\frac{1}{K}\right) \qquad K << 1 \qquad (1.7)$$

Since the interfaces on the two sides of the film surface are not same, therefore, specularity parameter is likely to be different for either surfaces. Using Fuchs method, Juretschke[6] and Lucas[7,8] derived the conductivity of thin film with unlike surfaces characterized by specularity parameters p and q as

$$\frac{\sigma_F}{\sigma_o} = 1 - \frac{3}{4K}\int_1^\infty \left(\frac{1}{t_1^3} - \frac{1}{t_1^5}\right)\frac{1-e^{-Kt_1}}{1-pqe^{-2Kt_1}} \times [2-p-q + (p+q-2pq)e^{-Kt_1}]\,dt_1 \qquad (1.8)$$

For thick and thin films this conductivity expression can be approximated as

$$\frac{\sigma_F}{\sigma_o} = 1 - \frac{3}{8K}\left(1 - \frac{p+q}{2}\right) \qquad K >> 1 \qquad (1.9)$$

and

$$\frac{\sigma_F}{\sigma_o} = \frac{3}{4}\frac{(1+p)\ (1+q)}{(1-pq)} K\ \ell n\ (\frac{1}{K}) \qquad K <<1 \qquad (1.10)$$

The temperature coefficient of resistivity (TCR) β_F($= \frac{1}{\rho_F}\frac{d\rho_F}{dT}$) depends on parameter K ($= \frac{d}{\ell_o}$) of the film. The limiting expression for the temperature coefficient of resistivity β_F of the film may be written as

For thick film K >> 1 $$\frac{\beta_F}{\beta_o} = 1 - \frac{3}{8}\frac{(1-p)}{K} \qquad (1.11)$$

For thin film K << 1 $$\frac{\beta_F}{\beta_o} = \frac{1}{\ell n\ \frac{1}{K} + 0.423} \qquad (1.12)$$

where β_o= Temperature Coefficient of resistivity (TCR) of bulk metal.

An alternative expression for the Fuchs-Sondheimer (FS) function was proposed by Cottey[9] who considered only continuous metal films with smooth parallel surfaces. Cottey assumed that bulk and surface scatterings are taking place independently and bulk mean free path of conduction electrons is independent of position, film thickness, and direction of motion of electrons. The Cottey function describing the size effects in conductivity is written as[9]

$$F(\mu) = \frac{\sigma_F}{\sigma_o} = \frac{3}{2}\mu\left[\mu - \frac{1}{2} + (1-\mu^2)\,\ell n\,(1+\mu^{-1})\right] \qquad (1.13)$$

where $$\mu = \frac{d}{\ell_o(1-p)} \qquad (1.14)$$

It has been found[10] that Cottey formulation agrees with FS model within 8%. However, Tellier et al.[11] has pointed out that using

$$\mu = K\left[\ell n \frac{1}{p}\right]^{-1} \qquad (1.15)$$

instead of equation (1.14), leads to satisfactory results (deviation less than 4%) in the larger K and p ranges.

In nearly all instances, it has been observed that single crystal films show a lower resistivity than the corresponding polycrystalline films. The polycrystalline films have also a resistivity contribution due to the scattering of conduction electrons from the grain boundaries. To consider the effect of grain boundary scattering on the conductivity of the film Mayadas and Shatzkes (MS)[12] presented a model. The MS model postulates that only the grain boundaries perpendicular to the electric field are the main additional contributors to the resistance. In this model, the total resistivity of a polycrystalline film including isotropic background scattering, grain boundary scattering,and external surface scattering, is given as

$$\frac{\rho_F}{\rho_g} = \left[1 - \frac{A}{G(\alpha)} \right]^{-1} \qquad (1.16)$$

where $A = \frac{6}{\pi K} (1-p) \int_0^{\pi/2} d\phi \int_1^{\infty} \frac{\cos^2\phi}{H^2(t_1,\phi)} \left[\frac{1}{t_1^3} - \frac{1}{t_1^5} \right]$

$$x \frac{1-\exp\left[-Kt_1 H(t_1, \phi)\right]}{1-p \exp\left[-Kt_1 H(t_1,\phi)\right]} dt_1 \qquad (1.17)$$

with

$$H(t_1,\phi) = 1 + \alpha(\cos\phi)^{-1} \left[1 - \frac{1}{t_1^2} \right]^{-1/2}$$

ρ_g, which represents the resistivity due to both isotropic background scattering and grain boundary scattering, is connected to the bulk resistivity ρ_o by the relation

$$\frac{\rho_o}{\rho_g} = G(\alpha) = 1 - \frac{3}{2}\alpha + 3\alpha^2 - 3\alpha^3 \ln\left(1 + \frac{1}{\alpha}\right) \qquad (1.18)$$

where $\alpha = \frac{\ell_o R}{D(1-R)}$

R = Reflection coefficient of conduction electrons at the grain boundaries

D = Average grain diameter

ϕ and t_1 = Integration Variables.

The equation (1.16) obtained by Mayadas and Shatzkes is non-analytic and complicated and for comparison with the

experimental results, numerical solutions are necessary. To make the MS theory more practicable, approximate linearized expressions have been derived. Thieme and Kirstein[13] obtained a simple analytic expression for the resistivity of a polycrystalline metal film which is written as

$$\rho_F = \rho_o \left[1 + \frac{3}{2}\alpha + \frac{3}{8}\frac{(1-p)}{K} \right] \qquad (1.19)$$

A similar equation has also been obtained by Dobierzewska et al.[14] They have found that film resistivity, under the condition that film is not very thin ($\mu > 1$) and grain boundary scattering is not very strong ($\alpha < 1$), is the sum of resistivities due to phonons and defects (ρ_o), due to surface scattering (ρ_s) and due to grain boundary scattering (ρ_{gb}) in accordance with Matthiessen's rule. The total film resistivity ρ_F is given as

$$\rho_F = \rho_o + \frac{3}{2}\alpha\rho_o + \frac{3}{8}\frac{\rho_o}{\mu}$$

$$= \rho_o + \frac{3}{2}\frac{\rho_o \ell_o R}{(1-R)D} + \frac{3}{8}\frac{\rho_o \ell_o (1-p)}{d} \qquad (1.20)$$

$$= \rho_o + \rho_{gb} + \rho_s \qquad (1.21)$$

with

$$\mu = \frac{d}{\ell_o (1-p)}$$

The approximation given by Wedler and Wissmann[15] also

leads to the similar expression as given by equation (1.20).

In contrast, phenomenological theories have been proposed by Warkusz[16-18] and Pichard et al.,[11,19-22] to consider the effects of grain boundary scattering on the electrical resistivity of films. In these theories, the conductivity characteristics are described by algebraic expressions. These models are based on more realistic physical models of the grain structure of the films. The three dimensional model of Pichard et al.[11,19,21] (PTT model) considers the effect of grain boundary scattering on the electrical properties of polycrystalline film through a simple probability calculation.

In this three dimensional PTT model, grain boundaries in polycrystalline films can be represented by three arrays of mutually perpendicular planar potentials. The average effect of grain boundary is represented by a specular transmission coefficient t which gives the fraction of electrons whose velocity in the electric field direction is not altered by the grain boundary, whereas the remainder electrons are diffusely scattered and do not contribute to the current.[19,21] In this model, the resistivity ρ_g due to both isotropic background scattering and grain boundary scattering, is expressed as [19,23]

$$\frac{\sigma_g}{\sigma_o} = \frac{\rho_o}{\rho_g} = \frac{3}{2}\ \frac{\nu}{1-C}\ \left[\ \gamma - \frac{1}{2} + (1-\gamma^2)\ \ell n\ (1+\gamma^{-1})\ \right] \qquad (1.22)$$

with

$$\gamma = \frac{\nu + C^2}{1-C} \quad ; \qquad C = \frac{4}{\pi}$$

and

$$\nu = \frac{D}{\ell_o} \left[\ell n \frac{1}{t} \right]^{-1} \tag{1.23}$$

whereas in thin polycrystalline films in which three types of electron scatterings (background, grain boundary, and external surface scattering) are simultaneously operative, the total electrical conductivity σ_F takes the simple analytical form[22,23]

$$\frac{\sigma_F}{\sigma_o} = \frac{3}{2b} \left[a - \frac{1}{2} + (1-a^2)\, \ell n\, (1+a^{-1}) \right] \tag{1.24}$$

with

$$b = \mu^{-1} + \nu^{-1}\,(1-C) \tag{1.25}$$

$$a = (1+C^2\nu^{-1})b^{-1} \tag{1.26}$$

and

$$\mu = \frac{d}{\ell_o} \left[\ell n \frac{1}{p} \right]^{-1} \tag{1.27}$$

This conductivity expression given by equation (1.24) is also valid for monocrystalline or columnar film provided that b is replaced by b_2 given by[20,24]

$$b_2 = \mu^{-1} - C\nu^{-1} \tag{1.28}$$

Recently, it has been pointed out that by using[25,26]

$$\nu = \frac{D}{\ell_o} \frac{(1+t)}{2(1-t)} \tag{1.29}$$

$$\mu = \frac{d}{\ell_o} \frac{(1+p)}{2(1-p)} \tag{1.30}$$

instead of definitions of ν and μ given by equations (1.23) and (1.27), the range of validity of electrical resistivity expressions can be extended to the whole experimental domain. For relatively high values of t and p, the more covenient definitions of ν (equation 1.23) and μ (equation 1.27) are also valid.[26] Thus, whatever be the film structure and its electrical state, equation (1.24) can be used for describing the electrical conductivity of metal films.

The behaviour of electrical conductivity and galvanomagnetic coefficients of thin metal films have been the subject of many investigations. Because the study of these properties is the main source of information on the behaviour of charge carriers. The previous studies made on lead (Pb) films were mainly concerned with its nucleation and growth properties[27,28] and its properties at liquid helium temperatures.[29-37] Aleksandrov[38] studied the size effect in ultra thin lead films at low temperatures. The transport properties of vapour deposited lead films have been studied in the low temperature region by Morgner et

al.[39] They have pointed out that in addition to the scattering of electrons on the external boundaries, scattering at grain boundaries also occurs. Tsalyy[40] has reported the effect of temperature on electron diffraction peaks for lead films and he determined Debye temperature θ at 300K as 59K, 69K and 77K for film thicknesses 90, 200 and 300 Å respectively. Chaudhuri et al.[41] have studied the electrical resistivity and temperature coefficient of resistivity (TCR) of lead films in a temperature range 30 to 150°C. They concluded that experimental results were in good agrement with Lucas model and scattering at both the surface was completely diffused. The values of $\ell_o(1-p)$ as obtained from ρ_F vs $\frac{1}{d}$ and β_F vs. $\frac{1}{d}$ plots were 46.0 nm and 42.6 nm respectively. The Fermi surface area was calculated as 1.683×10^6 cm^{-2}. Murakami[42] studied the thermal strain and effect of different substrates on thermal strain in Pb film. G. Chandra[43] have studied the structural and electrical properties of Pb films. He found that lattice parameter increased with decreasing film thickness. He also found that MS model was consistent with the experimental results on resistivity of Pb films. The dependences of the electrical resistivity and of its temperature coefficient on thickness, grain size, temperature,and annealing treatments were determined for lead films deposited on a liquid helium cooled substrate by Belevtsev et al.[44] The experimental data were interpreted on the basis of theories of Mayadas et al.(MS)[12] and of

Tosser et al.[45] They concluded that theory of Tosser et al. provides a better interpretation of the experimental results. B.K. Sarma et al.[46] have investigated the effects of annealing on the electrical resistivity of vacuum deposited lead films.

The previous investigations on tin films were carried out mainly to study its super conducting properties at liquid helium temperature[47-51] and its nucleation and growth properties.[52] At low temperature a study on size effect of Sn film was made by Niebuhr.[53] The experimental results were fitted well to the Fuchs theory. The value of mean free path and specularity parameter were estimated as 55.0 nm and 0.69 respectively. Pal et al.[54] have studied the electrical resistivity and TCR of Sn films in the temperature range 30 to 150°C. They concluded that MS theory reproduced the experimental observations more faithfully than F.S. theory. The values of term $\ell_o(1-p)$ from ρ_F vs $\frac{1}{d}$ and β_F vs $\frac{1}{d}$ plots were found to be 31.5 nm and 27.0 nm respectively. A comparatively high value of bulk resistivity ρ_o at room temperature for Sn films was extrapolated as 45.8 $\mu\Omega$ cm. The growth of tin films under electron microscope was examined by Malhotra.[55] He found that the grain size increased with the thickness of the film. The electrical properties and effect of annealing on electrical properties of polycrystalline tin films evaporated onto cold substrate were studied by Stolecki

et al.[56,57] They have found that film resistivity and TCR are the function of film thickness and annealing temperature. With increasing film thickness, annealing temperature, and annealing rate, the resistivity decreases and TCR is increased. Wissmann model was found to be consistent with the experimental data. They have concluded that grain boundary scattering is considerable and it also depends on both the annealing temperature and annealing rate. Patel et al.[58] studied the effects of the substrate (NaCl, KCl, KBr and KI) and substrate temperature (28-90^{o}C) on the crystallinity of tin films and found that crystallites of film deposited on KBr were more preferentially oriented than those deposited on NaCl, KCl or KI. Saif et al.[59] studied the structural, electrical, and optical properties of thin Sn films. The Sn films were polycrystalline in nature whose grain size increased with the film thickness. The experimental results on resistivity were fitted with the MS model. From the theoretical formula, the mean free path, mobility, and concentrations of conduction electrons were calculated in thin films. Varghese et al.[60] have reported a study of effect of gold, silver, tin, and aluminium electrodes on the electrical properties of tin films. They found that percentage variation in resistance was less for gold and silver electrode films and large for tin and aluminium electrode films. In case of Sn films, De et al.[61] have observed that thermoelectric power varies linearly with

temperature in temperature range 30 to 100°C. Temperature dependence of size effect in thin tin films in a temperature range 77 to 450K was studied by Angadi et al.[62] They found that with diffuse scattering FS theory explains the experimental results only in high thickness region. For R = 0.1, it was found a good agreement between the MS theory and experimental results. Pichard et al.[63] have reported the effect of grain boundary scattering on the TCR of thin tin films. It was observed that the effects of grain boundary were not temperature dependent from 65 to 140K. Recently, Chandra et al.[64] have studied the electrical properties of polycrystalline tin films in a temperature range 150 to 350K. They have observed that average grain size increases with the thickness linearly and resistivity and TCR exhibit the size effects. From ρ_F vs $\frac{1}{d}$ and β_F vs $\frac{1}{d}$ plots, they calculated the values of ℓ_o (1-p) equal to 43.6 nm and 34.0 nm respectively. The extrapolated bulk resistivity of Sn at 300K was found 12.6 $\mu\Omega$ cm. The electrical resistivity was found to be consistent with the Wissmann model for R = 0.60 and p = 0.

The tin-lead (SnPb) alloy is used as soldering material and it is also useful in high sensitive electronic circuits where large DC gain is needed. Ghosh et al.[65] have studied the electrical resistivity and TCR of SnPb alloy films. They have compared the experimental results on electrical resistivity and TCR with the values

calculated by assuming coexistence of two phases in the alloy. Chandra and Katyal[66] have tested the applicability of Mayadas model on the electrical resistivity of polycrystalline SnPb alloy films. By assuming that alloy film resistivity can be written as the weighted average of resistivities of the components (Sn, Pb), a theoretical expression from MS model was derived for the resistivity of alloy film. It was found that this theoretical equation with R = 0.92 and p = 0 reproduced the experimental results.

The transport properties of group V elements (Sb, Bi etc) have drawn the attention of many researchers and there have been extensive investigations on the thin films of these semimetals. There are two types of size effects observable in thin films - the classical and quantum size effects. The quantum size effect appears when film thickness becomes comparable to the de Broglie wavelength of the conduction carriers. At this thickness electronic energy states become discrete, resulting in oscillations in transport properties as a function of thickness with a period nearly equal to one half of the carrier wavelength. Komnik et al.[67,68] have observed quantum oscillation in antimony films. Leverton et al.[69] have reported measurements of Hall coefficient and resistivity of Sb films. Colombani et al.[70] have studied the transport properties of antimony films and found that film of

thickness smaller than 90 nm exhibited the size effect. The growth mechanism and structure of thin Sb films have been investigated by many authors.[71-74] The classical size effect in electrical properties of Sb films was studied by Barua et al.[75] The thickness dependence of electrical resistivity of Sb films deposited in oil pumped and ion pumped evaporators was studied by Maki[76] who found that films with thickness greater than 20 nm showed no size dependence. Horikoshi et al.[77] reported the observations in close agreement with those of Maki. The temperature dependence of conductivity, Hall coefficient, thermoelectric power (TEP), classical and quantum size effects in thin antimony films in the thickness range 15 to 800 nm were studied by Paprocki et al.[78] By using tunnel spectrometry techniques, the energy band edges along the trigonal axis were determined. From the experimental results they have estimated the mean free path of the carriers at 77K and specularity parameter p equal to 700 nm and 0.8 respectively. Pal et al.[79] have measured the electrical resistivity and TCR of polycrystalline Sb films in Situ. Recently, Deschacht et al.[80-84] have done an extensive study of electrical properties of thin antimony films. They investigated the effect of grain boundary scattering on the electrical conductivity both theoretically and experimentally and found excellent agreement between the theoretical and experimental results.[80] The experimental results on TEP and TCR of

polycrystalline Sb films[82] have been successfully explained by using a modified form of MS model[13] and assuming unequal hole and electron concentrations. These authors[82] derived an expression for the resistivity of an infinitely thick polycrystalline semimetal films using MS model and found a good agreement with the experimental results of Sb films. Deschacht et al.[83] have tested the applicability of new conductivity equations of thin films grown in a columnar fashion, proposed by Tellier et al.[24] The same group[84] also derived an expression for TCR in polycrystalline semimetal film by taking into consideration the influence of internal size effects on film resistivity in terms of MS function, thermal strains and the difference in the thermal expansion coefficients between the film and its substrate. They found a good agreement between the theoretical equations and experimental results in the temperature range 77 to 500K over a grain size range 30 to 200 nm, for antimony films of 200 nm thickness. The electrical resistivity of bismuth and antimony films deposited onto glass substrate at a pressure of 10^{-10} torr in a temperature range 20 to 500K was studied by Pariset.[85] He found that crystal size could be kept constant with increasing thickness by using appropriate heat treatments and epitaxial technique. The experimental results of Sb films were in good agreement with approximate form of FS and MS size effect theories. The specularity parameter p was greater than 0.7. Pal et al.[86] have reported the

measurements on the electrical and galvanomagnetic properties of Sb films in situ. The values of $\ell_o(1-p)$ obtained from ρ_F vs $\frac{1}{d}$ and β_F vs $\frac{1}{d}$ plots were 51 nm and 60 nm respectively. The bulk resistivity ρ_o and bulk TCR β_o were found to be 70 $\mu\Omega$ cm and 2.4 x $10^{-3}K^{-1}$ respectively. They observed that MS model with specularity parameter p = 0 and grain boundary reflection coefficient R = 0.15, reproduced the experimental results. The influence of preparative technique on the structural and galvanomagnetic properties of thin antimony films was systematically investigated by Mojejko et al.[87] They observed that it was possible to obtain antimony films of structure similar to that of single crystal over a broad range of the substrate temperatures (T_s = 50 to 110°C). From the experimental data on Sb films deposited at a substrate temperature T_s = 50 to 110°C, the values of ρ_o and $\ell_o(1-p)$ were calculated as 55 $\mu\Omega$ cm and 300 nm at 293K respectively. The results were analysed on the basis of FS and MS theories. They concluded that surface scattering was almost diffuse (p = 0 - 0.15) and grain boundary scattering was 16% - 25% specular. According to Akhtar et al.[88] the thickness dependence of both the electrical resistivity and the thermoelectric pwer for Sb and Bi films could be described by using FS theory. The values of ρ_o and $\ell_o(1-p)$ for Sb were obtained as 49 $\mu\Omega$ cm and 73 nm respectively.

The semimetal bismuth has comparatively large mean

free path and its conduction electrons have large de Broglie wavelength, small effective mass and low Fermi energy. Due to these properties, bismuth is best material to study the quantum size effect (QSE). Several authors have studied QSE in the Bi films.[89-96] In bismuth, the mean free path of the electron is large thus classical size effect (CSE) can be observed at larger thickness even at room temperature. Kaidanov et al.[97] have investigated the effect of thickness on the electrical properties of bismuth films in a temperature range -190 to +150^{o}C. They have found that as thickness decreases, the resistivity increases and Hall effect and the resistivity change due to magnetic field decrease. The electrical properties of Bi films were studied by A. Colombani et al.[98] Galvanomagnetic effect of evaporated Bi films in a temperature range 77 to 293K were reported by Sawatari et al.[99] They concluded that thickness dependence of resistivity was mainly due to the change of mean free path and of carrier concentrations with thickness. These authors observed that negative TCR was due to the difference in temperature dependence of the mobility between the bulk and thin film. Newman and Kao[100] investigated the dependence of conductivity on grain size of Bi films and found that scattering at grain boundary was the primary cause of decrease in the conductivity in Bi films. The electrical transport properties of well ordered, twinned Bi films between 1.15 and 300K were

studied by Hoffman et al.[101]. At 300K, the experimental results were fitted roughly with F.S theory with p = 0.60 but at low temperature the results could not be explained by F.S theory and p was found to be negative. This indicates that there exists an additional size dependent and temperature dependent scattering mechanism. At low temperatures, quantum oscillations were observed in all of the transport properties of thin Bi films. A more faithful study of bismuth films was reported by Garcia et al.[102] They have studied the thickness dependence of resistivity, Hall coefficient, and magnetoresistance, by gradually varying the thickness of a single film, which was kept under high vacuum during the entire experiment. They have concluded that infinite potential well model with boundary condition that wavefunction (ψ) vanishes at the surface, does not explain the experimental resuslts on Hall effect. On using the boundary condition that $\nabla\psi = 0$, the experimental results on Hall coefficient were found to be consistent with the theory. Subotowicz et al.[103] measured the classical (CSE) and quantum size effect (QSE) in thin Bi films. The results were fitted with F.S theory for p = 0.6. The mean free path was found to be 1000 nm. They studied the possible changes of work function with film thickness in connection with the metal-semiconductor transition. Mikolajczak et al.[104] studied the TEP of Bi thin film. The transport properties of glass coated bismuth films in a temperature range 77 to 300K were

studied by Inoue et al.[105] They found that Hall coefficient for thinner films (d < 50 nm) was p type at higher temperatures and became n type below a critical temperature T_c, where T_c increased with thickness, whereas the thicker ones with d > 50 nm were always n type. The thicknes dependence of resistivity was understood by the size effect theory. The value of ρ_o and ℓ_o were obtained as 1.14×10^{-4} Ωcm and 50 nm respectively. P. Sen et al.[106] reported the measurements on resistivity of Bi films in a temperature range -60 to 110°C. They have found that the negative TCR in thinner films changes with thickness becoming positive at higher thickness. This type of behaviour was attributed to the anomalous growth structure as observed by Ertl et al.[107] Inoue et al.[105] and Newman et al.[100] have also found that smoother polycrystalline structure exists at higher thickness. In the study of kinetic properties of thin Bi films Komnik et al.[108,109] have observed the following peculiarities: (1) in resistivity vs temperature curve, the resistivity goes through a minimum; (2) for very thin films at low temperatures, a maximum of resistivity occurs; (3) at very low temperature the decrease of film thickness is accompanied by a decrease of resistivity. The positions of minimum and maximum in ρ_F vs T plot were found to be thickness dependent. These authors[108,109] concluded that these peculiarities followed from the temperature dependence of the carrier density and carrier mobility, the

temperature coefficients of which are opposite in sign. They found that anomalous size effect was due to an increase in the carrier density with decreasisng thickness of Bi films. Komnik et al.[110] also studied the effect of a change in lattice spacing of small crystalline particles in bismuth island films due to surface pressure. Chaudhuri et al.[111] have measured Hall effect, resistivity, magnetoresistance, TCR of thin Bi films deposited at 150°C. They obtained a positive Hall coefficient. The values of $\ell_o(1-p)$ obtained from ρ_F vs $\frac{1}{d}$ and β_F vs $\frac{1}{d}$ plots were 668.7 and 742.7 nm respectively. The values of ρ_o and p were found as 1.182×10^{-4} Ωcm and 0.5 respectively. The TCR was negative for all thicknesses. They concluded that both FS and MS theories were more or less satisfactory to the same extent. The resistivity, Hall coefficient, magnetoresistance, and thermoelectric power for the temperature range 80 to 293K were measured by Kochowski et al.[112] From the data obtained, concentrations of electron (n) and holes (p_o) as well as their mobilities were determined without assuming that $n = p_o$. Similar kind of study was carried out by Vandamme et al.[113] They obtained the results which were in close agreement with those of Kochowski et al.[112] Kuijper et al.[114] also determined the mobilities and concentrations of electrons and holes using an anisotropic two carrier model. They found that electron and hole concentrations were approximately equal. Pariset[85] found that experimental results on electrical

resistivity of Bi films were in good agreement with approximate form of F.S and MS size effect theories. Electrical and structural properties of bismuth film have been studied by Buxo et al.[115] They have concluded that surface states play a major role in dictating the properties of conductivity. The surface state density and the energy barrier which controls the carrier transport across the grain boundaries have also been evaluated as a function of preparation technique. Saleh et al.[116] studied the elastoresistance properties of thin Bi films. From the study of electromagnetic properties of thin Bi films Asahi et al.[117] found that transverse magnetoresistance had a tendency of saturation with increasing magnetic fields. This tendency was stronger for thinner films. This behaviour was attributed to the scattering at the grain boundary planes parallel to the electric field. Asahi et al.[118] also studied the size effect in the electrical properties of thin epitaxial bismuth films. The MS theory was modified to make it applicable for a system with two carriers (electron and hole). The thickness dependence of the carrier densities was also considered. The specularity parameter p at the surface and reflection coefficient R at the grain boundaries were determined to be 0.7 and 0.2 to 0.3 respectively. Damodara Das et al.[96,119] studied the temperature dependence of resistivity of Bi film. They also found that resistivity vs temperature plots exhibited a minimum whose position was a function of thickness.

Thickness dependence of resistivity and TCR of polycrystalline Bi films were studied by Schnelle et al.[120] They modified the approximate MS equation for the resistivity to consider the thickness dependence of charge carrier concentration. Using this modified model, these authors successfully explained the resistivity behaviour and negative TCR of bismuth films. Recently Beutler et al.[121] have observed fluctuations in low temperature resistance of thin Bi wires and films. These fluctuations appeared most clearly as a function of time.

In the present work, the effect of grain boundary scattering and surface scattering on the electrical resistivity of tin, lead, and tin-lead alloy films have been studied at different temperatures. The size effect in temperature coefficient of resistivity (TCR) of tin and lead films have been studied at room temperature. For this study of electrical properties of Sn, Pb, and SnPb alloy films the experimental data has been used from reference 43. The electrical properties of thin Sb and Bi films have been studied at different temperatures. All the electrical measurements were made in Situ. The experimental observations have been correlated with structure of the film. The applicability of different models such as Mayadas, Pichard model etc. has been explored.

REFERENCES

1. T.J. Coutts, Electrical Conduction in Thin Metal Films (Elsevier, New York, 1974) Chapt. 6.
2. J.J. Thomson, Proc. Cambridge Phil. Soc. 11, 120 (1901).
3. K. Fuchs, Proc. Cambridge Phil. Soc.34, 100 (1938).
4. E.H. Sandheimer, Phys. Rev. 80, 401 (1950).
5. E.H. Sandheimer, Adv. Phys. 1, 1 (1952).
6. H.J. Juretschke, J. Appl. Phys. 37, 435 (1966).
7. M.S.P. Lucas, Appl. Phys. Lett. 4, 73 (1964).
8. M.S.P. Lucas, J. Appl. Phys. 36. 1632 (1965).
9. A.A. Cottey, Thin Solid Films 1, 297 (1968).
10. C.R. Tellier and A.J. Tosser, Int. Res. Rep. Nancy 1, (1979).
11. C.R. Tellier and A.J. Tosser, Size Effects in Thin Films (Elsevier, Amsterdam, New York, 1982) Chapt. 1.
12. A.F. Mayadas and M. Shatzkes, Phys. Rev. B1, 1382 (1970).
13. F. Thieme and W. Kirstein, Thin Solid Films 30, 371 (1975).
14. E. Dobierzewska-Mozrzymas and F. Warkusz, Thin Solid Films 43, 267 (1977).
15. G. Wedler and P. Wissmann, Ber. Bunsenges. Phys. Chem. 74, 934 (1970).
16. F. Warkusz, Acta. Phys. Pol A 54, 31 (1978).
17. F. Warkusz, Electrocomp. Sci. Technol. 5, 197 (1978).

18. F. Warkusz, Surf. Sci. 200, 394 (1988).

19. C.R. Pichard, C.R. Tellier, and A.J. Tosser, Thin Solid Films 62, 189 (1979).

20. C.R. Tellier and A.J. Tosser, Thin Solid films 70, 225 (1980).

21. C.R. Tellier, C.R. Pichard, and A.J. Tosser, Thin Solid Filoms 61, 349 (1979).

22. C.R. Pichard, C.R. Tellier, and A.J. Tosser, J. Mater. Sci. 15, 2236 (1980).

23. C.R. Pichard, C.R. Tellier, and A.J. Tosser, Phys. Status Solidi(a) 65, 327 (1981).

24. C.R. Tellier, C.R. Pichard, V.I. Vatamanyuk, and A.J. Tosser, J. Mater Sci. Lett. 2, 579 (1983); 3, 447 (1984).

25. M. Bedda, C.R. Pichard, and A.J. Tosser, J. Mater Sci. 21, 1405 (1986).

26. M. Bedda, S. Messaadi, C.R. Pichard, and A.J. Tosser, J. Mater. Sci. 21, 2643 (1986).

27. A.J. Learn and R.S. Spriggs, J. Appl. Phys. 34, 3012 (1963).

28. J.W. Matthews, Scr. Metall. 11, 233 (1977).

29. S.L. Lenhoczky and C.V. Briscoe, Phys. Letters 24, 880 (1977).

30. K.E. Gray, G.J. Everett, R.T. Kampwirth, and R.P. Huebener, Phys. Status Solidi(a) 7, K73 (1971).

31. H.P. Baltes and E.R. Hilf, Solid State Commu. 12, 369 (1973).

32. D.E. Banks and B.L. Blackford, Can. J. Phys. 51, 2505 (1973).

33. G.J. Dolan, J. Low. Temp. Phys. 15, 111 (1974).

34. L.G. Hayler, L. M. Geppert, J.T. Chen, and Y.W. Kim Phys. Rev. B 11, 1924 (1975).

35. V.P. Duggal and P.K. Ashwini Kumar, Phys. Lett. 53A, 397 (1975).

36. R.O. Smith, B. Serin, and E. Abrahm, Phys. Lett. 28A, 224 (1968).

37. M.G. Hapase, M.K. Gharpurey and A.B. Biswas, Surf. Science 12, 85 (1968).

38. B.N. Aleksandrov, Sov. Phys. - JETP 16, 286 (1963).

39. H. Morgner and G. Pompe, Phys. Status Solidi(a), 29, 459 (1975).

40. Z.P. Tsalyy, The Phys. of Metal and Metall. 36, 189 (1973).

41. S. Chaudhuri and A.K. Pal, J. Phys. D8, 1311 (1975).

42. M. Murakami, Thin Solid Films 59, 105 (1979).

43. Gyanesh Chandra, Ph.D. Thesis, Indian Institute of Technology, Kanpur (1985).

44. B.I. Belevtsev, Yu. F. Komnik, and V.I. Odnokozov, Sov. Phys.-Solid State 26, 1968 (1984).

45. A.J. Tosser, C.R. Tellier, and C.R. Pichard, J. Mater. Sci. 16, 944 (1981).

46. B.K. Sarma, R.K. Das, and J. Hatibaruah, Ind. J. Phy. 59A, 209 (1985).

47. R. Watton, J. Phys. C2, 1697 (1969).

48. Ch. K. Schiller and H. Bulow, Solid State Commu. 8, 1827 (1970).

49. E.R. Andrew, Proc. Phys. Soc. (London) A, 62, 77 (1949).

50. A.B. Pippard, Proc.R. Soc. (London) Ser. A, 191, 385 (1947).

51. R.G. Chambers, Proc. R. Soc. (London) Ser. A 215, 481 (1952).

52. H.P. Singh and L.E. Murr, Philos. Mag. 26, 649 (1972).

53. J. Niebuhr, Z. Phys. 132, 468 (1952).

54. A.K. Pal and Paramita Sen, J. Mater. Sci. 12, 1472 (1977).

55. G.L. Malhotra, S.K. Sharma, S. Chaudhuri, and A.K. Pal, J. Phys. Soc. (Japan) 45, 930 (1978).

56. B. Stolecki, F. Warkusz, A. Borodziuk-Kulpa, and C. Wesolowska, J. Mater. Sci. 14, 1349 (1979).

57. B. Stolecki, A. Borodziuk-Kulpa, and C. Wesolowska, Thin Solid Films 56, 299 (1979).

58. A.R. Patel and K.V. Rao, Thin Solid Films 70, 253 (1980).

59. E.A. Abou Saif, A.A. Mohamed, and M.G. El-Khodary, Thin Solid Films 94, 133 (1982).

60. S. Varghese, C.I. Muneera, and V.U. Nayar, Thin Solid Films 99, 385 (1983).

61. D. De, S. Chaudhuri, and A.K. Pal, Thin Solid Films, 99, 371 (1983).

62. M.A. Angadi and L.A. Udachan, J. Mater. Sci. Lett. 2, 379 (1983).

63. C.R. Pichard, Yu.F. Komnik, B.I. Belevtsev, and A.J. Tosser, J. Mater. Sci. Lett. 2, 360 (1983).

64. Gyanesh Chandra and O.P. Katyal, Phys. Status Solidi(a) 86, 765 (1984).

65. C.K. Ghosh and A.K. Pal, Ind. J. Phys. 55A, 193 (1981).

66. Gyanesh Chandra and O.P. Katyal, Phys. Status Solidi(a) 86, 759 (1984).

67. Yu.F. Komnik and E.I. Bukhshtab, JETP Lett. 6, 58 (1967).

68. Yu.F. Komnik, E.I. Bukshtab, and Yu.V. Nikitin, Fiz. Tvered. Tela (USSR) 12, 793 (1970).

69. W.F. Leverton and A.J. Dekker, Phys. Rev. 80, 732 (1950).

70. A. Colombani, C. Vautier and P. Huet; C.R. Acad. Sci. 21, 1838 (1958).

71. I. Mietz and H. Sprenger, Krist. Tech. 7, 123 (1972).

72. I. Rechenberg and H. Thieme, Krist. Tech 9, 19 (1974).

73. K. Mojejko, K. Paprocki, M. Subotowicz, and M. Radomsky, J. Cryst. Growth 36, 61 (1976).

74. M. Hashimoto, T. Niizeki, and K. Kambe, Jpn. J. Appl. Phys. 19, 21 (1980).

75. D.C. Barua and K. Barua, Ind. J. Phys. 49, 603 (1975).

76. K. Maki, Jpn. J. Appl. Phys. 12, 146 (1973).

77. H. Horikoshi and N. Tamura, Jpn. J. Appl. Phys. 2, 328 (1963).

78. K. Paprocki, K. Mojejko, M. Subotowicz, and M. Jalochowski, Thin Solid Films 36, 93 (1976).

79. A.K. Pal and P. Sen, J. Mater. Sci. 10, 1879 (1975).

80. D. Deschacht, A. Boyer, and E. Groubert, Thin Solid Films 70, 311 (1980).

81. A. Boyer, D. Deschacht, and E. Groubert, Thin Solid Films 76, 119 (1981).

82. D. Deschacht, A. boyer, E. Groubert, C.R. Pichard, A.J. Tosser, and C.R. Tellier, J. Mater. Sci. 17, 2753 (1982).

83. D. Deschacht and A. Boyer, J. Mater. Sci. Lett. 4, 25 (1985).

84. D. Deschacht and A. Boyer, J. Mater. Sci. 20, 807 (1985).

85. C. Pariset, Thin Solid Films 91, 301 (1982).

86. D. De, C.K. Ghosh, and A.K. Pal, Thin Solid Films 110, 193 (1983).

87. K. Mojejko-Kotlinska and M. Subotowicz, Thin Solid Films, 111, 235 (1984).

88. S.M.J. Akhtar and E.E. Khawaja, Phys. Status Solidi(a) 87, 335 (1985).

89. V.B. Sandomirskii, Sov. Phys.-JETP 16, 1630 (1963); 25, 101 (1967).

90. Yu.F. Ogrin, V.N. Lutskii, and M.I. Elinson, Sov. Phys.-JETP Lett. 3, 71 (1966); Sov. Phys.-JETP 26, 714 (1968)

91. V.P. Duggal, R. Rup, and P. Tripathi, Appl. Phys. Lett. 9, 293 (1966).

92. V.P. Duggal and R. Rup, J. Appl. Phys. 40, 492 (1969).

93. M. Inoue, H. Yagi, and Y. Tamaki, Jap. J. Appl. Phys. 12, 310 (1973).

94. Yu.F. Komnik and E.I. Bukhshtab, Sov. Phys.-JETP 27, 34 (1968).

95. H. Asahi, T. Humoto, and A. Kawazu, Phys. Rev. B 9, 3347 (1974).

96. V. Damodara Das and N. Jayaprakash, Vacuum 31, 199 (1981); 31, 133 (1981).

97. V.I. Kaidanov and A.R. Regel, Sov. Phys.-Tech. Phys. 3, 376 (1958).

98. A. Colombani and P. Huet, C.R. Acad. Sci. 244, 755 (1957); 244, 865 (1957); 254, 1988 (1962); 254, 2566 (1962).

99. Y. Sawatari, A. Kinbara, and T. Nakao, Oyo Butsuri 33, 461 (1964).

100. M.R. Newman and W.H. Kao, J. Appl. Phys. 37, 3327 (1966).

101. R.A. Hoffman and D.R. Frankl, Phys. Rev. B 3, 1825 (1971).

102. N. Garcia, Y.H. Kao, and M. Strongin, Phys. Rev. B 5, 2029 (1972).

103. M. Subotowicz, M. Jalochowski, B. Mikolajczak, and P. Mikolajczak, Phys. Status Solidi(a) 17, 79 (1973).

104. P. Mikolajczak, W. Piasek, and M. Subotowicz, Phys. Status Solidi(a) 25, 619 (1974).

105. M. Inoue, Y. Tamaki, and H. Yagi, J. Appl. PHys. 45, 1562 (1974).

106. Paramita Sen and A.K. Pal, Jap. J. Appl. Phys. 14, 1473 (1975).

107. M.E, Ertl, P. Marchant, and H.L. Johnson, J. Mater. Sci. 4, 1114 (1969).

108. Yu.F. Komnik, E.I. Bukhshtab, Yu.V. Nikitin, and V.V.Andrievskii, Sov. Phy.-JETP 33, 364 (1971).

109. Yu.F. Komnik and V.V. Andrievsky, Thin Solid Films 42, 1 (1977).

110. Yu.F. Komnik, V.V. Pilipenko, and L.A. Yatsuk, Thin Solid Films 52, 313 (1978).

111. S. Chaudhuri and A.K. Pal, J. Appl. Phys. 48, 3455 (1977).

112. S. Kochowski and A. Opilski, Thin Solid Films 48, 345 (1978).

113. L.K.J. Vandamme and J. Kedzia, Thin Solid Films 65, 283 (1980).

114. A.H. DE Kuijper and J. Bisschop, Thin Solid Films 110, 99 (1983).

115. J. Buxo, M. Saleh, G. Sarrabayrouse, G. Dorville, J. Berty, and M. Brieu, Rev. De Physique Appliquee 15, 961 (1980).

116. M. Saleh, J. Buxo, G. Dorville, and G. Sarrabayrouse, Rev. De Physique, Appliquee 14, 405 (1979).

117. H. Asahi, S. Baba, and A. Kinbara, J. Appl. Phys. 48, 129 (1977).

118. H. Asahi and A. Kinbara, Thin Solid Films 66, 131 (1980).

119. V. Damodara Das and S. Vaidehi, Phys. Status Solidi(a) 71, 351 (1982).

120. W. Schnelle and U. Dillner, Phys. Status Solidi(a) 44, 197 (1977).

121. D.E. Beutler, T.L. Meisenheimer, and N. Giordano Phys. Rev. Lett. 58, 1240 (1987).

CHAPTER II

EXPERIMENTAL DETAILS

2.1 *Preparation of Sb and Bi Films*

Sb and Bi films were prepared by thermal evaporation method. The glass slides were used as substrates, as glass surface is atomically smooth, chemically inactive, and nonporous. For the preparation of thin films, a vacuum coating unit (Hind Hivac model 12A4) which was fitted with a oil diffusion pump and a liquid nitrogen cold trap, was used (Fig. 2.1). A vacuum of about 10^{-6} torr was maintained in the vaccum chamber of this coating unit. The distance of glass substrate from the source was about 20 cm. The glass substrate was cleaned prior to deposition by the following method.

The glass substrate was washed by detergent solution and rinsed properly in distilled water. Then this glass substrate was kept in boiling distilled water for 15 to 20 minutes. After this, it was cleaned, ultrasonically, in acetone. During ultrasonic cleaning due to vibrations microscopic cavities were formed in the cleaning fluid. These cavities had a powerful scrubbing and cleaning action because of which impurities were easily removed. Finally glass substrate was degreased in the vapours of isopropyl alcohol for 20 minutes.

Fig. 2.1 'HIND HI VAC' 12A4 VACUUM COATING UNIT.

The cleaned glass slide was placed horizontally on the substrate holder in the vacuum chamber. A piece of the film material was placed in molybdenum boat. When the pressure was reduced to about 10^{-6} torr, the boat carrying the film material was heated. As a result of evaporation, the evaporated atoms got deposited onto the substrate. Four silver (99.99%) spots were first deposited onto the cleaned substrate using a suitable mask. These silver spots served as electrical contacts. Sb(99.999%) and Bi(99.999%) supplied by Chempure (Pvt.) Ltd., Calcutta, India were used for the preparation of the sample films. A suitable mica mask was used to obtain a definite rectangular shape of the film. Film obtained in this way, made a bridge over the silver electrodes. Before the evaporation, the metals Ag, Sb, and Bi were etched with very dilute hydrochloric acid for the removal of surface oxide then these metals were washed by deionized distilled water and finally rinsed by acetone. The molybdenum boat was also heated to a high temperature in a vacuum of 10^{-5} torr before the evaporation. The deposition was controlled by controlling the current through the boat. For the deposition of Sb films, the substrate was kept at 350K, while the deposition of Bi films was carried out at room temperature.

2.2 *Electrical Measurements*

Measurements of film resistance were carried out in situ. For this purpose a metallic cold finger was designed (Fig. 2.2). The substrate deposited with electrodes was attached to the bottom plate of the cold finger where a heater was fitted near to the substrate so that its temperature can be varied. After making the electrical connections, the cold finger was fitted to the vacuum chamber and then film was prepared. The resistance of the film was measured by using four probe method. The outer two electrodes were used as current leads when a constant current of few milliamperes was passed through the outer electrodes, the potential drop was measured across the inner two electrodes by a K-3 potentiometer (Leeds and Northrup). Extra care was taken to eliminate any thermoelectric voltage by reversing the direction of current for each measurements. A standard resistance was connected in the series with the sample. By measuring the potential drop across the standard resistance with the help of K-3 potentiometer, the current across the sample was calculated. The resistance of the film R_F was calculated by using the simple relation

$$\frac{V_F}{R_F} = \frac{V_{st}}{R_{st}}$$

where V_F = Potential drop across the film

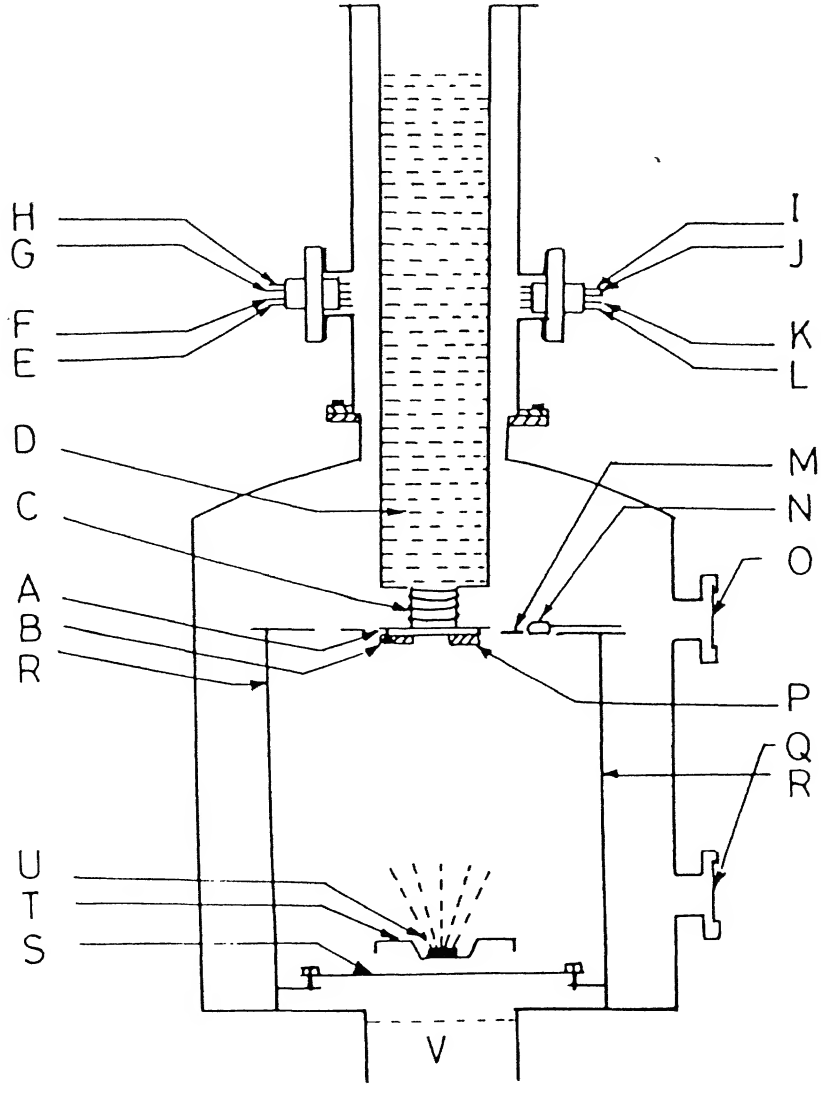

A: Substrate
B: Thermocouple
C: Heater
D: Liquid Nitrogen
E,F: Thermocouple leads
G H: Heater leads
I,J: Current leads
K,L: Leads for emf measurements
M: Horizontal plate
N: Thickness monitor
O,Q: Glass windows
P: Mica mask
R: Supporting rods
S: Plate
T: Boat
U: Bulk material
Y: Connection to pumping system

Fig. 2.2 EXPERIMENTAL SETUP.

V_{st}= Potential drop across the standard resistance

R_{st}= Value of standard resistance.

During the measurements of resistance, the temperature of the film was varied by cold finger filled with liquid nitrogen and fitted with a heater. The temperature was raised by passing a d.c. current through the heater. A copper-constantan thermocouple fixed rigidly on the substrate was used to measure the temperature of the film. These measurements of resistance of Sb and Bi films in situ, were made in a temperature range 150 to 350K. The resistance of bismuth film was also measured at 77K. For this, the film was directly immersed in liquid nitrogen and the resistance was recorded. The distance of inner two electrodes and the width of the film were measured by a travelling microscope.

2.3 *Thickness Measurements of the Films*

A quartz crystal thickness monitor (model CFM-1, Hind Hivac) was used to measure the evaporation rate and thickness of the film during the deposition. This thickness monitor has two oscillatory quartz crystals, one is monitor quartz crystal (6.0M.Hz-frequency) positioned in the vacuum chamber at the level of substrate and other is reference quartz crystal (6.5M.Hz-frequency) mounted in the control unit outside the vacuum chamber. The mass of the

deposited material (the thin film) causes a change in the frequency of monitor crystal, which results a change in the frequency difference of two crystals. This change is converted into D.C. signals and displayed on the conventional meters. Before doing the actual measurements, this frequency shift was calibrated in terms of thickness for antimony and bismuth films. These calibration curves were used to determine the thickness of the film during the actual experiments.

The thickness of the film was also measured by optical method. A cleaned glass slide was placed in the vacuum chamber near to the film substrate at the same level. The half portion of this glass slide was covered during film deposition so that a step was formed on it. This slide, which had deposited film on its half portion, was then covered by the silver coating. Another partially silvered glass plate was brought into contact with the film surface at a slight wedge angle so that a wedge shaped air gap was formed between the two glass slides. When the interferometer was illuminated with a parallel monochromatic beam of yellow light (589.3nm) from a sodium lamp at normal incidence and viewed with a microscope, dark fringes were observed against a bright background. By adjusting the relative positions of plates to form a wedge shaped air gap, fringes were made to run in straight lines perpendicular to the step. These fringes showed a

displacement as they passed over the film step edge. The separation of the interference fringes and the displacement or step height were measured with the help of a calibrated microscope eyepiece. The thickness of the film was calculated by using the relation

$$d = \frac{\lambda_{Na}}{2} \times \frac{\Delta\omega}{\omega}$$

where λ_{Na} = Wavelength of sodium light (589.3nm)

d = Film thickness

$\Delta\omega$ = Displacement or step height

ω = Fringe width.

2.4 *Electron Microscopy*

For the study of structural properties and grain size measurements of Sb and Bi films, scanning electron microscopes (JEOL JSM-35 and PHILIPS PSEM 500) were used. Since the films were deposited onto the substrate of insulating material, therefore, to avoid the damage caused by the incident electrons, the grounding of film surface was made by silver paste. The film was seen on the screen of the electron microscope at magnifications of 5000x and 10000x. The photographs of the structure seen on the screen were taken on 35mm films by using a camera. The positive prints were used for the grain size study. The

grain size was measured by a travelling optical microscope. The micron marker was used for the indication of the magnification.

2.5 *X-ray Diffraction Techniques*

The structural properties of Sb and Bi films were also studied with the help of X-ray diffractograms. For this X-ray diffraction profiles were chart recorded at a scanning speed of 1.2° in 2θ per minute and a chart speed of 15mm/minute with a time constant of 10 second on a X-ray diffractometer (ISO-DEBYEFLEX 2002D) operated at 30KV and 20mA. X-ray was generated from a nickel filtered CuK_{α} target. Knowing the exact position where the diffraction peak occurs, the interplanar spacing d may be found by using the relation

$$2d\sin\theta = \lambda$$

where θ = Angle at which diffraction peak occurs

λ = Wavelength of X-ray.

Sb and Bi, both, have rhombohedral structure. The rhombohedral lattice may be referred to hexagonal axes.[1] Therefore knowing d values and lattice parameters a and c, the indices of planes were determined by using the following relation

$$\frac{1}{d^2} = \frac{4}{3}\left[\frac{h^2 + hk + k^2}{a^2}\right] + \frac{\ell^2}{c^2}$$

Grain size D was also measured from the diffraction peaks using Scherrer formula[2]

$$D = \frac{\lambda}{B_c \mathrm{Cos}\theta}$$

where B_c = True width of diffraction peak at half of the maximum intensity.

This true width of diffraction peak occurs due to particle size only.[3] The recording of instrumental profiles which acts as standard was made under identical instrumental settings from the pure bulk powder. To remove the effect of nonuniform strain in broadening, the bulk powder was properly annealed. The true width due to grains was calculated by using the following formula[2]

$$B_c = B_F - \frac{B_{St}^2}{B_F}$$

where B_F = Observed width of diffraction peak at half of the maximum intensity in films

B_{St} = Corresponding width of diffraction peak at half of the maximum intensity in bulk sample.

References

1. B.D. Cullity, Elements of X-ray Diffraction (Addison-Wesley, London, 1959) Appendix 2.
2. Suchitra Sen, S.K. Halder and S.P. Sen Gupta, J. Phys. Soc. (Jpn) 38. 1641 (1975).
3. B.E. Warren, X-ray Diffraction (Addison-Wesley, London, 1968) Chapt. 13.

CHAPTER IIIA

EFFECT OF GRAIN BOUNDARY SCATTERING ON THE ELECTRICAL RESISTIVITY OF POLYCRYSTALLINE TIN, LEAD, AND TIN-LEAD ALLOY FILMS

3.1 *Experimental Results and Discussion*

Chandra and Katyal[1-3] have studied the electrical properties of tin, lead, and tin-lead alloy films in a temperature range 150 to 350K. They found that experimental results on film resistivity were consistent with the approximate form of MS model[4,5] for completely diffused scattering i.e. p=0. In this chapter, using the experimental data from reference 1, the effect of grain boundary scattering on the electrical resistivity of polycrystalline tin, lead, and tin-lead alloy films have been studied.

Figures 3.1A and 3.1B show that in Pb, Sn, and SnPb films the average grain diameter increases with the film thickness. According to Matthiessen's rule the resistivity of a thin metal film can be calculated by superimposing the contributions to the resistivity due to all sources of electronic scatterings.[6,7] Estimating the contribution to the film resistivity due to surface ρ_s by using the relation

$$\rho_s = \frac{3}{8} \frac{\rho_o \ell_o (1-p)}{d} \qquad (3.1)$$

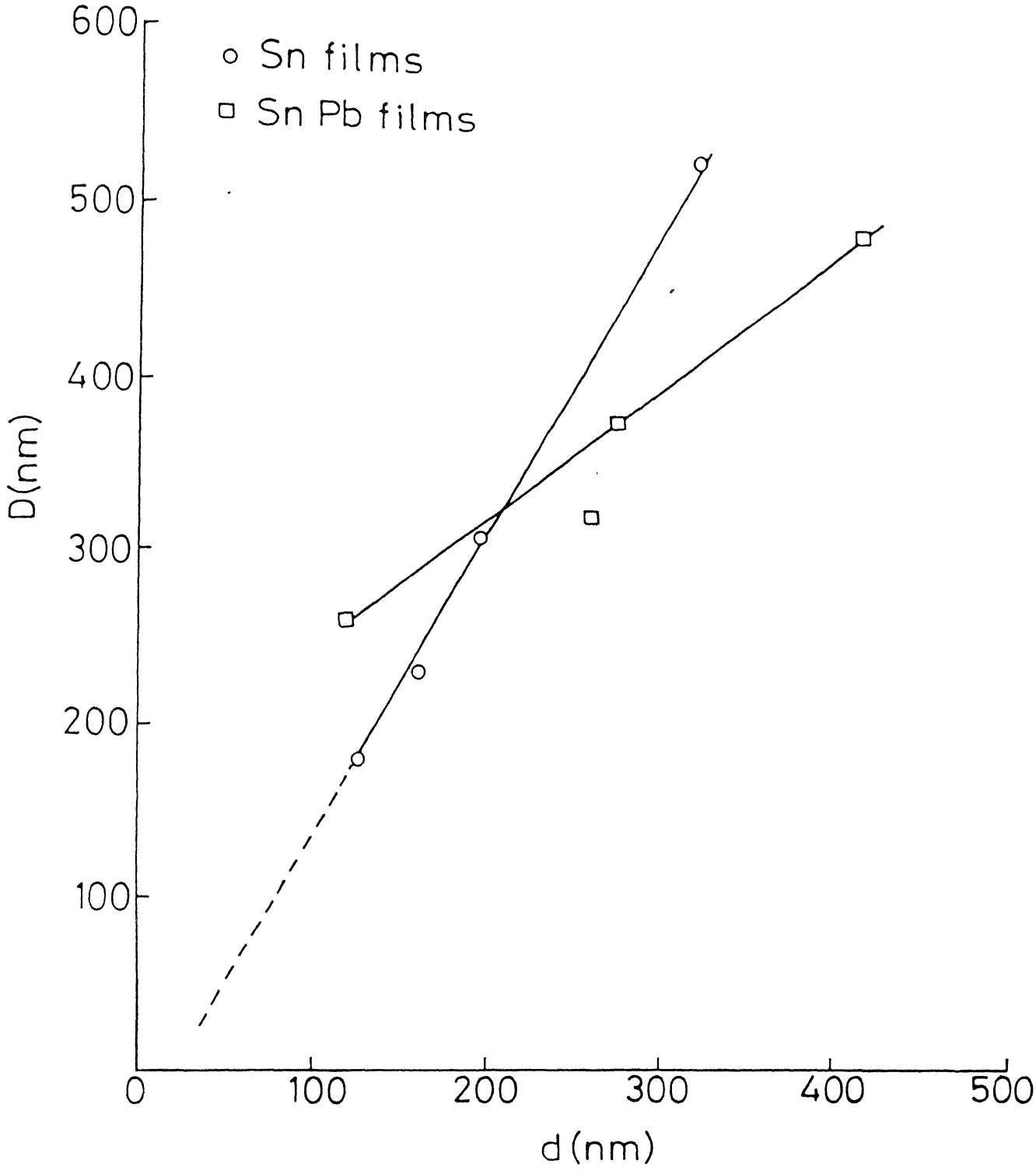

Fig. 3.1B PLOT OF AVERAGE GRAIN SIZE D vs. FILM THICKNESS d FOR TIN AND TIN-LEAD ALLOY FILMS.

with the completely diffuse scattering (p=0) and attributing the difference to the grain boundaries,[8] the experimental value of grain boundary resistivity ρ_g have been calculated. Figures 3.2 and 3.3 show the dependence of ρ_g on average grain diameter D at temperatures 175K and 300K for Sn and Pb films respectively. The grain boundary resistivity ρ_g of each films (Sn and Pb) is found to increase with the decreasing grain diameter D and thus exhibits the size effect. Such Type of size effect which arises due to grain size, is known as internal size effect.

In polycrystalline films, the resistivity is also influenced by the scattering of conduction electrons from the grain boundaries. The effect of grain boundary scattering becomes more significant when grain size is comparable to the mean free path of charge carriers. Mayadas and Shatzkes(MS)[4] developed a theory which takes into account the effect of grain boundary scattering. In this model the resistivity of an infinitely thick film is given as

$$\frac{\rho_o}{\rho_g} = G(\alpha) = 1 - \frac{3}{2}\alpha + 3\alpha^2 - 3\alpha^3 \ln(1+\alpha^{-1}) \qquad (3.2)$$

with $$\alpha = \frac{\ell_o}{D}\frac{R}{(1-R)} \qquad (3.3)$$

where ρ_g = Grain boundary resistivy due to both isotropic background scattering and grain boundary scattering

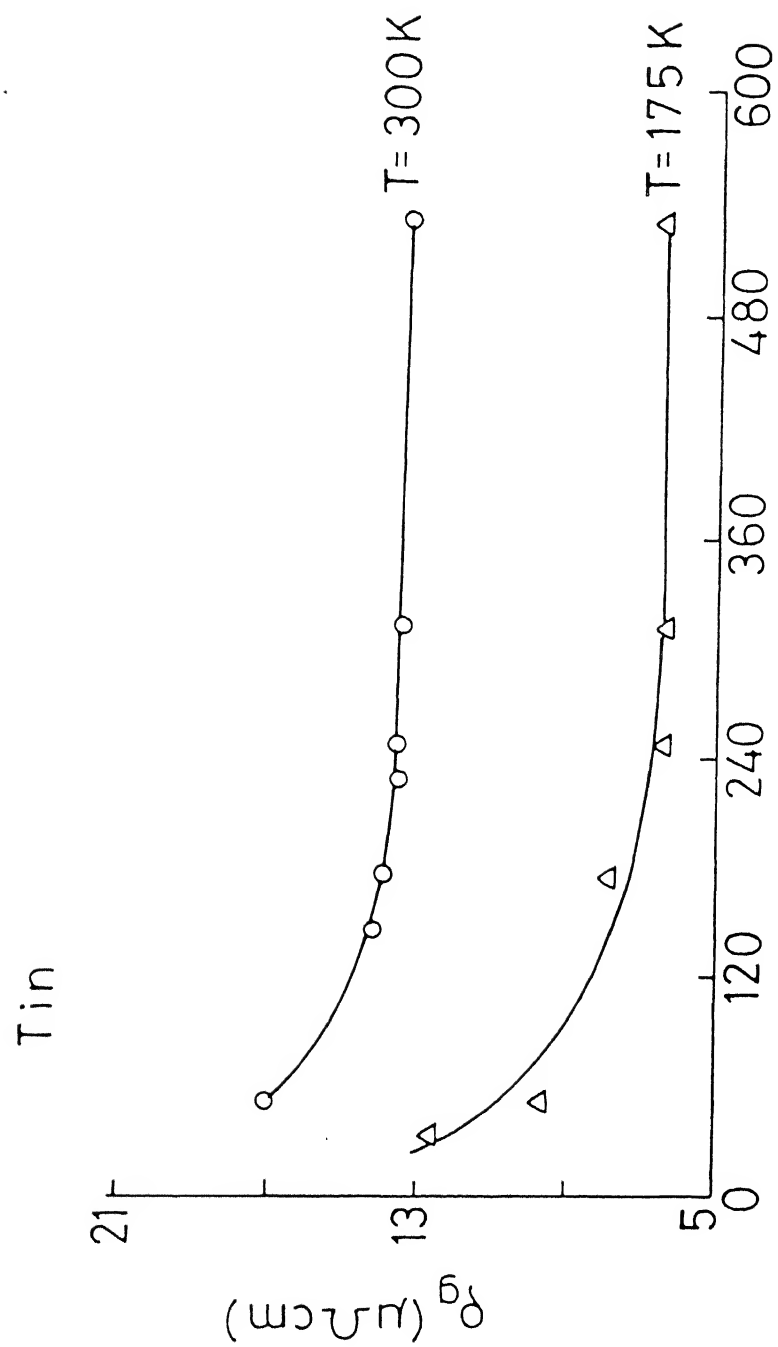

Fig. 3.2 PLOTS OF RESISTIVITY ρ_g vs. AVERAGE GRAIN DIAMETER D FOR TIN FILMS AT 175 AND 300 K.

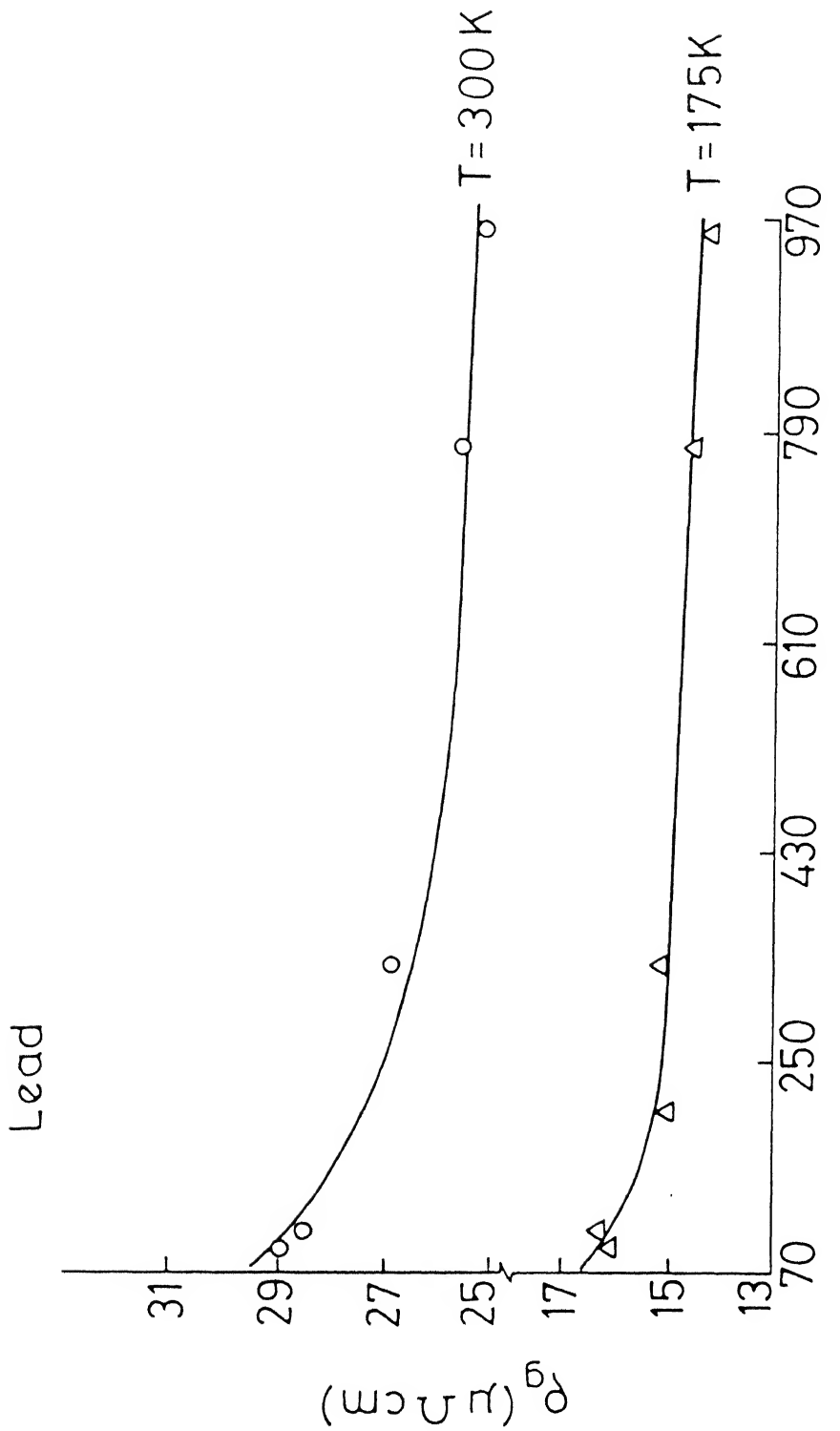

Fig. 3.3 PLOTS OF RESISTIVITY ρ_g vs. GRAIN DIAMETER D FOR LEAD FILMS AT 175 AND 300 K.

ρ_o = Bulk resistivity

ℓ_o = Bulk mean free path

D = Average grain diameter

R = Reflection coefficient.

To consider grain boundary scattering, a phenomenological theory was proposed by Pichard et al. (PTT model).[9] In this three dimensional PTT model, a statistical transmission coefficient t was introduced for describing the effect of roughness of the grain boundary.[7,10] The ratio of an infinitely thick film conductivity σ_g to that in bulk material is expressed as[9-12]

$$\frac{\sigma_g}{\sigma_o} = \frac{\rho_o}{\rho_g} = \frac{3}{2}\frac{\nu}{1-C}\left[\gamma - \frac{1}{2} + (1-\gamma^2)\ell n\ (1+\gamma^{-1})\right] \qquad (3.4)$$

with

$$\gamma = \frac{\nu + C^2}{1 - C} \qquad (3.5)$$

$$C = 4/\pi$$

and

$$\nu = \frac{D}{\ell_o}\left[\ell n\ \frac{1}{t}\right]^{-1} \quad \text{for } t > 0.3 \qquad (3.6)$$

$$\nu = \frac{D}{2\ell_o}\frac{(1+t)}{(1-t)} \qquad (3.6')$$

where t = Transmission coefficient.

Equation (3.6') defines the grain boundary parameter ν without any restriction in t values.

The experimental results on ρ_g of Sn and Pb have been

explained with the help of equations (3.2) and (3.3) of MS model[4] and equations (3.4) to (3.6') of PTT model.[9,11] In case of Sn films on using the bulk parameter[1] ρ_o = 12.6 $\mu\Omega$ cm and ℓ_o = 8.3 nm we see from Fig. 3.4 that MS equation (3.2) with R = 0.60 and PTT equation (3.4) with t = 0.15 reproduce the experimental results at 300K. Similarly at 175K on using ρ_o = 5.2 $\mu\Omega$ cm and ℓ_o = 20.2 nm (reference 1) equation (3.2) with R = 0.66 and equation (3.4) with t = 0.075 reproduce the results. In case of Pb films[1] ρ_o = 24.4 $\mu\Omega$ cm and ℓ_o = 4.3 nm, at 300K the experimental results are consistent with MS equation (3.2) for R = 0.72 and with PTT equation (3.4) for t = 0.005 (Fig 3.5). At 175K for Pb films[1] ρ_o = 13.7 $\mu\Omega$ cm and ℓ_o = 7.7 nm, the results are consistent with equations (3.2) and (3.4) for R = 0.67 and t = 0.05 respectively. Figures 3.4 and 3.5 show that there is a good agreement between the experimental and theoretical results on ρ_g. Both the models, the MS model and PTT model, give almost same results for Sn and Pb films. To see the effect of surface scattering and grain boundary scattering on the total film resistivity of Sn and Pb films, different contributions to the resistivity have been calculated in Table 3.1. It is well known that if the grain size becomes comparable to the mean free path, the grain boundary scattering may produce a deviation from Matthiessen's rule. However, according to MS[4] and Pichard et al.[13] this deviation is less than 5% therefore with a good approximation $\rho_g$can be expressed as the sum of

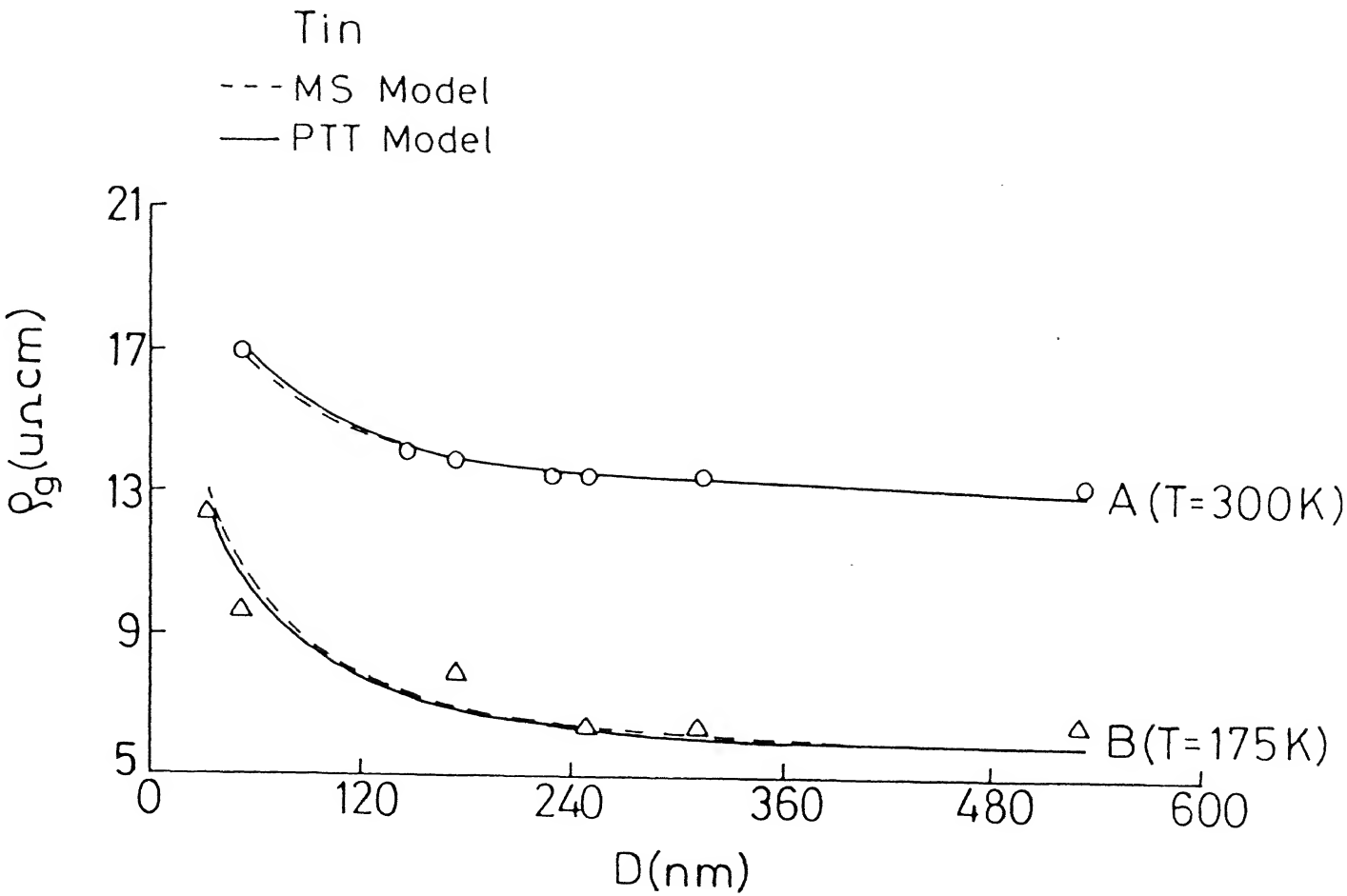

Fig. 3.4 Plots of grain boundary resistivity ρ_g vs. grain size D for tin films. Curves : (A) o experimental points at 300 K, --- MS curve (eqn. 3.2) for R = 0.6, —— PTT curve (eqn. 3.4) for t = 0.15; (B) Δ experimental points at 175 K,--- MS curve for R = 0.66, —— PTT curve for t = 0.075.

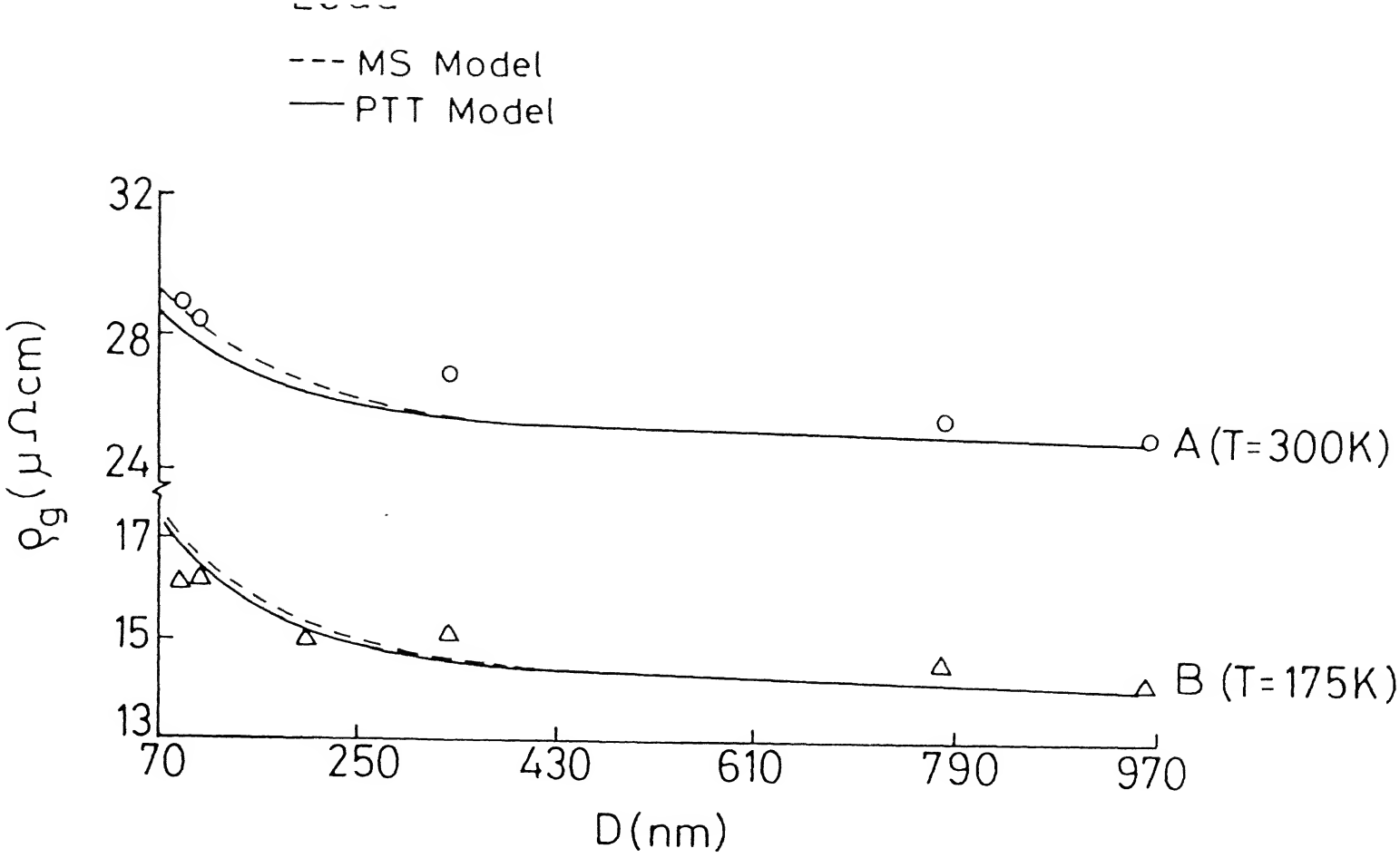

Fig. 3.5 Plots of grain boundary resistivity ρ_g vs. grain size D for lead films. Curves : (A) o experimental points at 300 K, --- MS curve (eqn. 3.2) for R = 0.72, —— PTT curve (eqn. 3.4) for t = 0.005; (B) Δ experimental points at 175 K, --- MS curve for R = 0.67, —— PTT curve for t = 0.05.

resistivity ρ_{gb} due to only grain boundary and ρ_o due to background. Table 3.1 shows that the contribution to the film resistivity due to surface scattering ρ_s is small and enhancement in the film resistivity due to grain boundary scattering ρ_{gb} is considerably large. Thus the resistivity of Sn and Pb films is mainly dominated by grain boundary scattering.

The alloy is a mixture of two phases.[14] The SnPb alloy film have nearly the same concentration as that of bulk alloy (i.e. 63 at.% of Sn and 37 at.% of Pb).[15] The resistivity of an alloy can be given by the weighted average of the resistivities of two components. The total resistivity of the alloy can be expressed as[16]

$$\rho = \rho_1 x_1 + \rho_2 x_2 \qquad (3.7)$$

where

ρ_1 = Resistivity of Sn

ρ_2 = Resistivity of Pb

and x_1 and x_2 are the volume percentage of Sn and Pb respectively.

The resistivity of a film under the conditions that film is not very thin ($K = \frac{d}{\ell_o} > 1$)and grain boundary influence is not very strong ($\alpha < 1$), can be written as[17-19]

$$\rho_F = \rho_o + \frac{3}{2}\frac{\rho_o \ell_o R}{(1-R)D} + \frac{3}{8}\frac{\rho_o \ell_o (1-p)}{d} \qquad (3.8)$$

where d = Film thickness.

Thieme et al.[18] have shown that this equation (3.8) is an approximation to the MS equation if $K > 0.1$ and $\alpha < 1$. Equation (3.8) represents the film resistivity as the sum of resistivities due to scattering of conduction electrons from phonons and defects, from film surfaces, and from grain boundaries, in accordance with the Matthiessen's rule.

The total resistivity of alloy film can be obtained by introducing film resistivities of the component (Sn and Pb) films in equation (3.7) and assuming the effective reflection coefficient in alloy films R for both Sn and Pb films in alloy films. The resistivity of alloy film then may be written as[3]

$$\rho_F = \left[\rho_{o1} + \frac{3}{2}\frac{\rho_{o1}\ell_{o1}R}{(1-R)D} + \frac{3}{8}\frac{\rho_{o1}\ell_{o1}(1-p)}{d}\right] x_1$$

$$+ \left[\rho_{o2} + \frac{3}{2}\frac{\rho_{o2}\ell_{o2}R}{(1-R)D} + \frac{3}{8}\frac{\rho_{o2}\ell_{o2}(1-p)}{d}\right] x_2$$

$$\rho_F = (\rho_{o1}x_1 + \rho_{o2}x_2) + \left[\frac{3}{2}\frac{R}{(1-R)D} + \frac{3}{8}\frac{(1-p)}{d}\right] X$$

$$(\rho_{o1}\ell_{o1}x_1 + \rho_{o2}\ell_{o2}x_2) \qquad (3.9)$$

where ρ_{o1} and ρ_{o2} are bulk resistivities of Sn and Pb respectively

and ℓ_{o1} and ℓ_{o2} are bulk mean free paths of Sn and Pb respectively.

From equation (3.9) we have

$$\rho_s = \frac{3}{8}\frac{(1-p)}{d}\ (\rho_{o1}\ell_{o1}x_1 + \rho_{o2}\ell_{o2}x_2) \qquad (3.10)$$

and $\rho_g = (\rho_{o1}x_1 + \rho_{o2}x_2) + \frac{3}{2}\frac{R}{(1-R)D}\ (\rho_{o1}\ell_{o1}x_1 + \rho_{o2}\ell_{o2}x_2)$ ... (3.11)

The values of constants are

For Sn $\rho_{o1}\ell_{01} = 0.105 \times 10^{-10}\ \Omega\ cm^2$

$\rho_{o1} = 11.35\ \mu\Omega\ cm$

For Pb $\rho_{o2}\ell_{o2} = 0.106 \times 10^{-10}\ \Omega\ cm^2$

$\rho_{o2} = 21.31\ \mu\Omega\ cm$

$x_1 = 0.603$ and $x_2 = 0.397$

Estimating the contribution to the resistivity due to surface scattering ρ_s from equation (3.10) with p = 0 and attributing the difference to the grain boundaries, the experimental values of grain boundary resistivity ρ_g have been calculated. Figure 3.6 show that in SnPb films, ρ_g increases with the decrease of grain diameter and thus exhibits the size effect.

Experimental results on ρ_g of SnPb films can be explained with the help of equation (3.11) which expresses the film resistivity when background and grain boundary

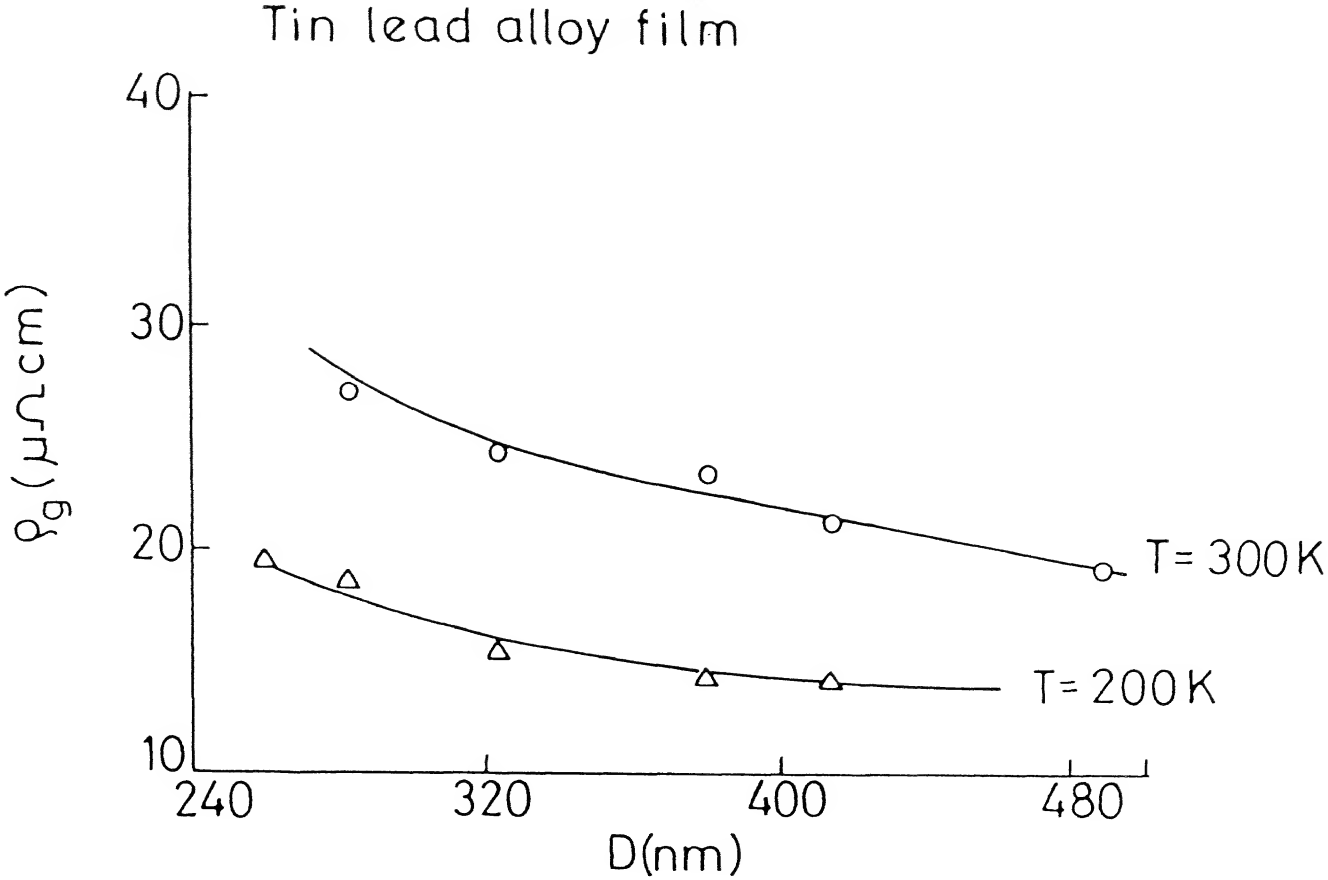

Fig. 3.6 PLOTS OF GRAIN BOUNDARY RESISTIVITY ρ_g vs. GRAIN DIAMETER D FOR SnPb ALLOY FILMS AT 200 AND 300 K.

scatterings are simultaneously operative. On putting the values of ρ_{o1}, ρ_{o2}, x_1, and x_2 in equation (3.7), the bulk resistivity ρ_o of SnPb alloy at 300K is calculated as 15.3 $\mu\Omega$ cm which is very close to the experimental value ρ_o = 15.5 $\mu\Omega$ cm obtained by Chandra and Katyal.[1,3] At 300K on using ρ_o = 15.5 $\mu\Omega$ cm, we see that equation (3.11) with R = 0.945 reproduces the experimental results (Fig. 3.7). Similarly at 200K, with ρ_o = 9.5 $\mu\Omega$ cm and R = 0.935 the equation (3.11) reproduces the experimental results on ρ_g. Figure 3.7 shows that there is a fairly good agreement between the experimental results and theoretical curves. The second term of equation (3.11) represents the resistivity ρ_{gb}, due to only grain boundary scattering. From Table 3.1 it is clear that in SnPb alloy films, the surface scattering effect on resistivity is negligibly small and the film resistivity is mainly contributed by the grain boundary scattering.[20] Therefore, in Sn, Pb,and SnPb alloy films, the grain boundary scattering plays an important role. Particularly in SnPb alloy films, the reflection coefficient R and the resistivity ρ_{gb} due to only grain boundary scattering are rather large in comparison to that in Sn and Pb films, this may be due to defects and impurities.

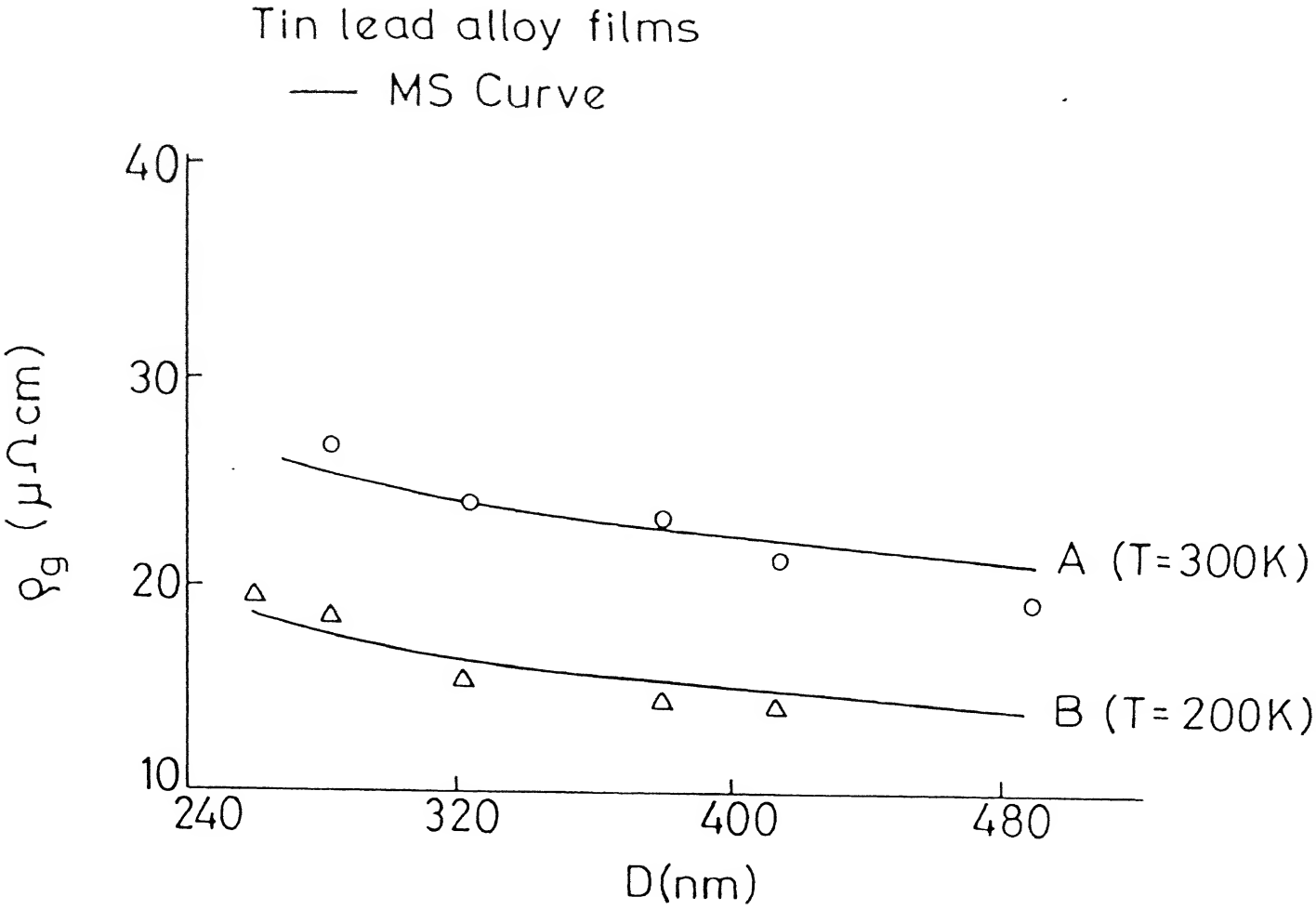

Fig. 3.7 Plots of grain boundary resistivity ρ_g vs. grain size D for SnPb alloy films. Curves : (A) o experimental points at 300 K, —— MS curve (eqn. 3.11) for R = 0.945; (B) Δ experimental points at 200 K, —— MS curve for R = 0.935.

Table 3.1 Different contributions to the resistivity for Sn, Pb and SnPb films

Film	d (nm)	D (nm)	ρ_F ($\mu\Omega$cm)	ρ_{gb} ($\mu\Omega$cm)	ρ_s ($\mu\Omega$cm)
Sn	50.0	51.0	17.9	4.51	0.79
	106.0	147.0	14.6	1.63	0.37
	129.0	177.0	14.3	1.40	0.30
	163.0	229.0	13.8	0.96	0.24
	166.0	248.0	13.8	0.96	0.24
	195.0	311.0	13.7	0.90	0.20
	319.0	530.0	13.4	0.68	0.12
Pb	91.0	90.0	29.4	4.57	0.43
	110.0	104.0	28.9	4.14	0.36
	122.0	206.0	28.5	3.78	0.32
	165.0	334.0	27.2	2.56	0.24
	320.0	776.0	25.8	1.28	0.12
	386.0	960.0	25.2	0.70	0.10
SnPb	119.5	260.0	31.7	15.87	0.33
	156.0	282.0	27.2	11.45	0.25
	260.0	323.0	24.5	8.85	0.15
	275.0	379.0	23.6	7.96	0.144
	323.0	414.0	21.4	5.75	0.122
	415.0	487.7	19.2	3.60	0.095

CHAPTER III(B)

THICKNESS DEPENDENCE OF TEMPERATURE COEFFICIENT OF RESISTIVITY (TCR) OF TIN AND LEAD FILMS

3.2 *Results and Discussion*

The experimental results on temperature coefficient of resistivity (TCR) of Sn and Pb films at room temperature are given in Figs 3.8 and 3.9. The TCR β_F of Sn and Pb films is observed to vary with the thickness. With the increase of film thickness, the TCR of Sn and Pb films increases and thus exhibits the size effect.

In the framework of three dimensional model,[9] for a polycrystalline film in which three types of electron scatterings i.e. background scattering, grain boundary scattering, and external surface scattering, are simultaneously operative, Pichard et al.[11,12,21] obtained an expression for the electrical resistivity of the film, which is written as

$$\frac{\rho_o}{\rho_F} = \frac{3}{2}\frac{1}{b}\left[a - \frac{1}{2} + (1-a^2)\, \ell n\, (1+a^{-1}) \right] \qquad (3.12)$$

with

$$b = \mu^{-1} + \nu^{-1}\,(1-C) \qquad (3.13)$$

$$a = (1 + C^2\nu^{-1})\, b^{-1} \qquad (3.14)$$

$$\mu = \frac{d}{\ell_o}\left[\ell n\, \frac{1}{p} \right]^{-1} \quad \text{for } \mu > 0.3 \qquad (3.15)$$

$$\mu = \frac{d}{2\ell_o}\frac{(1+p)}{(1-p)} \qquad (3.15')$$

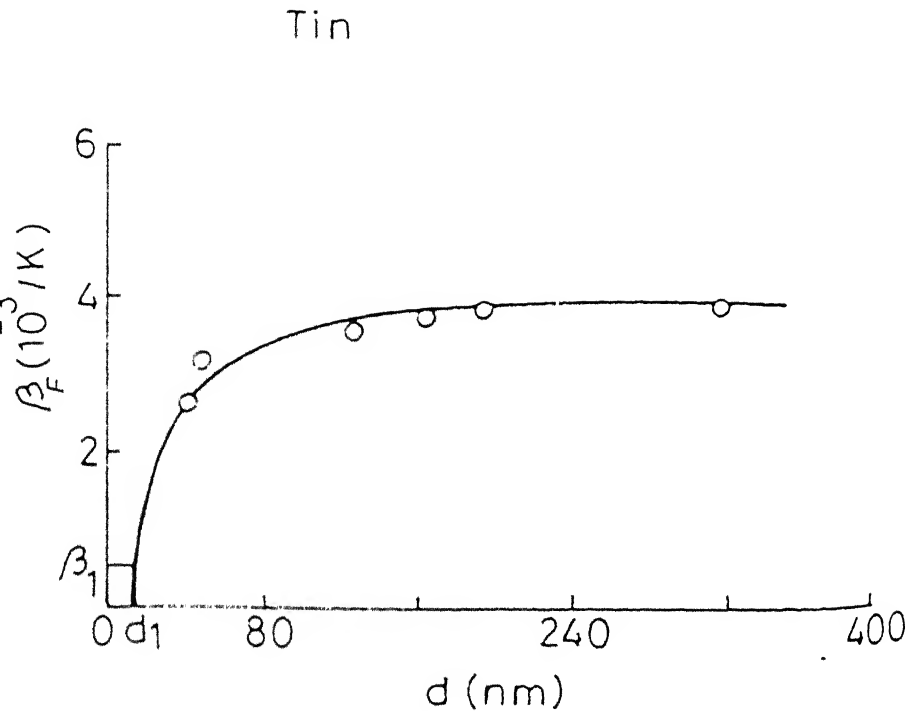

Fig. 3.8 PLOT OF TCR β_F vs. THICKNESS d FOR TIN FILMS.

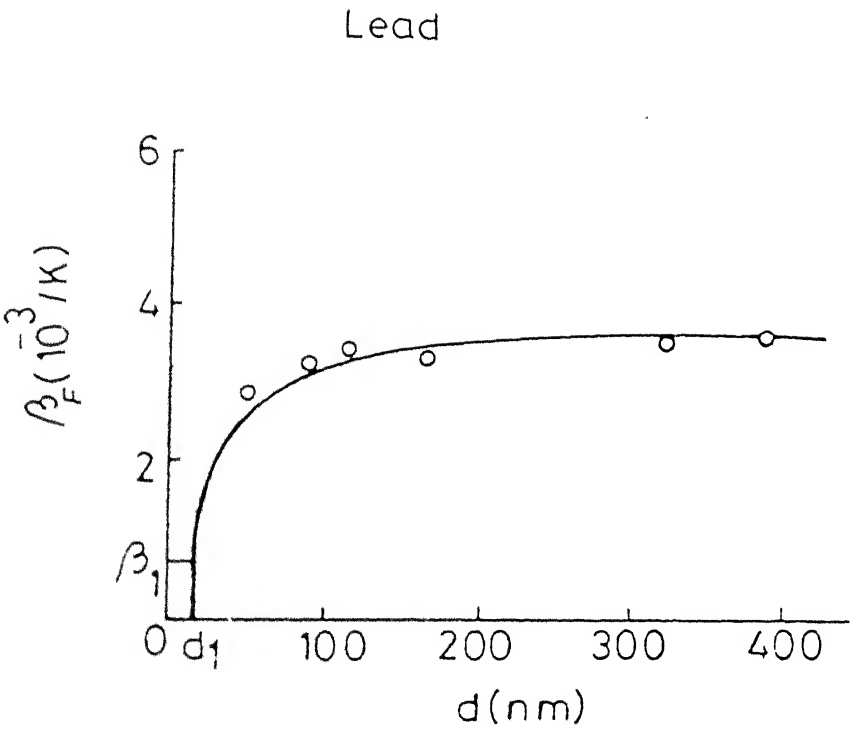

Fig. 3.9 PLOT OF TCR β_F vs. THICKNESS d FOR LEAD FILMS.

where ρ_F = Electrical resistivity of film

p = Specularity parameter

μ = External surface parameter

ν = Grain boundary parameter.

Equations (3.6') and (3.15') defines ν and μ respectively without any restriction on t and p values, while for relatively high values of t and p, the definitions of ν (equation 3.6) and μ (equation 3.15) are also valid.[11]

To analyse the data on the temperature coefficient of resistivity (TCR) in terms of the size effect theories, following assumptions have been made

(i) the rigid band model of metals is valid,

(ii) the number of conduction electrons per unit volume is temperature independent,

(iii) the thermal expansions of the grains and film's dimensions are negligible in comparison to that of mean free path.

In the framework of the three dimensional model, Pichard et al.[22] studied the TCR of polycrystalline film. From equation (3.4) they derived an expression for grain boundary TCR as[22,23]

$$\frac{\beta_g}{\beta_o} = \frac{\nu}{1-C} \frac{\gamma^{-1} - 2 + 2\gamma \ln (1 + \gamma^{-1})}{\gamma - \frac{1}{2} + (1-\gamma^2) \ln (1 + \gamma^{-1})} \qquad (3.16)$$

where β_g = Grain boundary TCR of film

β_o = TCR of bulk metal.

In the case when $\nu >> 1$, this equation (3.16) becomes

$$\frac{\beta_g}{\beta_o} \simeq 1 + \frac{1}{\nu}\left[\frac{3}{8}(1-C) - C^2\right] \qquad (3.17)$$

While the total film TCR was obtained from equation (3.12) as[12,22,24-26]

$$\frac{\beta_F}{\beta_o} = \frac{1}{b} \; \frac{a^{-1} - 2 + 2a\,\ell n\,(1 + a^{-1})}{a - \frac{1}{2} + (1-a^2)\,\ell n\,(1 + a^{-1})} \qquad (3.18)$$

where β_F = TCR of metal film.

It has been observed that single layer model is not appropriate, therefore, to explain the experimental results on TCR of Sn and Pb films at room temperature, the idea of two layer model proposed by Tellier and Tosser[7,27] have been used. In this model the films consist of two layers; the bottom layer has a constant thickness d_1 known as the first critical thickness and second layer is homogeneous and polycrystalline. Since the total conductivity is the sum of the reciprocal resistance r_1' and r_2', the TCR of second layer can be written as[28]

$$\beta_2 = \beta_F + (\beta_F - \beta_1)\,\frac{r_2'}{r_1'} \qquad (3.19)$$

where β_1 = TCR of first layer of thickness d_1

β_2 = TCR of second layer of thickness d_2

r_1' = Resistance of first layer

r_2' = Resistance of second layer.

The critical thickness d_1 has been extrapolated from the experimental data on the TCR of Sn and Pb films as d_1 = 12.0 nm for Sn (Fig. 3.8) and d_1 = 17 nm for Pb (Fig. 3.9). From Figs. 3.8 and 3.9 the value of TCR of critical thickness d_1 has been extrapolated as $\beta_1 \approx 0.5 \times 10^{-3} K^{-1}$ for Sn and $\beta_1 \simeq 0.7 \times 10^{-3}\ K^{-1}$ for Pb. For the calculation of resistance r_1', the value of ρ_1 has been deduced from the variation of $\frac{\rho_F}{\rho_o}$ with the reduced thickness K $\left[= \frac{d}{\ell_o}\right]$. At reduced thickness $K_1 = \frac{d_1}{\ell_o}$, $\frac{\rho_F}{\rho_o}$ will become $\frac{\rho_1}{\rho_o}$. From Fig. 3.10 and taking ρ_o = 12.6 $\mu\Omega$ cm, ℓ_o = 8.3 nm^1 and d_1 = 12 nm, the value of ρ_1 is found to be 25.7 $\mu\Omega$ cm for Sn films. Similarly, for lead films for which ρ_o = 24.4 $\mu\Omega$ cm. ℓ_o = 4.3 nm^1 and d_1 = 17.0 nm, Fig. 3.11 gives ρ_1 = 55.0 $\mu\Omega$ cm. Knowing ρ_1, the resistance of Ist layer r_1' can be calculated by the relation $r = \frac{\rho L}{d\ell}$ (L and ℓ are the length and width of the film respectively).

The TCR of second layer β_2 has been calculated by using equation (3.19). Figures 3.12 and 3.13 show that the plot of $\frac{d_2}{\beta_2}$ against d_2 yields a straight line of slope β_g^{-1} as expected.[22] From Figs 3.12 and 3.13 we obtained $\beta_g \approx$ 4.07 x $10^{-3}K^{-1}$ for Sn films and $\beta_g \approx 3.75 \times 10^{-3}K^{-1}$ for Pb films. With the known value of β_g, the value of ν can be

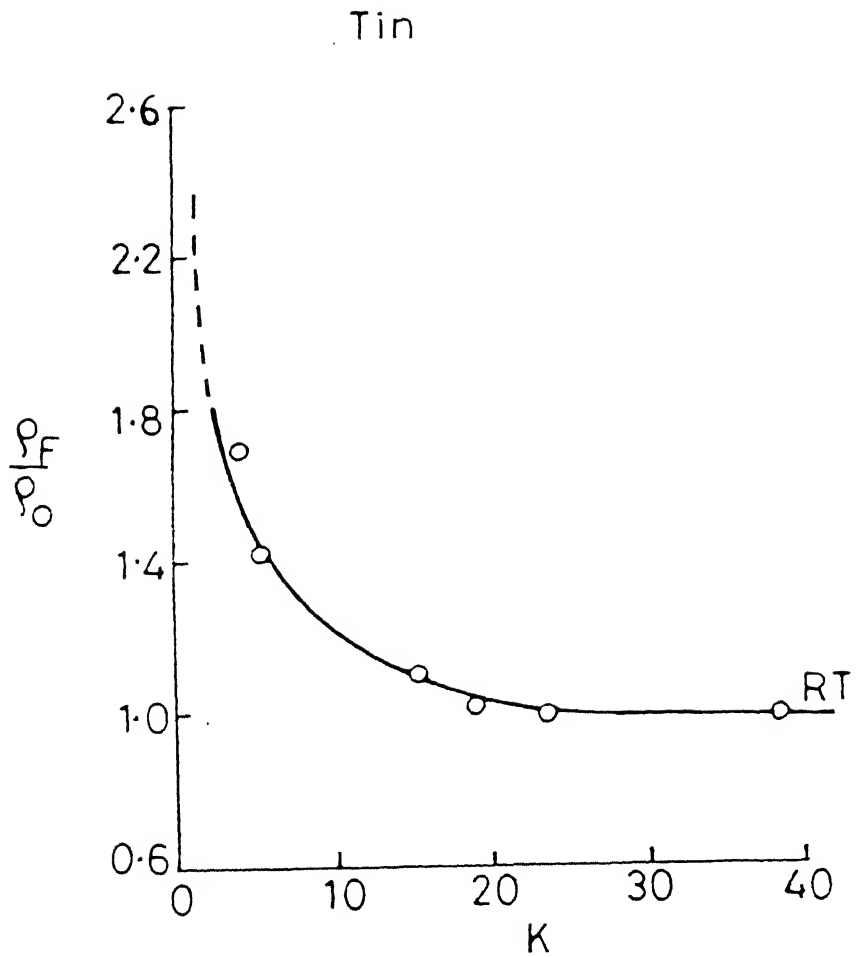

Fig. 3.10 VARIATION OF $\frac{\rho_F}{\rho_o}$ WITH REDUCED THICKNESS K FOR TIN FILMS.

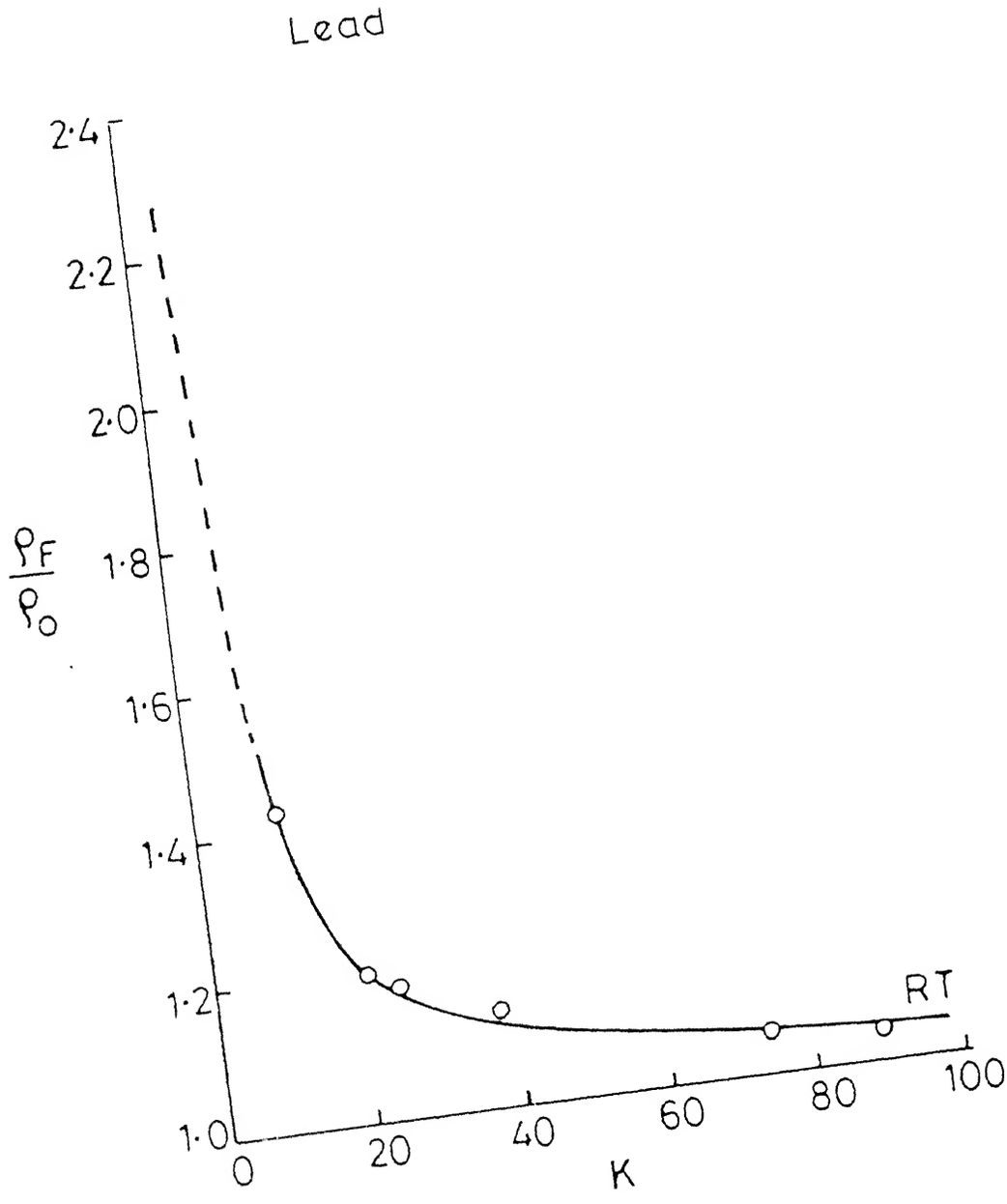

Fig. 3.11 VARIATION OF $\frac{\rho_F}{\rho_o}$ WITH REDUCED THICKNESS K FOR LEAD FILMS.

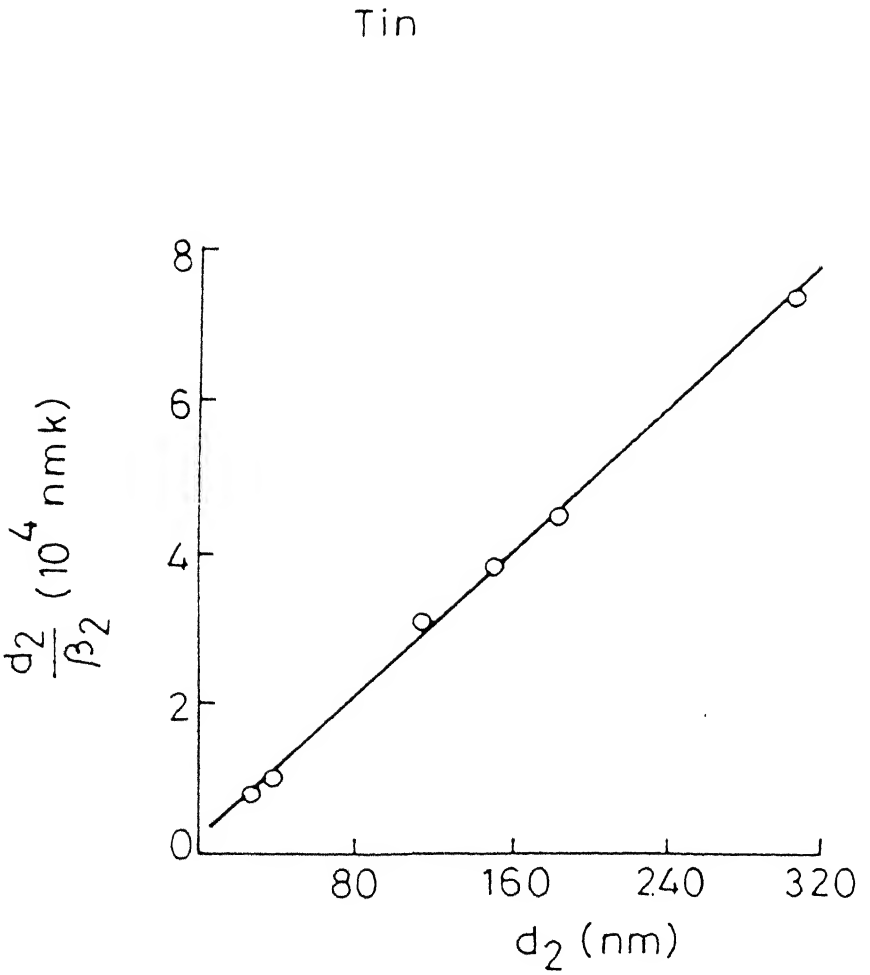

Fig. 3.12 PLOT OF $\frac{d_2}{\beta_2}$ vs. THICKNESS d_2 OF SECOND LAYER FOR TIN FILMS.

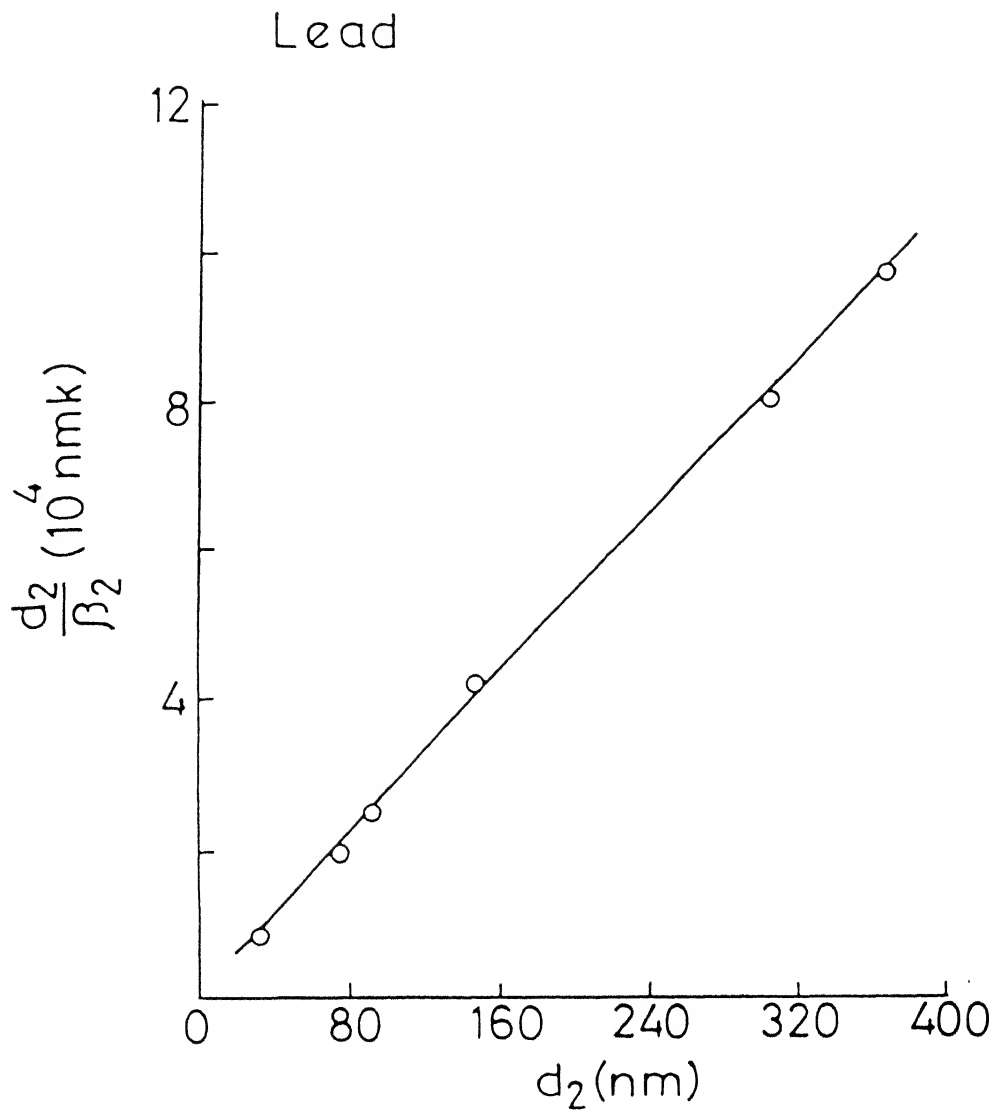

Fig. 3.13 PLOT OF $\frac{d_2}{\beta_2}$ vs. THICKNESS d_2 OF SECOND LAYER FOR LEAD FILMS.

determined by using equation (3.16). Taking β_o = 4.35 x $10^{-3}K^{-1}$ for Sn films[29] and β_o = 4.3 x $10^{-3}K^{-1}$ for Pb films[29] we obtained ν = 24.0 for Sn and ν = 11.0 for Pb films at 300K.

The values of ν and β_g obtained from the experimental results and the usual bulk mean free path have been used to determine the theoretical variation of β_2 with thickness d_2 given by equation (3.18) for the different values of specularity parameter p. The parameter b, a, and μ are determined from equations (3.13), (3.14) and (3.15'). The theoretical thickness dependence of TCR from equation (3.18) and the experimental results are shown in Figs. 3.14 and 3.15. One can see that there is a good agreement between the experimental data and the theoretical variations. The best fit is found for p = 0.2 in case of Sn and Pb films both. The low values of the specularity parameter p are expected because the films were not thoroughly annealed.

As no marked discrepancies are observed in the value of p and the experimental results are consistent with the theoretical predictions,[30] therefore, thickness dependence of TCR is well understood. Thus it can be assumed that TCR model[22] of Pichard et al. give a suitable description of the TCR of polycrystalline Sn and Pb metal films.

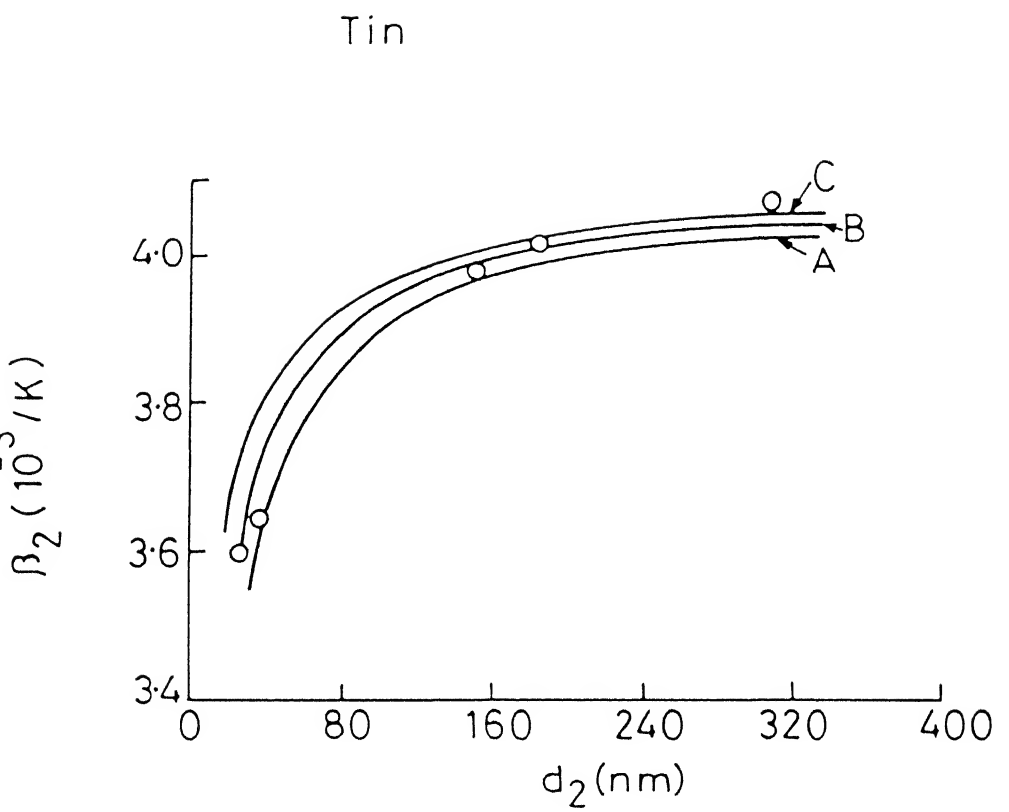

Fig.3.14 Thickness dependence of TCR β_2 of tin films. o-experimental points and —— theoretical curve from equation (3.18) for ν = 24.0, curves: (A) p = 0.1; (B) p = 0.2; (C) p = 0.3.

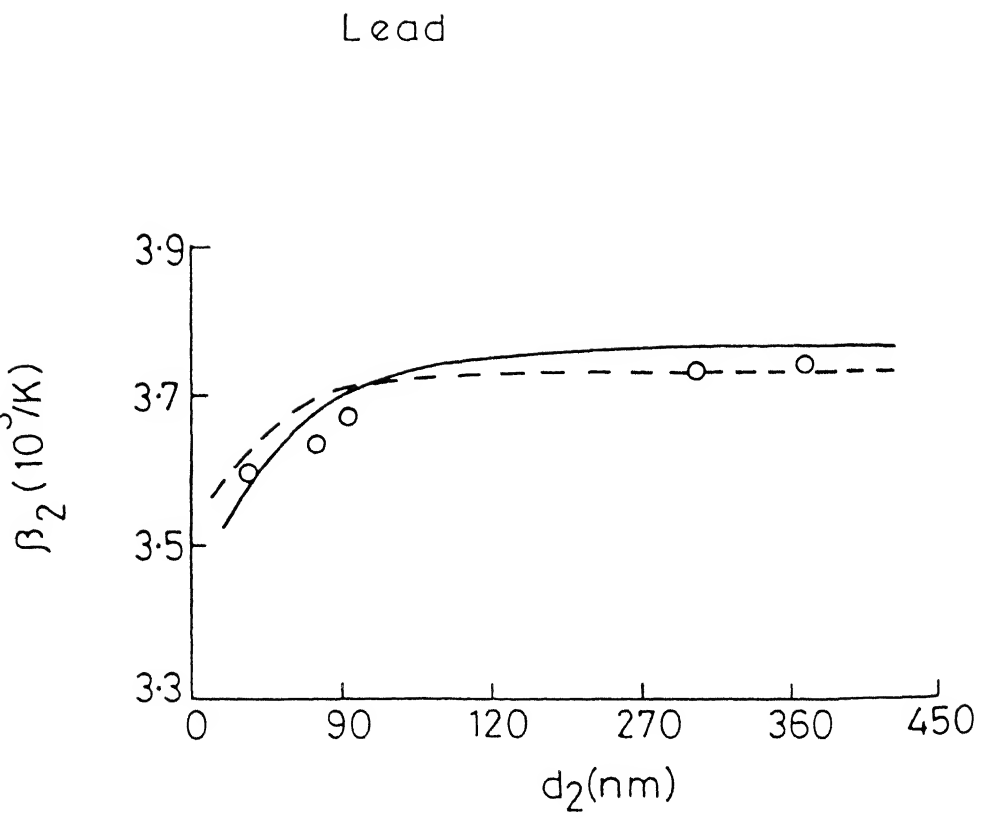

Fig.3.15 Thickness dependence of TCR β_2 of lead films. .o-experimental points and continuous line and dashed line show the theoretical variations of equation (3.18) for p = 0.2 and p = 0.3 respectively.

REFERENCES

1. Gyanesh Chandra, Ph.D. Thesis, Indian Institute of Technology, Kanpur (1985).
2. Gyanesh Chandra and O.P. Katyal, Phys. Status Solidi(a) 86, 765 (1984).
3. Gyanesh Chandra and O.P. Katyal, Phys. Status Solidi(a) 86, 759 (1984).
4. A.F. Mayadas and M. Shatzkes, Phys. Rev. B1, 1382 (1970).
5. P. Wissmann, Thin Solid Films 5, 329 (1970).
6. J.M. Jiman, Electrons and Phonons (Oxford Univ. Press, London 1962) p285.
7. C.R. Tellier and A.J. Tosser, Size Effect in Thin Films (Elsevier, Amsterdam, New York, 1982) Chapt. 1.
8. C.R. Pichard, C.R. Tellier, and A.J. Tosser, J. Phys. D 12, L101 (1979).
9. C.R. Pichard, C.R. Tellier, and A.J. Tosser, Thin Solid Films 62, 189 (1979).
10. C.R. Tellier, C.R. Pichard, and A.J. Tosser, Thin Solid Films 61, 349 (1979).
11. M. Bedda, S. Messaadi, C.R. Pichard, and A.J. Tosser, J Mater. Sci 21, 2643 (1986).
12. M. Bedda, C.R. Pichard, and A.J. Tosser, J. Mater Sci 21, 1405 (1986).
13. C.R. Pichard, C.R. Tellier, and A.J. Tosser, Phys. Status Solidi(b) 99, 353 (1980).

14. G. Pascoe, J. Phys. E9, 1121 (1976).

15. L.S. Platnik, G.V. Fedorov, and P.B. Bogatov, Fiz. Metallov i Metallovedenie 21, 89 (1966).

16. C.K. Ghosh and A.K. Pal, Ind. J. Phys. 55A, 193 (1981).

17. G. Wedler and P. Wissmann, Ber. Bunsenges Phys. Chem. 74, 934 (1970).

18. F. Thieme and W. Kirstein, Thin Solid Films 30, 371 (1975).

19. E. Dobierzewska-Mozrzymas, and F. Warkusz, Thin Solid Films 43, 267 (1977).

20. Ajay Kumar, Gyanesh Chandra, and O.P. Katyal, Phys. Status Solidi(a) 100, 169 (1987).

21. C.R. Pichard, C.R. Tellier, and A.J. Tosser, J. Mater. Sci. 15, 2236 (1980).

22. C.R. Pichard, C.R. Tellier, and A.J. Tosser, Phys. Status Solidi(a) 65, 327 (1981).

23. C.R. Pichard, C.R. Tellier, and A.J. Tosser, J. Phys. F10, L101 (1980).

24. C.R. Pichard, Yu.F. Komnik, B.I. Belevtsev, and A.J. Tosser, J. Mater. Sci. Lett. 2, 360 (1983).

25. C.R. Pichard, V.I. Vatamanyuk, A. Khalid-Naciri, C.R. Tellier, and A.J. Tosser J. Mater. Sci. Lett. 3, 447 (1984).

26. V.I. Vatamanyuk, A.J. Tosser, C.R. Pichard, and C.R. Tellier, J. Mater. Sci. 19, 4138 (1984).

27. C. Tellier and A. Tosser, Thin Solid Films 37, 207 (1976).

28. C.R. Tellier and A.J. Tosser, Thin Solid Films 43, 261 (1977).

29. Robert B. Ross, Metallic Materials Specification Handbook (Spon, London, 1960) p254.

30. Ajay Kumar, Gyanesh Chandra, and O.P. Katyal, J. Mater. Sci. 23, 2361 (1988).

CHAPTER IV

RESULTS AND DISCUSSION ON STRUCTURAL AND ELECTRICAL PROPERTIES OF ANTIMONY AND BISMUTH FILMS

4.1 *Results on Antimony Films*

The sample dimensions of antimony films have been given in Table 4.1. The rate of evaporation was approximately 1nm/sec. The structure of the film was studied with a scanning electron microscope and a X-ray diffractometer. Figures 4.1 and 4.2 show that films are polycrystalline in nature. We see from Fig. 4.2 and Table 4.2 that diffraction peaks correspond to (0003) , $(11\bar{2}1)$, (0006), and (0009) planes. These films are strongly textured as evidenced by strong (0003), (0006), and (0009) reflections. The variation of average grain size with the film thickness has been shown in Fig. 4.3. The grain size was measured from the micrographs and X-ray diffraction method. These two methods give approximately the same results. The average grain size is found to increase with the thickness. The average grain size varies from 47.5 nm to 234.2 nm for the corresponding change of thickness from 41.1 nm to 335.5 nm.

Figure 4.4 shows the temperature dependence of restivity for the antimony films of different thicknesses. The resistivity of the film increases linearly with the

temperature in the temperature range 150 to 350 K for all thicknesses. Thus, the temperature coefficient of resistivity (TCR) is positive and, therefore, antimony films exhibit metallic behaviour. The film resistivity increases with the decreasing thickness and thus exhibits the size effect (Fig. 4.5). At 300 K, the electrical resistivity of antimony films is nearly constant for thicker films (d > 225 nm) but for thinner films it increases considerably with the decrease of thickness. At different temperatures (150, 225,and 300 K) the resistivity versus thickness curves follow different paths. The TCR of the film is also observed to vary with thickness. The film TCR increases with increasing film thickness and approaches to the bulk values at higher thickness. The TCR of Sb

Table 4.1 Sample dimensions of Sb films

Sample	Thickness (nm)	Width (cm)	Length (cm)	Evaporation rate (nm/sec)	Substrates temp.
Sb 1	41.1	0.442	0.902	1.0	350 K
Sb 2	55.2	0.576	0.880	1.0	350 K
Sb 3	61.0	0.548	0.883	1.0	350 K
Sb 4	79.4	0.619	0.882	1.0	350 K
Sb 5	103.0	0.610	0.880	1.0	350 K
Sb 6	167.5	0.625	0.883	1.0	350 K
Sb 7	239.0	0.654	0.870	1.0	350 K
Sb 8	335.5	0.627	0.873	1.0	350 K

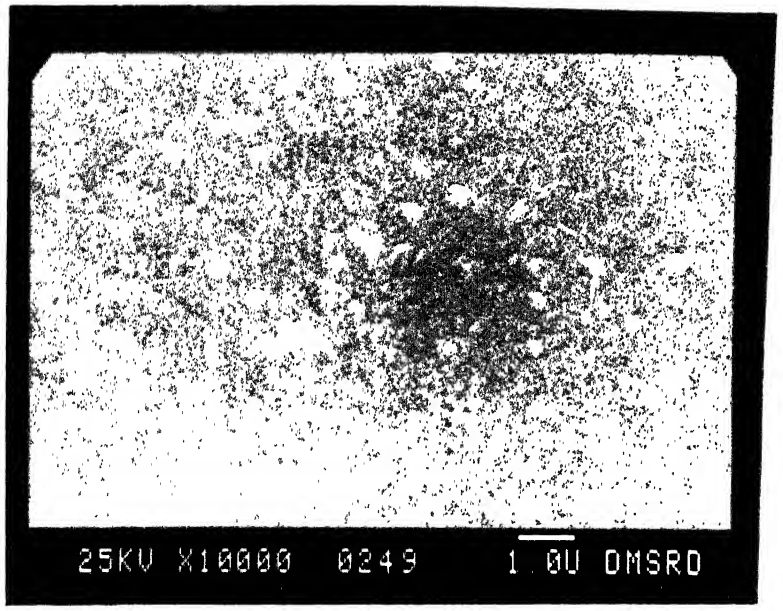

Fig. 4.1 SCANNING ELECTRON MICROGRAPH OF ANTIMONY FILM OF THICKNESS 335.5 nm (magnification 10000X).

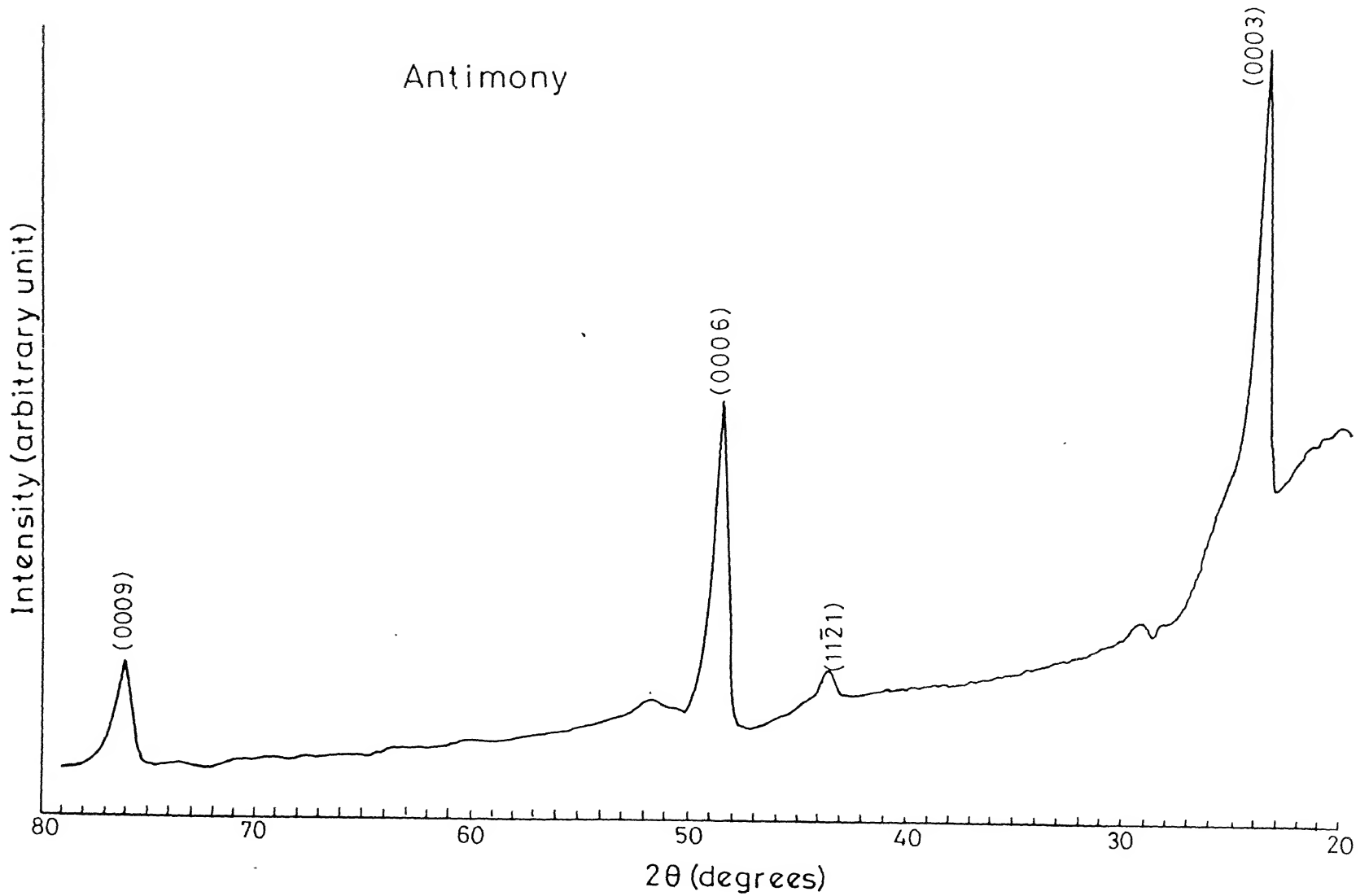

Fig. 4.2 X-RAY DIFFRACTOGRAM OF ANTIMONY FILMS OF THICKNESS 335.5 nm.

Table 4.2 X-ray diffraction study of antimony films

Sample thick-ness (nm)	Interplanar spacing (nm)	(h k i l) plane	Relative intensity	Grain size (nm)
41.1	0.3767	0003	87	47.5
	0.1880	0006	100	
55.2	0.3767	0003	88	59.8
	0.1878	0006	100	
	0.1253	0009	13	
61.0	0.3761	0003	89	64.4
	0.1877	0006	100	
	0.1253	0009	14	
79.4	0.3751	0003	85	76.5
	0.1877	0006	100	
	0.1253	0009	21	
239.0	0.3772	0003	82	169.0
	0.2084	$11\bar{2}1$	6	
	0.1876	0006	100	
	0.1251	0009	54	
335.5	0.3772	0003	79	
	0.2080	$11\bar{2}1$	5	
	0.1877	0006	100	
	0.1251	0009	25	

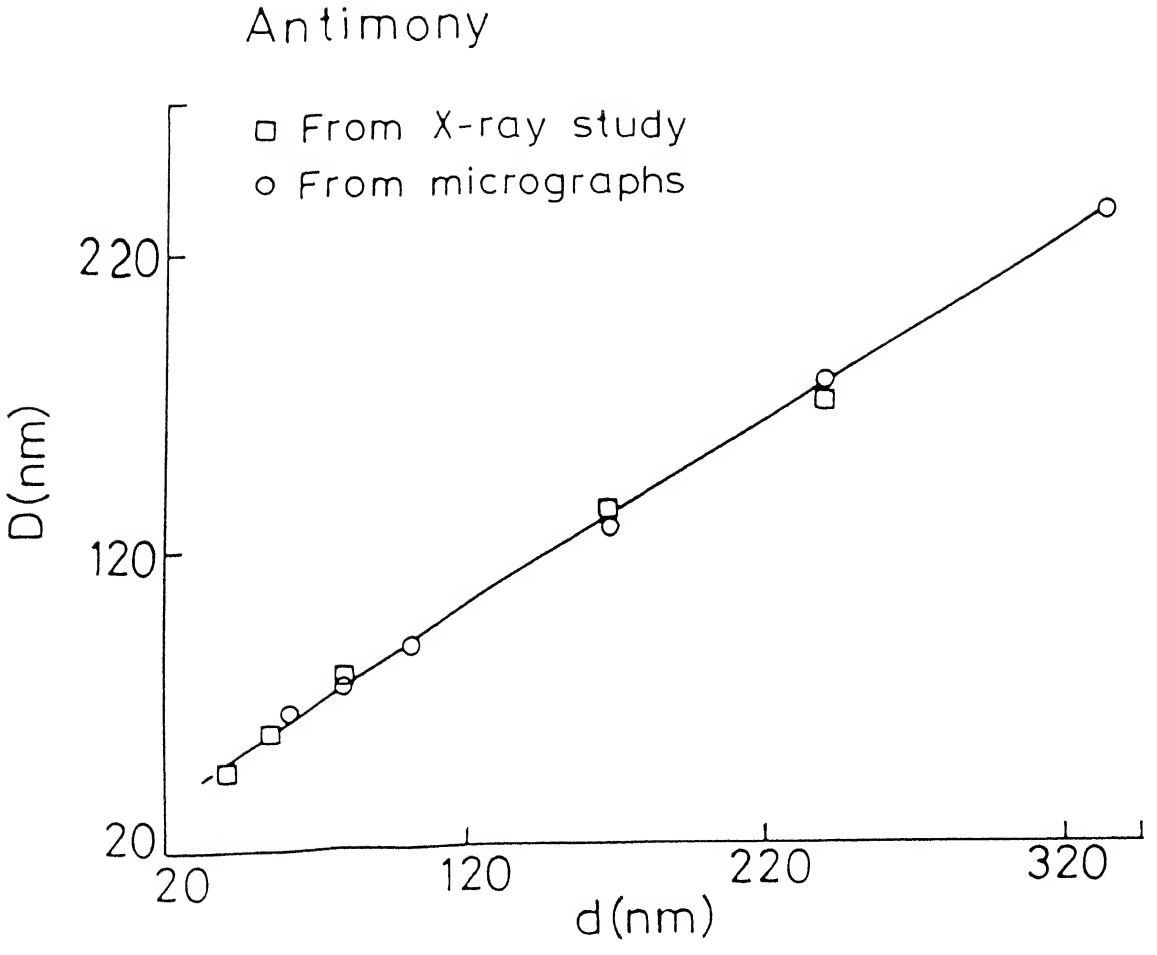

Fig. 4.3 VARIATION OF AVERAGE GRAIN SIZE D WITH THICKNESS d OF ANTIMONY FILMS.

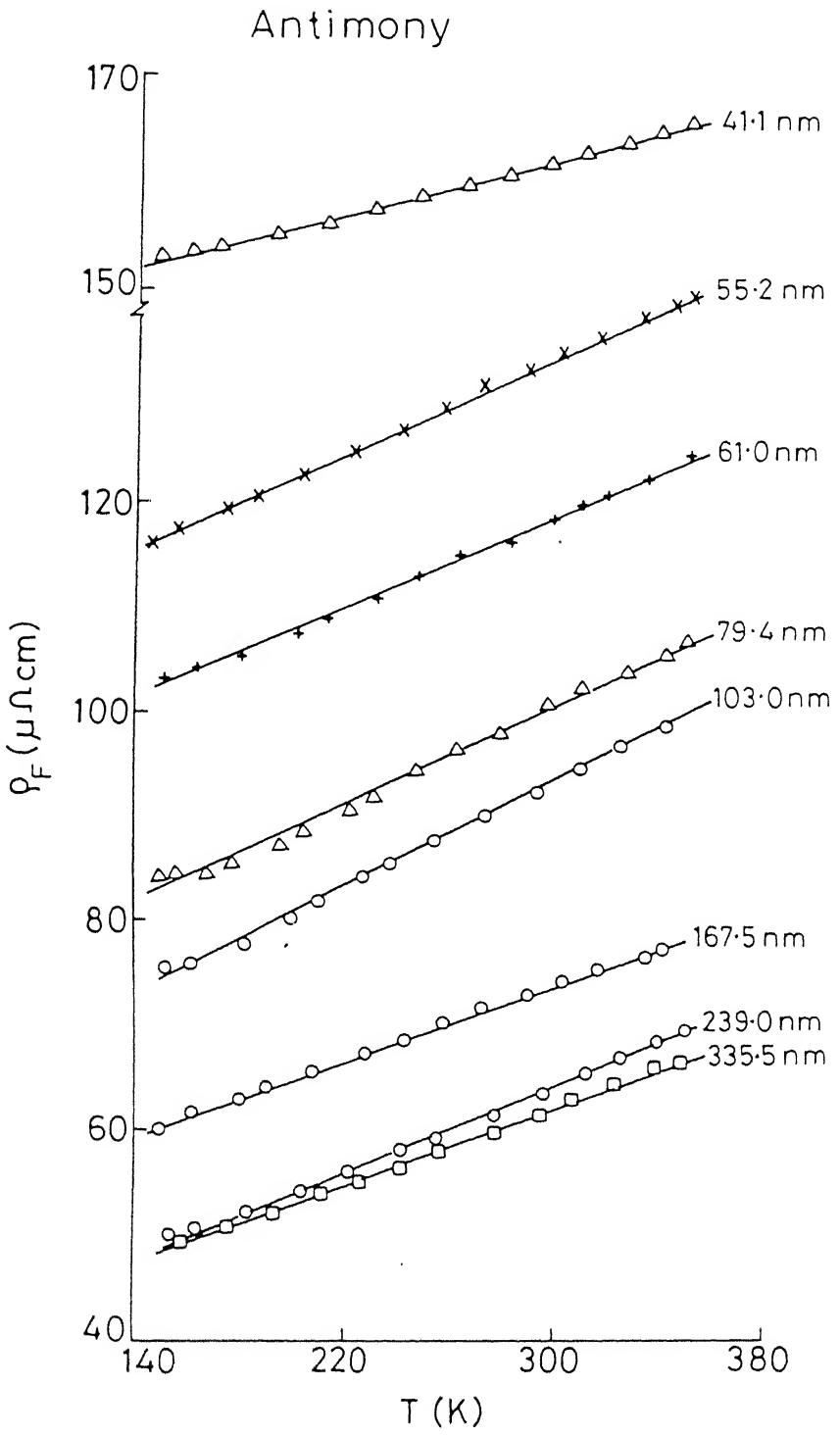

Fig. 4.4 TEMPERATURE DEPENDENCE OF RESISTIVITY ρ_F OF ANTIMONY FILMS.

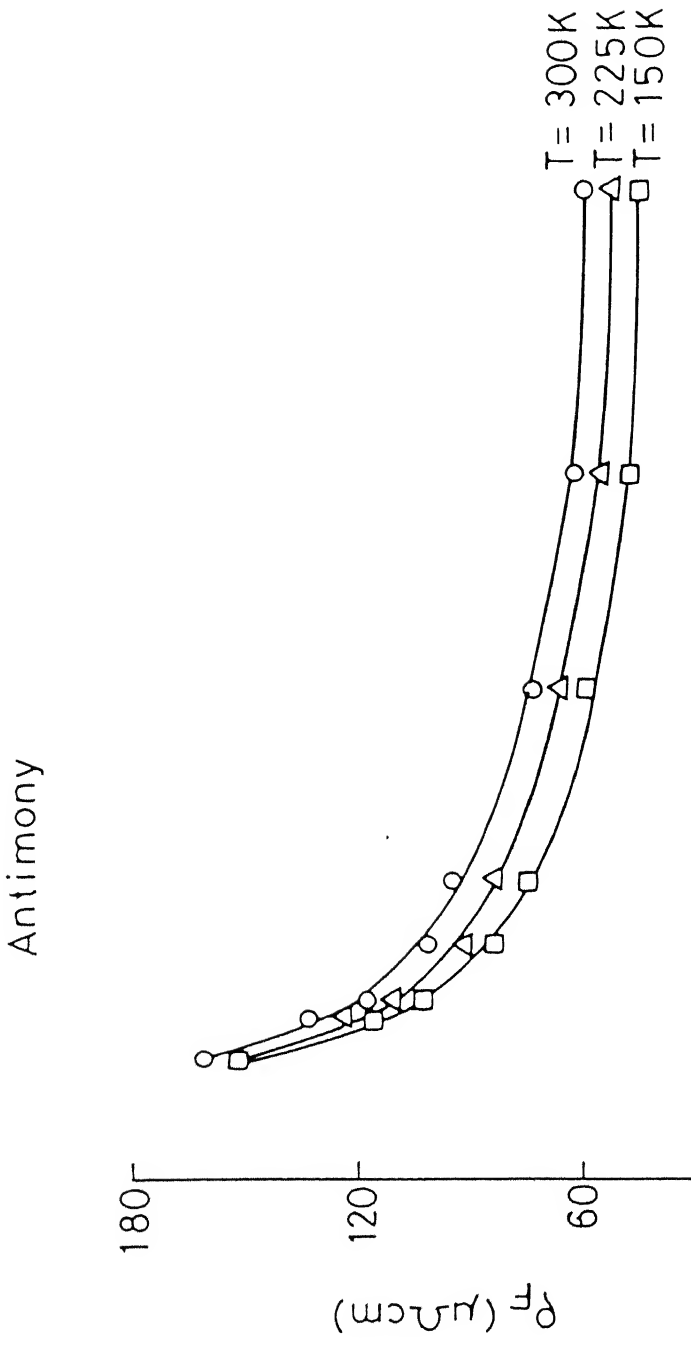

Fig. 4.5 THICKNESS DEPENDENCE OF RESISTIVITY ρ_F OF ANTIMONY FILMS AT 150, 225, AND 300 K.

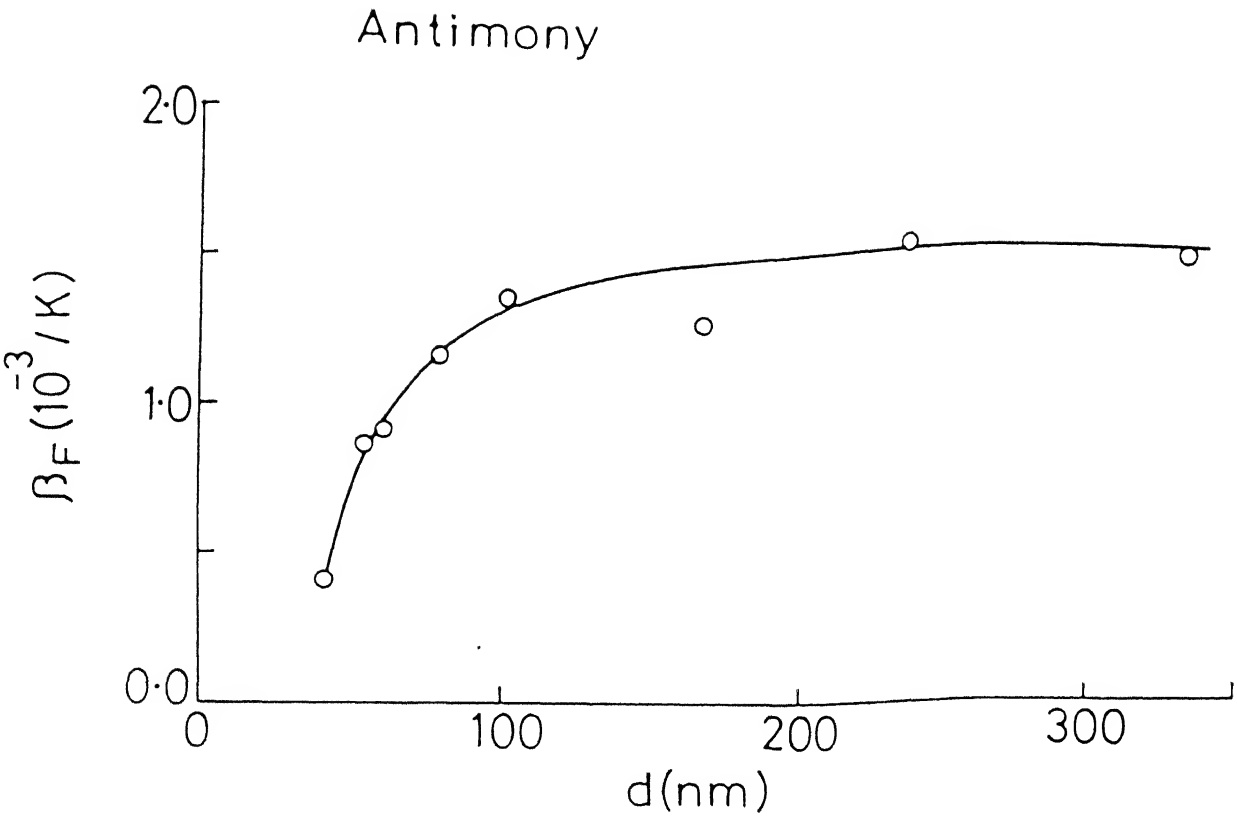

Fig. 4.6 THICKNESS DEPENDENCE OF TCR β_F OF ANTIMONY FILMS.

films changes from 0.41 x 10^{-3}/K to 1.51 x 10^{-3}/K for corresponding change of thickness from 41.1 nm to 200.0 nm. The TCR of thicker films (d > 200.0 nm) become nearly constant (Fig. 4.6).

4.2 *Results on Bismuth Films*

The sample dimensions of bismuth films are given in Table 4.3. The evaporation rate was approximately 1 nm/sec. The scanning electron micrographs (Figs. 4.7 and 4.8) show that films are made up of small grains with different orientations. From the diffraction pattern shown in Fig. 4.9 and Table 4.4 we see that diffraction peaks correspond to (0003), ($\bar{1}$012), (0006), (0$\bar{2}$22), and (0009) planes. These SEM and diffraction studies show that bismuth films are polycrystalline in nature. From the diffraction pattern it is also observed that reflections corresponding to (0003), (0006), and (0009) planes are relatively strong, therefore, the films are highly textured. From Fig. 4.10 it is found that average grain size measured from the micrograph and diffraction broadening is nearly same. The average grain size increases with the film thickness. The average grain size is found to vary from 93.1 nm to 297.2 nm for the corresponding change of thickness from 41.0 nm to 255.4 nm.

Table 4.3 Sample dimensions of Bi films

Sample	Thickness (nm)	Width (cm)	Length (cm)	Evaporation rate (nm/sec)	Substrates temp.
Bi 1	41.0	0.457	0.896	1.0	R.T.
Bi 2	45.7	0.595	0.898	1.0	R.T.
Bi 3	54.0	0.660	0.868	1.0	R.T.
Bi 4	68.7	0.614	0.883	1.0	R.T.
Bi 5	72.5	0.625	0.889	1.0	R.T.
Bi 6	89.6	0.685	0.870	1.0	R.T.
Bi 7	98.3	0.630	0.852	1.0	R.T.
Bi 8	165.4	0.570	0.884	1.0	R.T.
Bi 9	225.9	0.687	0.869	1.0	R.T.
Bi 10	255.4	0.576	0.860	1.0	R.T.

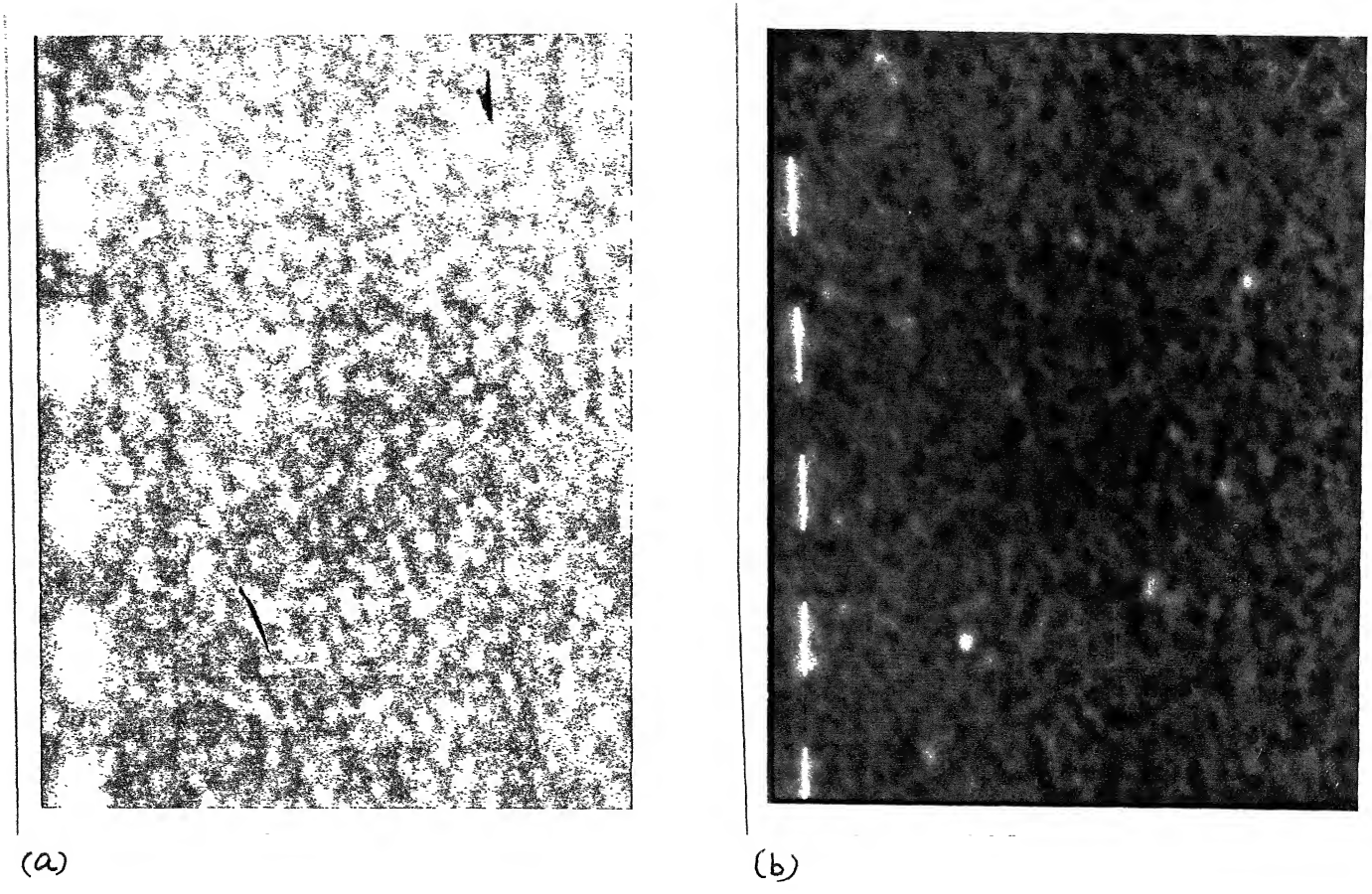

Fig. 4.7 Scanning electron micrographs of bismuth films of thicknesses (a) 45.7 nm, (b) 68.7 nm (magnification 10000X).

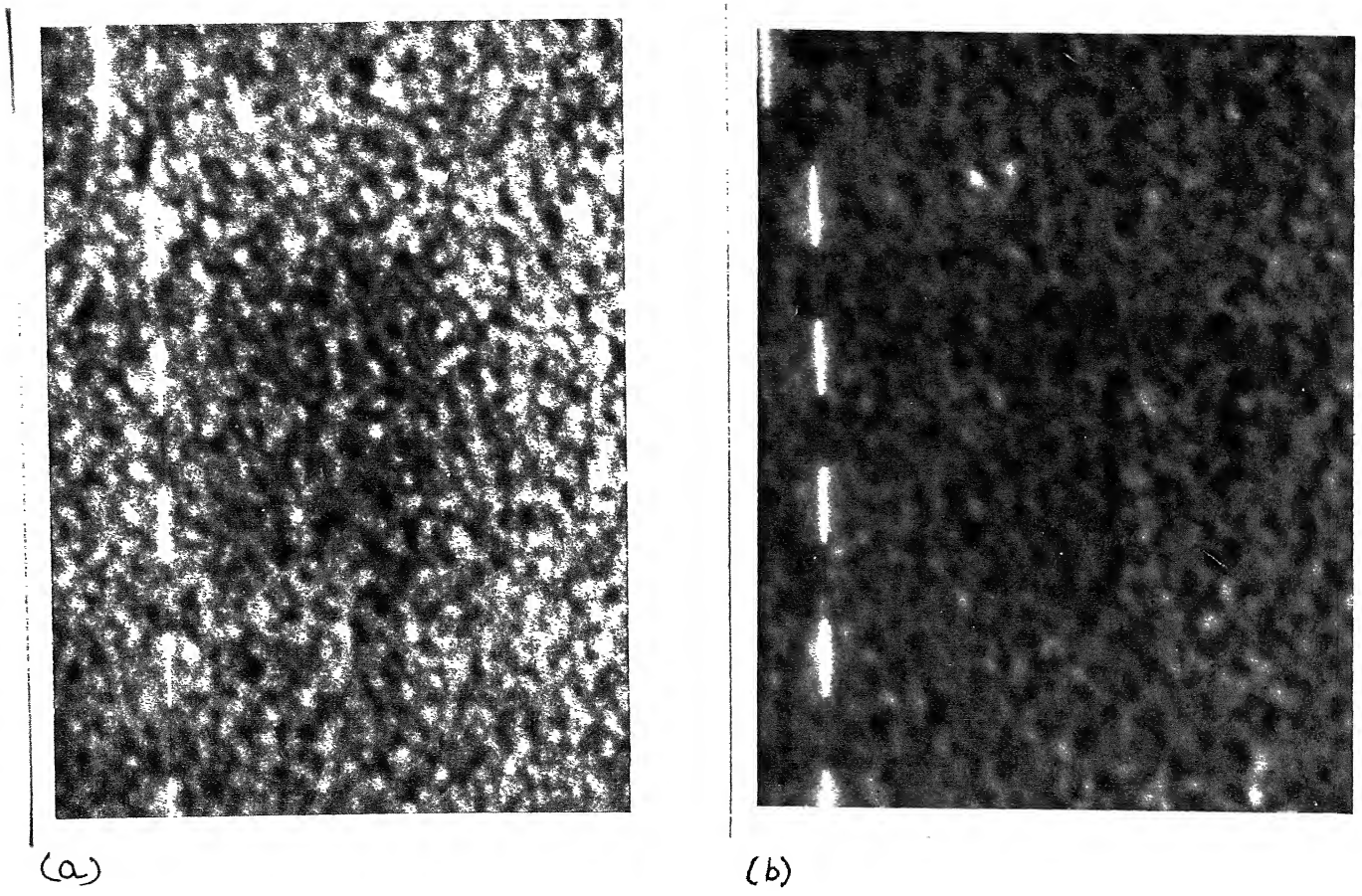

Fig. 4.8 Scanning electron micrographs of Bi films of thicknesses (a) 98.3 nm, (b) 225.9 nm (magnification 10000X).

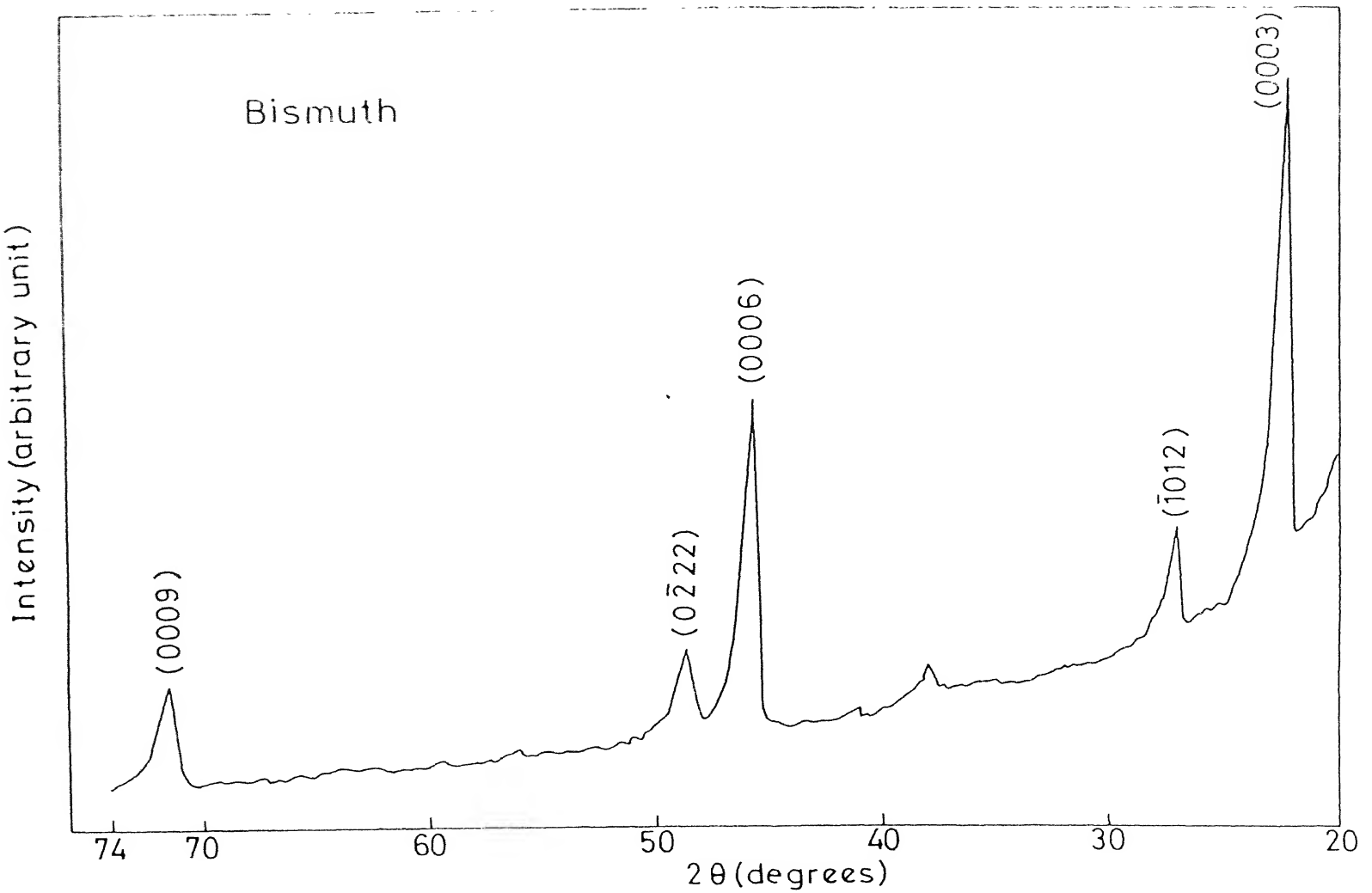

Fig. 4.9 X-RAY DIFFRACTOGRAM OF BISMUTH FILM OF THICKNESS 165.4 nm.

Table 4.4 X-ray diffraction study of bismuth films

Sample thick-ness (nm)	Interplanar spacing (nm)	(h k i l) plane	Relative intensity	Average Grain size (nm)
	0.3956	0003	53	
41.0	0.1984	0006	100	94.8
	0.1324	0009	19	
	0.3966	0003	54	
45.7	0.1981	0006	100	104.6
	0.1323	0009	21	
	0.3946	0003	49	
	0.3274	$\bar{1}012$	2	
68.7	0.1981	0006	100	129.2
	0.1321	0009	22	
	0.3962	0003	44	
	0.3267	$\bar{1}012$	1	
98.3	0.1978	0006	100	156.1
	0.1868	$0\bar{2}22$	2	
	0.1322	0009	20	
	0.3956	0003	56	
	0.3272	$\bar{1}012$	15	
165.4	0.1978	0006	100	
	0.1870	$0\bar{2}22$	14	
	0.1320	0009	21	

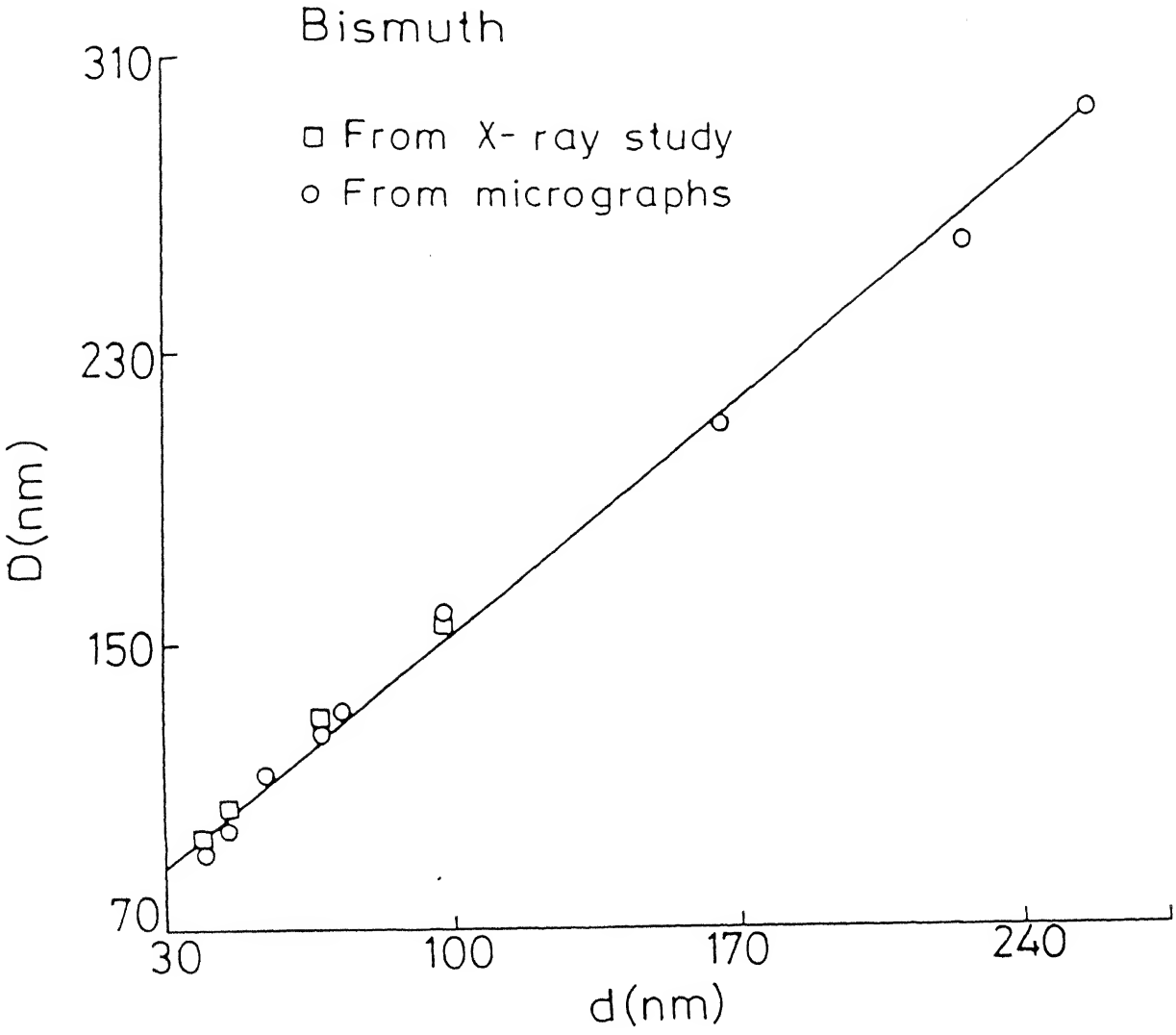

Fig. 4.10 VARIATION OF AVERAGE GRAIN SIZE D WITH THICKNESS d OF BISMUTH FILMS.

The temperature dependence of resistivity in the temperature range 150 to 350 K for few bismuth films of different thicknesses is shown in Fig. 4.11. The results on resistivity at 77 K are not included because at 77 K, the resistivity was not measured in situ. Figure 4.11 shows that with the increase in temperature, the resistivity decreases and, therefore, bismuth films exhibit negative TCR. It also appears from the curves of 98.3 nm and 225.9 nm thick films that there exists a minimum in resistivity at some temperature T_c. This minimum in restivity shifts towards higher temperature for thin samples and lies above 350 K. Figure 4.12 shows the thickness dependence of resistivity of bismuth films at temperatures 77, 150, and 300 K. The film resistivity increases with the decreasing thickness and thus exhibits the size effect. At 300 K, the resistivity is observed nearly constant above the thickness 160 nm and increases considerably with the decreasing thickness. At different temperatures the resistivity versus thickness curve follow different paths. At the low temperature, the size effects are observable even at some more higher thickness.

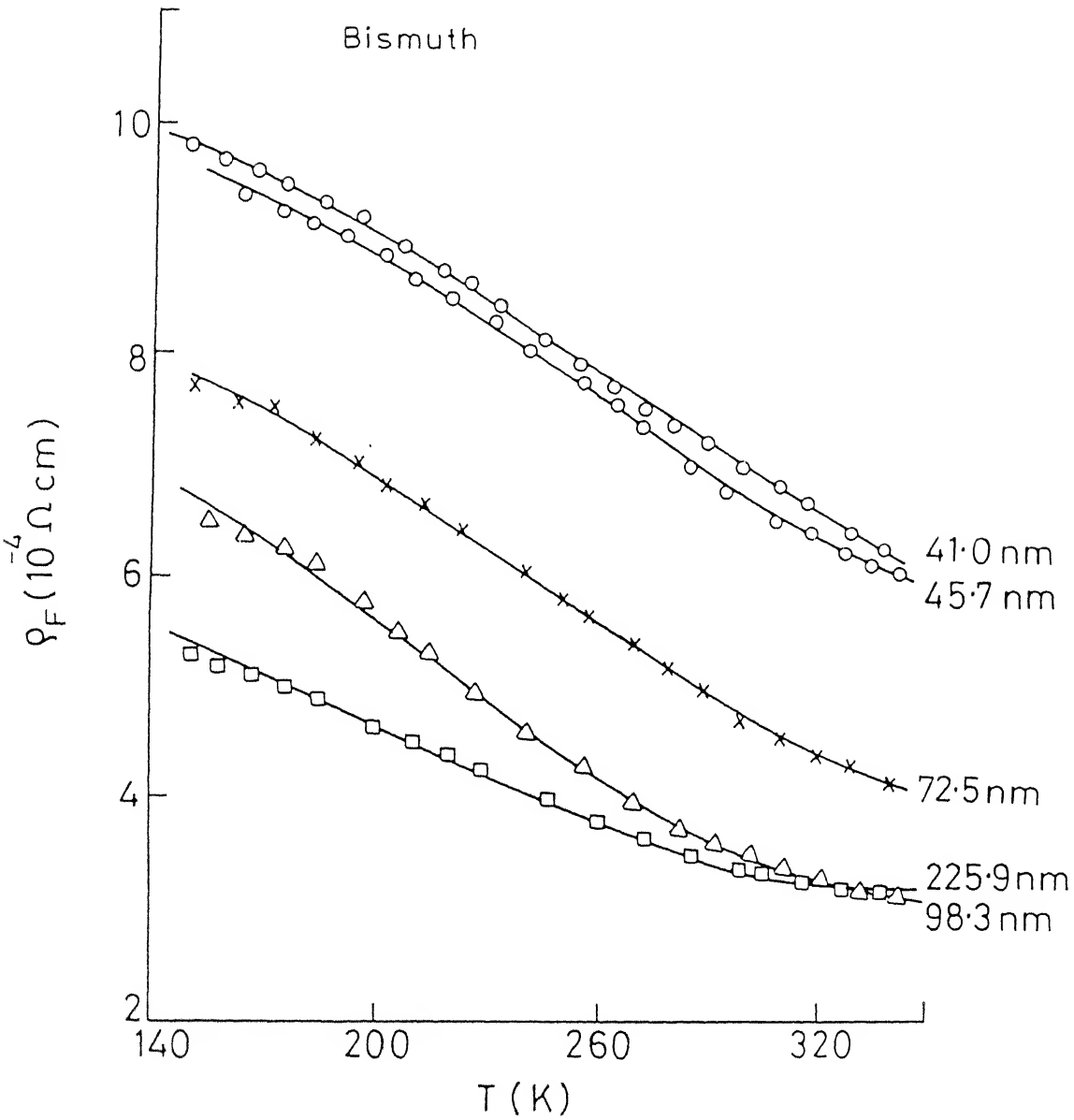

Fig. 4.11 Temperature dependence of resistivity ρ_F of bismuth films. (The results at 77K have not been shown because at 77K the resistivity was not measured in situ.)

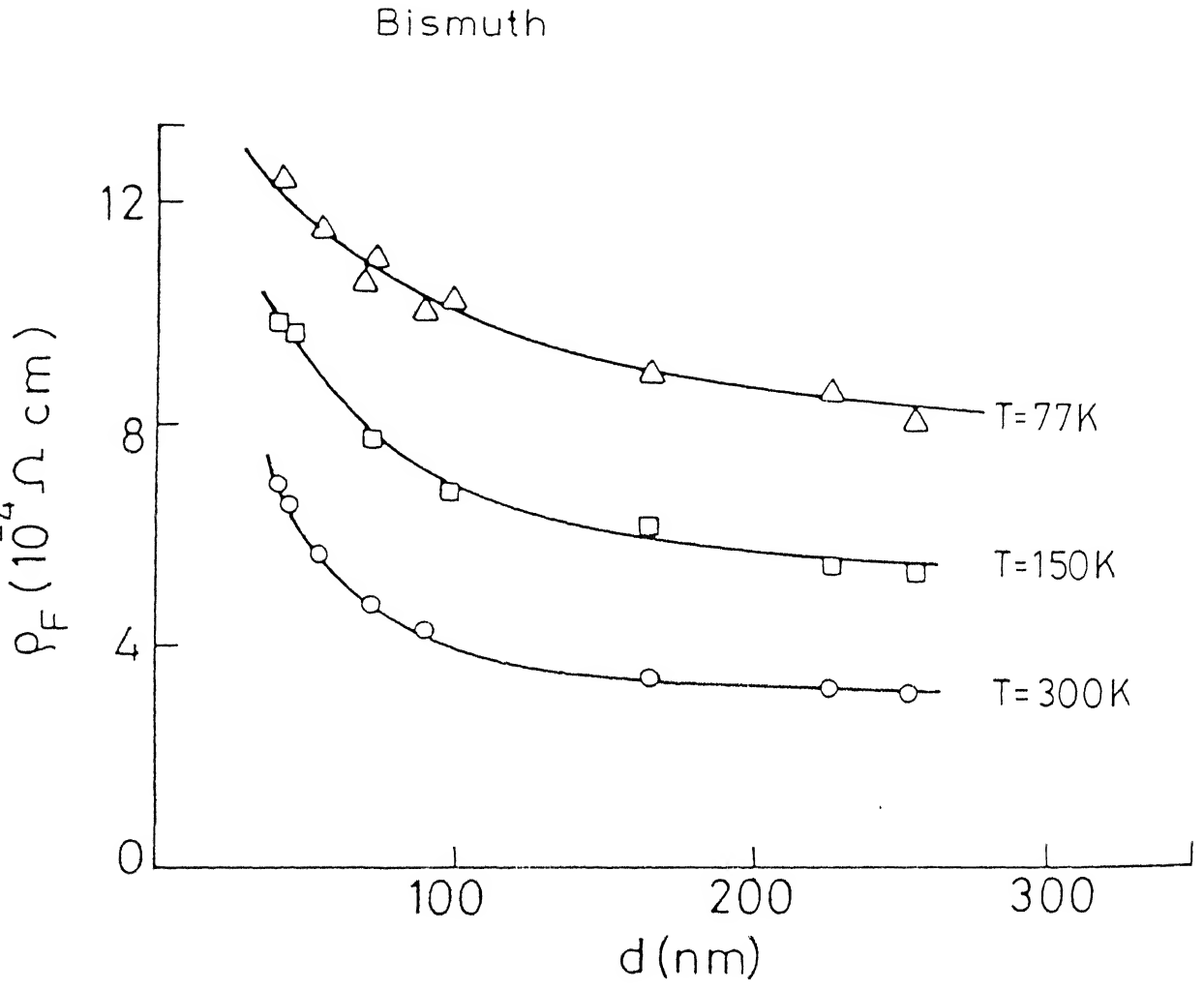

Fig. 4.12 THICKNESS DEPENDENCE OF RESISTIVITY ρ_F OF BISMUTH FILMS AT 77, 150, AND 300 K.

DISCUSSION

4.3 *Structural and Electrical Properties of Antimony Films*

The structural studies show that the antimony films are polycrystalline, highly textured and the grain size of the film increases with the thickness.The thickness dependence of resistivity is shown in Fig. 4.5. The first analysis of electrical measurements data for thin film was carried out by Fuchs[1] and Sondheimer[2] (FS model). The film resistivity in FS model is written as

$$\rho_F = \rho_o \left[1 + \frac{3}{8} \frac{\ell_o (1-p)}{d} \right] \qquad (4.1)$$

where ρ_F = Film resistivity

p = Specularity parameter

d = Film thickness

and ρ_o and ℓ_o are, respectively, the resistivity and mean free path of the bulk material having the same defect density as that of the film.

Equation (4.1) indicates a linear dependence of resistivity on $(\text{thickness})^{-1}$. The measured film resistivity at temperatures 150, 225, and 300 K is plotted as a function of $\frac{1}{(\text{thickness})}$ in Fig. 4.13. The variations are found to be linear. The bulk resistivity can be obtained from the intercept of the corresponding plot,

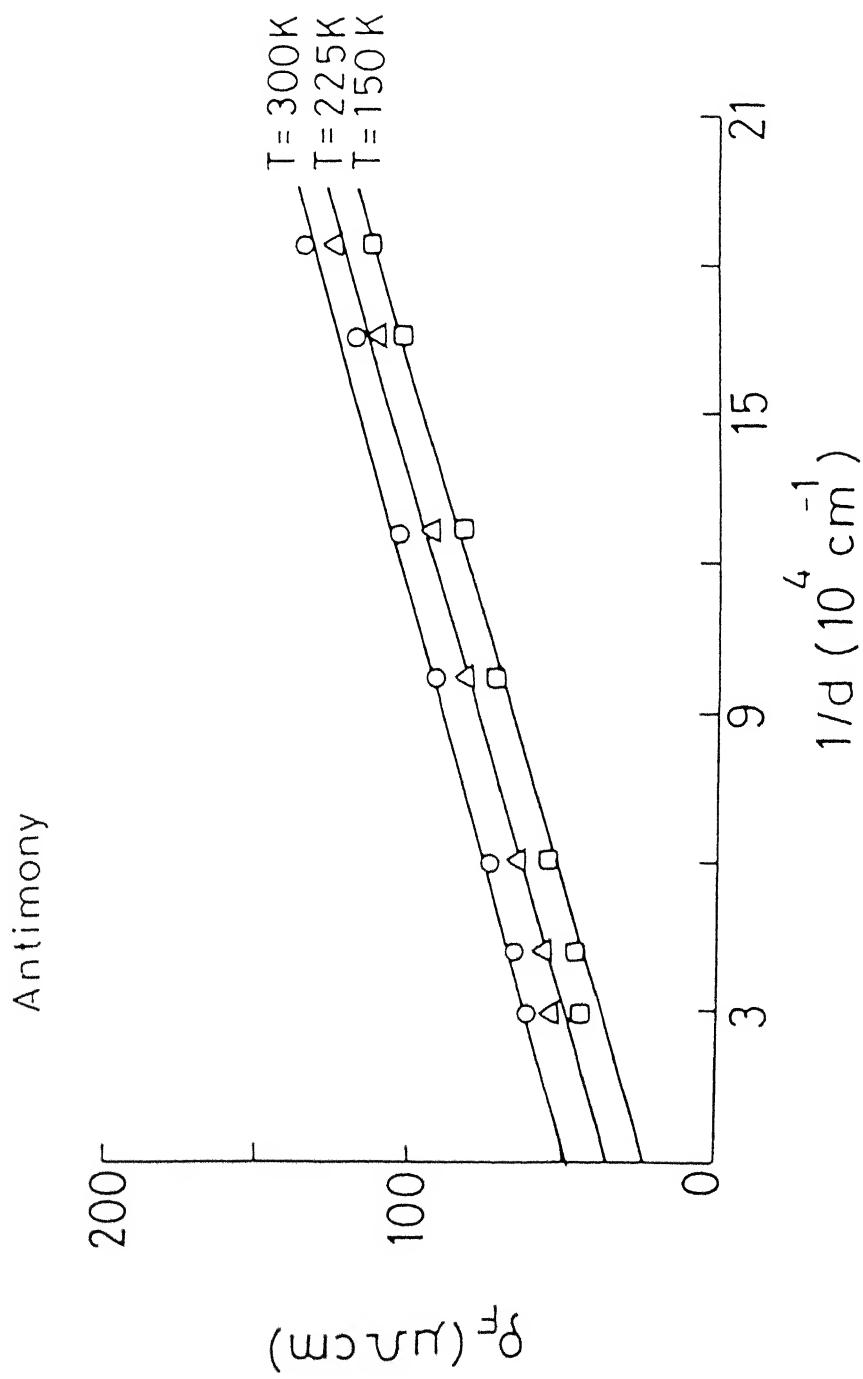

Fig. 4.13 PLOTS OF RESISTIVITY ρ_F vs. $(\text{THICKNESS})^{-1}$ OF ANTIMONY FILMS AT 150, 225, AND 300 K.

while the slope of the curve in Fig. 4.13 will give the value of $\frac{3}{8}\ \rho_o \ell_o(1-p)$. At 300 K, the value obtained for ρ_o and $\ell_o(1-p)$, in the present study of Sb films, are 49.0 $\mu\Omega$ cm and 241.8 nm respectively, whereas Pal et al.[3] obtained ρ_o = 70.0 $\mu\Omega$ cm and $\ell_o(1-p)$ = 51.0 nm, and Kotlinska et al.[4] obtained ρ_o = 55.0 $\mu\Omega$ cm and $\ell_o(1-p)$ = 300.0 nm in their study of Sb films. Thus the values of ρ_o and $\ell_o(1-p)$ obtained in the present study are close to the values obtained by Kotlinska et al.[4] . The values of ρ_o obtained here are very close to the pure bulk resistivity ρ_b and this difference $(\rho_o-\rho_b)$ remains approximately constant at the other temperatures (Table 4.5). Knowing the value of ρ_o, the bulk mean free path can be evaluated by using the relation $\rho_o \ell_o$ = constant.[5] The calculated values of ρ_o, $\ell_o(1-p)$ etc. at temperatures 150, 225, and 330 K are given in Table 4.5. For comparison the results of other researchers[3-6] are also included in Table 4.5. Bulk parameters are taken from the reference 7. In Fig. 4.13 we see that the slope of the curves remains constant which indicates that the specularity parameter p has no temperature dependence.

Fuchs model[1,2] is not appropriate to explain our experimental results on the resistivity of antimony films as it reproduces the results only in the high thickness region and deviates appreciably in the low thickness region

Table 4.5 Comparison of electrical properties of antimony films

T_S† (K)	Temp (K)	ρ_b ($\mu\Omega$cm) Bulk	ℓ_b (nm) Bulk	ρ_o ($\mu\Omega$cm)	$\ell_o(1-p)$ (nm)	p	R	T	Ref.
	150			22.00	538.6	0.49	0.176	0.820	
350	225	31.5	335.0	35.0	338.6	0.49	0.16	0.845	Present study
	300	46.0	230.0	49.0	241.8	0.48	0.135	0.877	
423	300	-	-	70.0	51.0	0	0.15		3
333-383	293	-	-	55.0	300.0	0.15	0.24		4
	300	-	-	52.0 to 63.0*	50.0 to 55.0*	0.75 to 0.68*			5
	300	-	-	45.0 to 95.0*	40.0 to 16.0*	0.83 to 0.86*			6

† T_S is the substrates temperature.

* depending on the preparation conditions.

but one can find the value of bulk resistivity by applying Fuchs model.

The effect of the grain boundaries on the film conductivity was studied by Mayadas and Shatzkes[8] and Pichard et al. (PTT).[9-11] The equation (3.2) of MS model and equation (3.4) of PTT model given in Chapter III, describe the resistivity of an infinitely thick polycrystalline film when only two types of electron scatterings (background scattering and grain boundary scattering) are operative. In the present study, estimating ρ_s, the contribution to the film resistivity due to surface by using the relation[6]

$$\rho_s = \frac{3}{8} \frac{\rho_o \ell_o (1-p)}{d} \qquad (4.2)$$

with the determined value of p and attributing the difference to the grain boundaries, we have calculated the experimental values of grain boundary resistivity ρ_g of antimony films. The ρ_g is found to increase with the decrease in grain size D. To describe this behaviour of ρ_g, MS model and PTT model have been used. The MS equation (3.2) with R = 0.135 and the PTT equation (3.4) with t = 0.86 at 300 K reproduce the experimental results on grain boundary resistivity. The experimental results on ρ_g and theoretical curves at temperatures 150, 225, and 300 K have

been shown in Fig. 4.14. We see from Fig. 4.14 that there is a good agreement between the experimental results and theoretical curves. The MS model and PTT model give almost the same results on grain boundary resistivity and the degree of agreement of the experimental results with the both theoretical curves i.e. MS and PTT, is satisfactory to the same extent.

In MS model[8], expression for the total resistivity of polycrystalline film (equation 1.16 of Chapter I) is complicated. Therefore, to explain the results on the thickness dependence of film resistivity, equation (3.12) (Chapter IIIB) of PTT model[11-15] have been used. The values of parameters ν, b, a, and μ were calculated from the equations (3.6), (3.13), (3.14), and (3.15) respectively. With t = 0.877, p = 0.48, ρ_o = 49.0 $\mu\Omega$ cm and ℓ_o = 215.0 nm, it is found that equation (3.12) reproduces the experimental results on total film resistivity at 300 K. From Fig. 4.15 one can see that there is a good agreement between the experimental results and theoretical variations of equation (3.12) of PTT model at temperatures 150, 225, and 300 K.

Hence the experimental results on the resistivity of polycrystalline antimony films[16] can be successfully explained by a simple analytic equation of three dimensional model of Pichard et al. The specularity

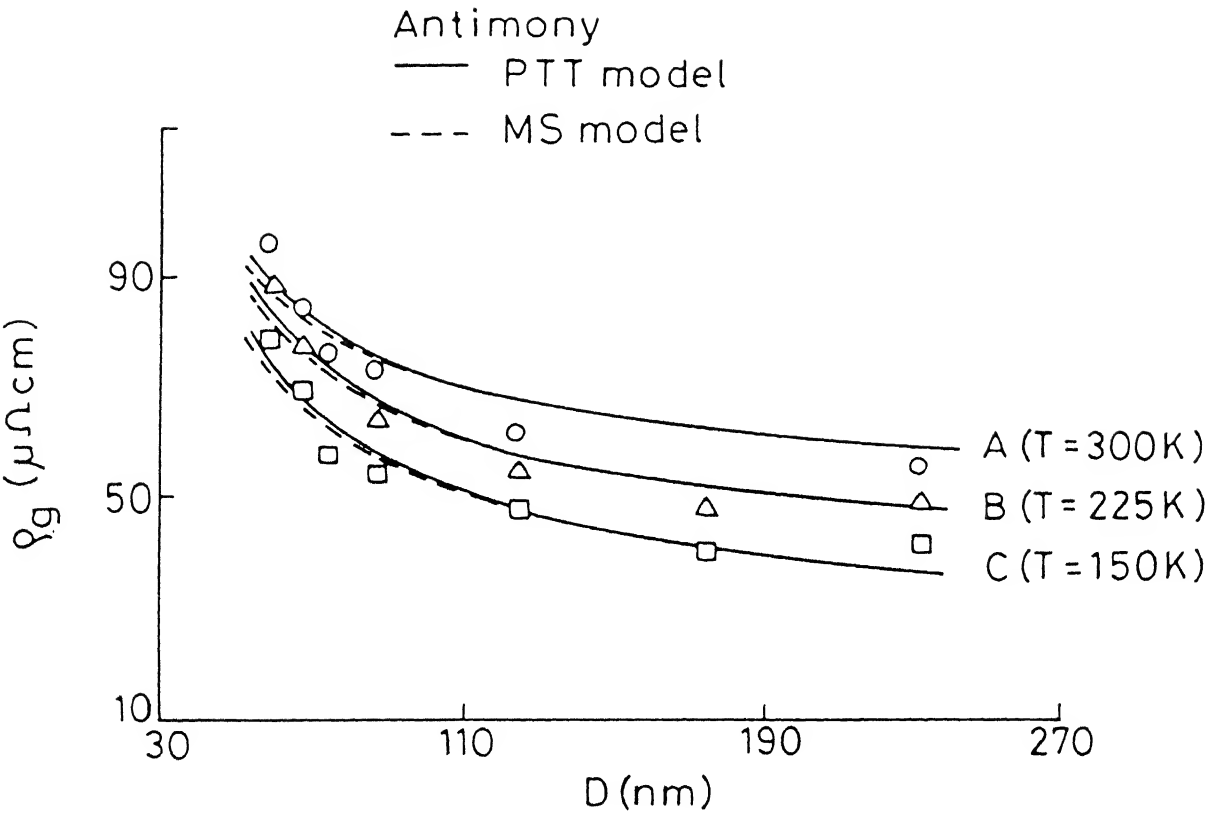

Fig. 4.14 Plots of grain boundary resistivity ρ_g vs. grain size D of antimony films. Curves: (A) o experimental points at 300K, --- MS curve for R = 0.135, —— PTT curve for t = 0.86; (B) Δ experimental points at 225 K, --- MS curve for R = 0.16, —— PTT curve for t = 0.835; (C) □ experimental points at 150 K, --- MS curve for R = 0.176, —— PTT curve for t = 0.82.

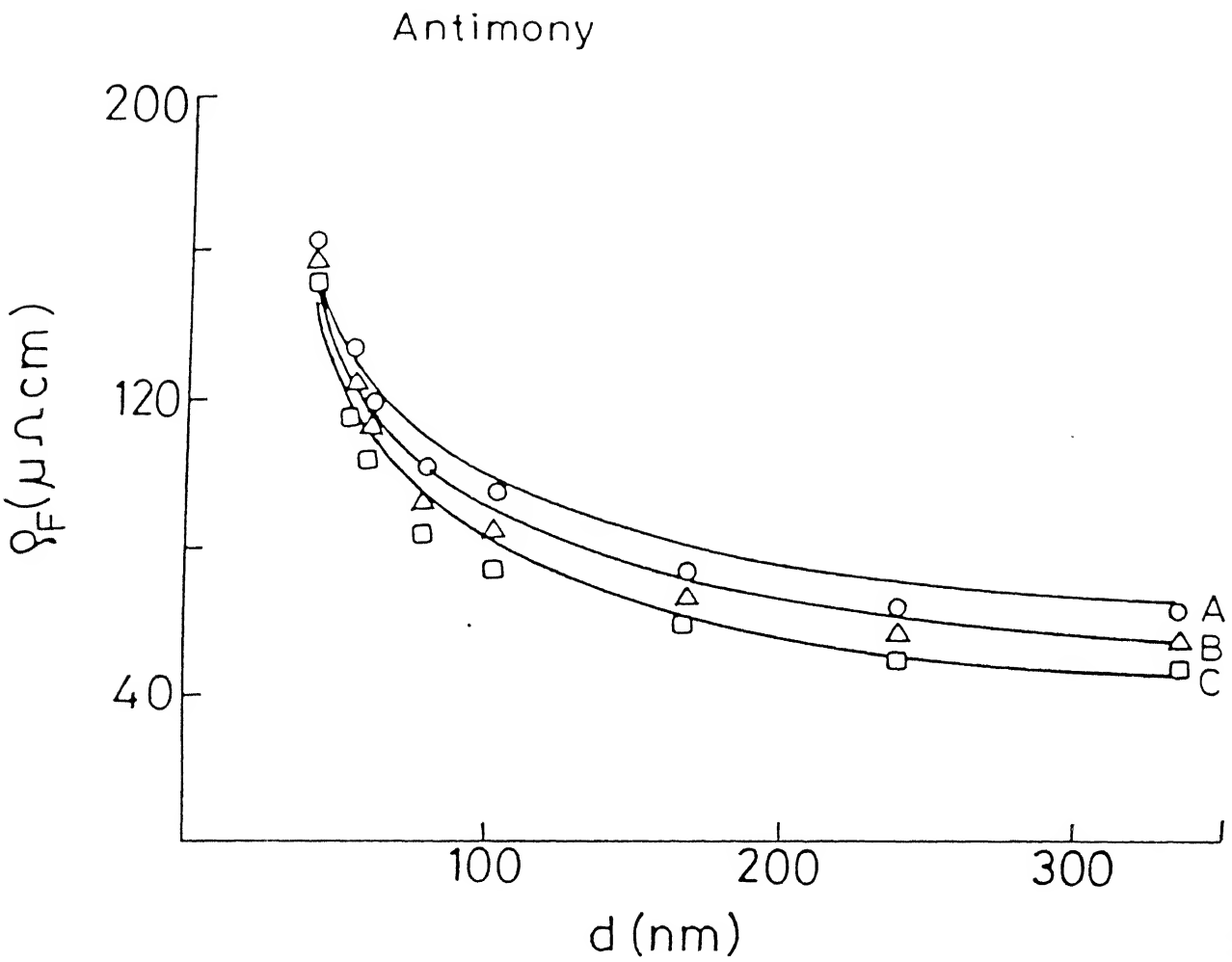

Fig. 4.15 **Plots of resistivity ρ_F vs. thickness d of antimony films.** Continuous curves are drawn using equation (3.12). Curves: (A) p = 0.48, t = 0.877, o experimental points at 300 K; (B) p = 0.49, t = 0.845, Δ experimental points at 225 K; (C) p = 0.49, t = 0.82, □ experimental points at 150 K.

parameter $p \simeq 0.49$ and it has no temperature dependence. The value of reflection coefficient R is about 0.135 - 0.176 while the value of transmission coefficient t is about 0.82 - 0.877 in the temperature range 150 to 300 K (Table 4.5). The grain boundary resistivity behaviour can be described by the PTT model and MS model. The comparatively large dispersion of mean free path values reported by several researchers (Table 4.5) is probably due to the different experimental conditions used during the deposition of the films.

4.4 *Structural and Electrical Properties of Bismuth Films*

Figures (4.7 to 4.10) show that bismuth films are polycrystalline, highly textured and the average grain size of the film increases with the increase in thickness.

Figure 4.11 shows that as the temperature is increased, the resistivity of Bi films decreases. The results agree well with those reported by other workers.[17,18] It also appears from the curves of 98.3 nm and 225.9 nm thick films in Fig. 4.11 that there exists a minimum in resistivity at some temperature T_c. This minimum in resistivity shifts towards higher temperature for thin samples and lies above 350 K. The same type of behaviour had been observed by several workers.[19-21] This type of temperature dependence of resistivity arises as a

result of competition between the temperature dependences of carrier density and their mobilities, which have different characters and opposite signs. As temperature increases the mobility decreases rather weakly.[20,21] This decrease in mobility is attributed to the decrease of mean free path due to the scattering of charge carriers at the surface of film and at the grain boundaries. On the other hand the charge carrier density unlike their mobilities increases noticeably faster and, therefore, resistivity ρ_F decreases with temperature. The thickness dependence of minimum in resistivity which lies above 350 K in the present work can be understood in terms of change of temperature variation of carrier mobilities with changing film thickness. With decreasing film thickness the mobility becomes smaller and its temperature dependence also becomes rather weak, therefore, the minimum in resistivity will shift towards higher temperature.

From the thickness dependence of resistivity curves of Bi films shown in Fig. 4.12, we see that as the film thickness is decreased, the resistivity increases. To study the electric conduction in bismsuth films with the help of three dimensional model of Pichard et al.[9-12] (given in Chapter III), one should also consider the known fact that carrier concentration varies with the film thickness.[20-23] The carrier concentration increases with

the decrease in thickness. The increase in charge carrier concentrations with the decreasing thickness of Bi film can be accounted for by using a model involving potential bending near the film surface.[21] The simplest approximation of the potential in bismuth film is a square well with infinitely high sides. Due to the large de Broglie wavelength and small Fermi energy of electrons in bismuth, a region of wavefunction "attenuation" near the crystal surface sets up which is appreciably larger than the interatomic distance. Thus an excess positive charge is created near the surface which corresponds to a rise in potential for electrons. Furthermore, Bi has large Thomas-Fermi screening radius, therefore, an electron charge due to, for examaple, the filling of surface states appearing at the surface is accompanied by a rise in potential near the surface at screening radius wavelength. A shift of chemical potential level and an increase in the mean concentration of charge carriers should also occur for a non-uniform potential in a semimetal film.

The dependence of carrier densities on thickness is well approximated by[20]

$$n_F = n_o \left[1 + \frac{2d_o}{d} \right] \qquad (4.3)$$

where n_F = Carrier concentrations in Bi films

n_o = Carrier concentration in bulk bismuth

d = Film thickness.

Similar dependence of n_F on thickness has been reported by Asahi et al.[22] and Sawatari et al.[23] The parameter d_o depends on the density of occupied surface states n_s and may be written as

$$n_s = 2d_o n_o$$

hence

$$n_F = n_o + \frac{n_s}{d} \qquad (4.4)$$

Buxo et al.[24] have studied the influence of surface states on the film conductivity with the help of surface states model. The property according to which $\sigma_2 > \sigma_1$ (where subscripts 2 and 1, respectively, stand for annealed and unannealed films) have been accounted for within the framework of this model. To estimate n_s, a relationship between $(\phi_1 - \phi_2)$ i.e. the barrier height and n_s have been derived by solving Poisson equation in the crystallite surface region. The effective density of states in bismuth conduction band N_C was given by

$$N_C = 2 \left(\frac{2\pi \, m^*_{de} \, kT}{h^2} \right)^{3/2} \qquad (4.5)$$

where m^*_{de} = Electron effective mass density

k = Boltzmann's constant

T = Absolute temperature

h = Planck's constant.

On using $m^*_{de} = 0.05\ m_o$, this equation yields $N_C = 2.62 \times 10^{23}\ m^{-3}$ at 300 K. Finally, Buxo et al.[24] have obtained an expression for n_s as (for detail please see the reference 24)

$$en_s = 4 \left(\frac{2N_C\ k\ T\ K\ \varepsilon_o}{15.\pi} \right)^{1/2} \left(\frac{E_F - E^s_{CB}}{kT} \right)^{5/4} \qquad (4.6)$$

where K = Relative intergrain dielectric constant

ε_o = Permittivity constant

e = Electronic charge.

Taking K = 3, and $\varepsilon_o = 8.85 \times 10^{-12}$ Farad/meter, the surface state density in unannealed film was given as[24]

$$n_s = 8.59 \times 10^{14} \left(\frac{\phi_1 - \phi_2}{kT} \right)^{5/4} \qquad (4.7)$$

For barrier height $\phi_1 - \phi_2 = 0.3$ eV, equation (4.7) gives $n_s \simeq 2 \times 10^{12}\ cm^{-2}$. Knowing n_s i.e. d_o, n_F can be calculated from equation (4.3).

In order to introduce this dependence of charge carriers on thickness, the FS equation (4.1) for film resistivity is modified as

$$\rho_F = \frac{1}{H} \left[\rho_o + \frac{3}{8} \frac{\rho_o \ell_o (1-p)}{d} \right] \qquad (4.8)$$

while the conductivity equations (3.4) and (3.12) of PTT model (See Chapter III) are modified as

$$\frac{\rho_g}{\rho_o} = \frac{1}{H} \left\{ \frac{3}{2} \frac{\nu}{1-C} \left[\gamma - \frac{1}{2} + (1-\gamma^2) \ell n \ (1+\gamma^{-1}) \right] \right\}^{-1} \qquad (4.9)$$

and

$$\frac{\rho_F}{\rho_o} = \frac{1}{H} \left\{ \frac{3}{2} \frac{1}{b} \left[a - \frac{1}{2} + (1-a^2) \ell n \ (1+a^{-1}) \right] \right\}^{-1} \qquad (4.10)$$

where $H = \frac{n_F}{n_o}$ (4.11)

The parameters γ, ν, b, a, and μ are defined by the equations (3.5), (3.6), (3.13), (3.14), and (3.15) respectively.

Fuchs model[1,2] is not appropriate to explain our results on resistivity completely as it reproduces the results only in high thicknes region and deviates appreciably in the low thickness region, but one can find the value of bulk resistivity by using this model. Modified equation (4.8) of Fuchs model indicates a linear dependence of film resistivity ρ_F on $(Hd)^{-1}$ for thick films.[19] Figure 4.16 shows a plot of measured resistivity ρ_F vs $(Hd)^{-1}$ at different temperatures. All variations are found to be linear. The bulk resistivity is obtained from

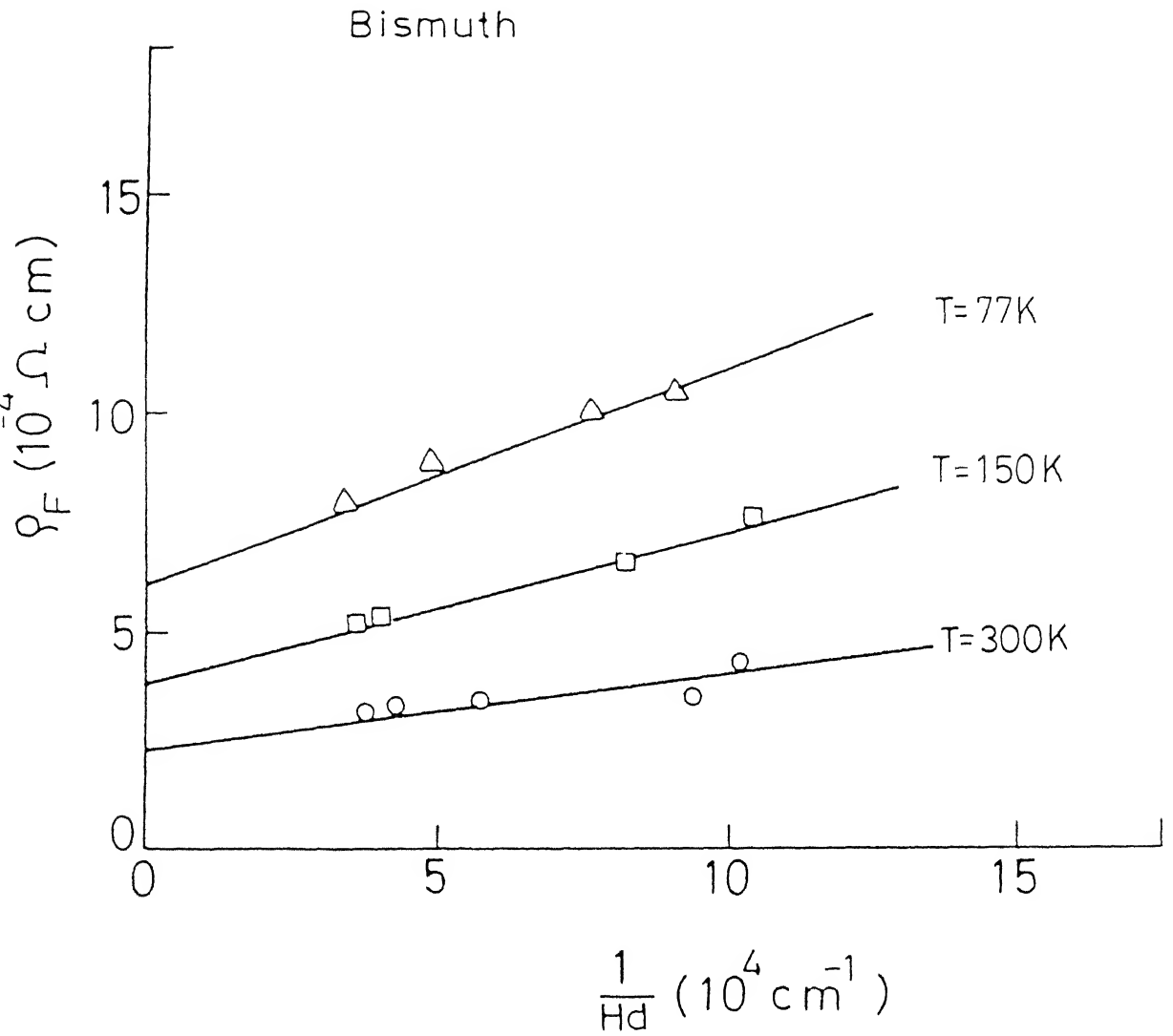

Fig. 4.16 PLOTS OF RESISTIVITY ρ_F vs. $\frac{1}{Hd}$ FOR BISMUTH FILMS AT 77, 150, AND 300 K.

the intercept at $\frac{1}{(Hd)} = 0$ because at infinite thickness $H \approx 1$, while the slope of corresponding plot will give the value of $\frac{3}{8} \rho_o \ell_o (1-p)$. Knowing the value of ρ_o and $\ell_o(1-p)$, it remains to determine the value of specularity parameter p. In case of bismuth, it is a well known fact[5,19,25] that mobility of electron is much larger than the hole mobility, therefore, we can estimate the bulk mean free path from one carrier formula

$$\rho_o \ell_o = \frac{(3\pi^2)^{1/3} \hbar}{e^2 n_o^{2/3}} \qquad (4.12)$$

In the present study, the values obtained for ρ_o, ℓ_o, and p at 300 K, are 2.25 x 10^{-4} Ωcm, 0.331 μm, and 0.43 respectively. The calculated values of ρ_o, ℓ_o, p etc at temperatures 77, 150, and 300 K are given in Table 4.6. For comparison the results of other researchers[5,19,26] are also included in Table 4.6. Bulk parameters are taken from the paper of Ables and Meiboom.[27] From Table 4.6 we see that specularity parameter p is temperature independent.

Now to estimate the variation of carrier concentration as a function of thickness d, we have used the values of various constant terms given in reference 24. Using equations (4.5) to (4.7), we obtained the concentration of surface states n_s as 2 x 10^{12} cm^{-2}. The corresponding value of d_o at 300 K is found to be 4.5 nm,

Table 4.6 Comparison of electrical properties of bismuth films

T_S^{++} (K)	Temp. (K)	$n_o^{\dagger}$ (10^{18} cm^{-3})	$\rho_b^{\dagger}$ (10^{-4} Ωcm)	$\ell_b^{\dagger}$ (μm)	ρ_o (10^{-4} Ωcm)	ℓ_o (μm)	p	t	d_o (nm)	Ref
	77	0.46	0.35	5.80	6.00	0.353	0.41	0.87	21.4	Present
300	150	0.83			3.75	0.384	0.41	0.91	12.0	Study
	300	2.2	1.20	0.59	2.25	0.331	0.43	0.90	4.5	
428-438	77	-	-	-	0.58	3.5	-0.02			19
	300	-	-	-	1.14	0.59	0.56			
423	300	-	-	-	1.182	1.41	0.5			26
	80	-	-	-	2.2 to 7.0*	1.0 to 0.3*	0.6 to 0.7*			5
	300	-	-	-	1.2 to 2.1*	0.6 to 0.35*	0.75 to 0.85*			

$^{\dagger}n_o$, ρ_o and ℓ_b are the standard bulk parameters for bismuth (ref. 27)

* depending on preparation conditions.

$^{++}T_s$ is the substrate temperature.

whereas Schnelle and Dillner[28] obtained d_o = 10.0 nm by fitting simply the theoretical curve to the results of measurements. At 77 K, from this model d_o is found to be 21.4 nm, whereas Asahi et al.[22] explained the experimental results on n_F using equation (4.3) with $d_o \simeq 52.0$ nm. Therefore, the results are not same. But at 4.2 K, this model gives $d_o \simeq 40.0$ whereas Komnik et al.[20] estimated d_o as 50.0 - 55.0 nm, which is not very much different. Knowing the value of d_o, n_F has been calculated as a function of thickness by using equation (4.3).

To include the thickness dependence of charge carrier concentrations, the equation (4.2) is modified as

$$\rho_s = \frac{3}{8} \frac{\rho_o \ell_o (1-p)}{Hd} \qquad (4.13)$$

where ρ_s = Resistivity due to surface scattering.

Estimating the contribution to the film resistivity due to surface scattering from the equation (4.13) with the calculated value of p and attributing the difference to the grain boundaries, we have calculated the experimental values of grain boundary resistivity ρ_g. This ρ_g is found to increase with the decrease of grain size and thus exhibits the size effect. Equation (4.9) with t = 0.86 at 300 K reproduces the experimental results. The experimental values of ρ_g and theoretical predictions of equation (4.9) at different temperatures are shown in Fig.

4.17. From Fig. 4.17 one can see that experimental results agree well with the theoretical curves. At 150 K, the ρ_g is almost constant and does not depend on grain size while at 77 K, ρ_g is found to decrease when grain size decreases and becomes smaller than 140.0 nm. This type of behaviour is due to the variation of carrier densities with the thickness of Bi film.

To explain the results of measurements on thickness dependence of film resistivity , equation (4.10) have been used. The values of ν, μ, b, and a were calculated from equations (3.6), (3.15), (3.13), and (3.14) respectively. For various calculations DEC10 computer was used. Using the values ρ_o = 2.25 x 10^{-4} Ωcm, ℓ_o = 3.31 x 10^2 nm, p = 0.43 (obtained from Fig. 4.16), and t = 0.90, we see that equation (4.10) reproduces the results on film resistivity at 300 K. Figure 4.18 shows that experimental results are in good agreement with the theoretical variations of equation (4.10) at temperatures 77, 150, and 300 K.

Therefore in bismuth film, the surface states play an important role, because of which the electrical properties are drastically altered. The variation of carrier densities with thickness can be estimated from the presence of surface states. To include this thickness dependence of carrier densities, conductivity equations of PTT model are modified. The experimental results on resistivity can be

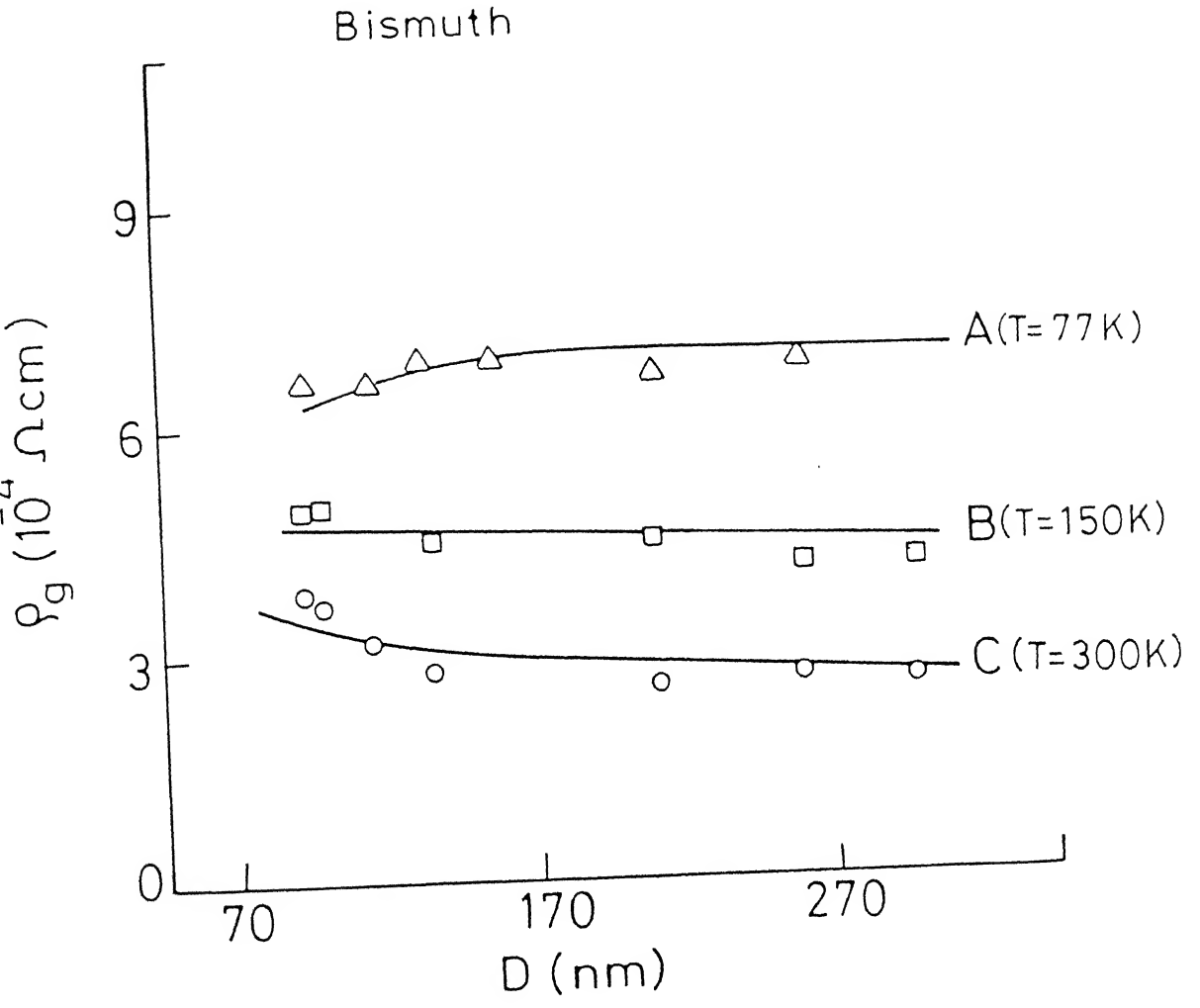

Fig. 4.17 Plots of grain boundary resistivity ρ_g vs. grain size D for bismuth films. Continuous curves are drawn from equation (4.9). Curves : (A) t = 0.82, Δ experimental points at 77 K; (B) t = 0.86, □ experimental points at 150 K; (C) t = 0.86, 0 experimental points at 300 K.

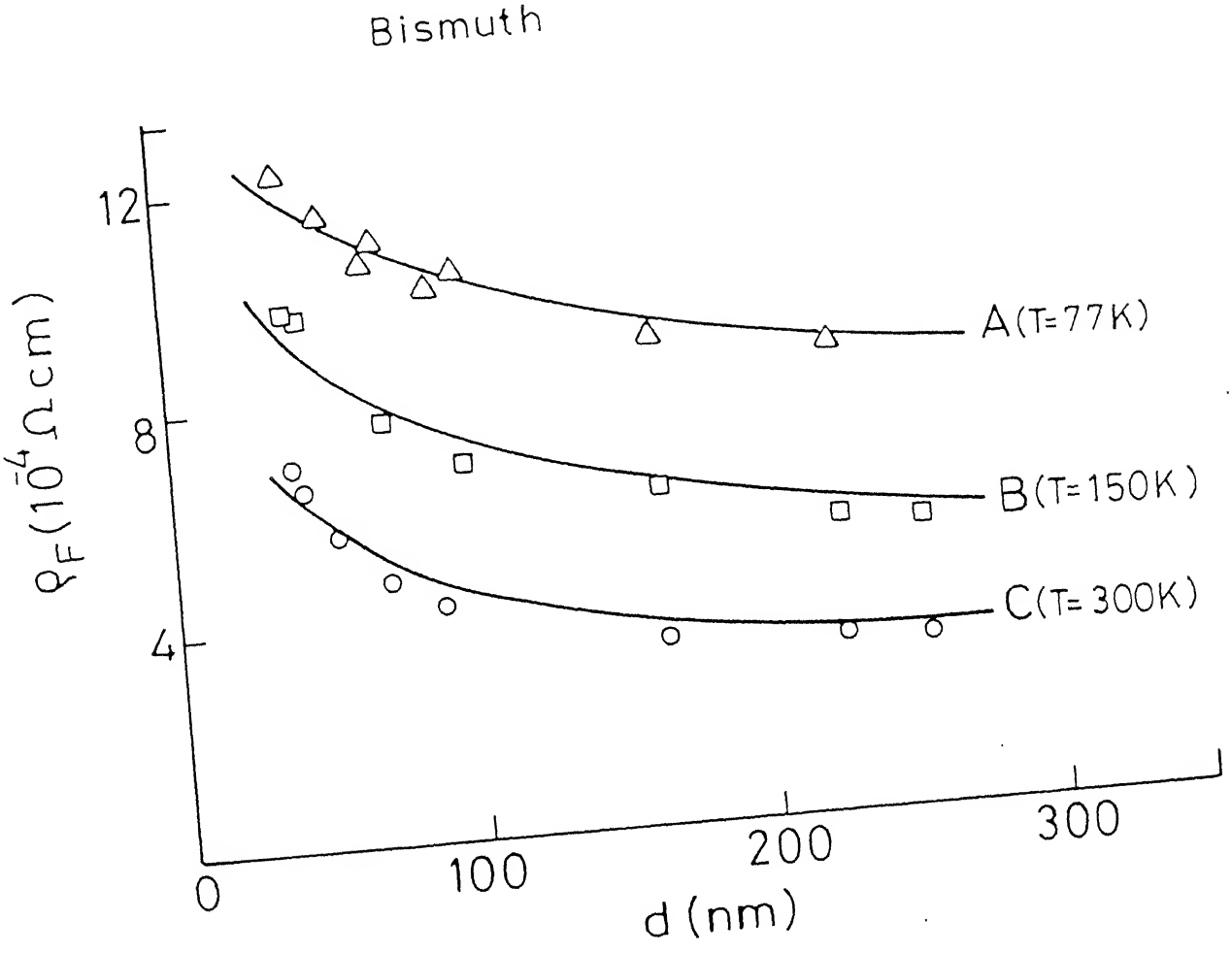

Fig. 4.18 Plots of resistivity ρ_F vs. thickness d of bismuth films. Continuous curves are drawn from equation (4.10). Curves: (A) p = 0.41, t = 0.87, Δ experimental points at 77K; (B) p = 0.41, t = 0.91, □ experimental points at 150 K; (C) p = 0.43, t = 0.90, ○ experimental points at 300 K.

successfully explained by this modified PTT model. The specularity parameter $p \simeq 0.43$ and has no temperature dependence. The transmission coefficient is about 0.86 - 0.91 in the temperature range 77 to 350 K.

REFERENCES

1. K. Fuchs, Proc. Camb. Phil. Soc. 34, 100 (1938).
2. E.H. Sondheimer, Adv. Phys. 1, 1 (1952).
3. D. De, C.K. Ghosh, and A.K. Pal, Thin Solid Films 110, 193 (1983).
4. K. Mojejko-Kotlinska and M. Subotowicz, Thin Solid Films 111, 235 (1984).
5. C. Pariset, Thin Solid Films 91, 301 (1982).
6. D. Deschacht, A. Boyer, and E. Groubert, Thin Solid Films 70, 311 (1980).

   D. Deschacht and A. Boyer, J. Mater. Sci. 20, 807 (1985).
7. O. Oktu and G.A. Saunders, Proc. Phys. Soc. 91, 156 (1967).
8. A.F. Mayadas and M. Shatzkes, Phys. Rev. B 1, 1382 (1970).
9. C.R. Pichard, C.R. Tellier, and A.J. Tosser, Thin Solid Films 62, 189 (1979).
10. C.R. Tellier, C.R. Pichard, and A.J. Tosser, Thin Solid Films 61, 349 (1979).
11. C.R. Pichard, C.R. Tellier, and A.J. Tosser, Phys. Status Solidi(a) 65, 327 (1981).
12. C.R. Pichard, C.R. Tellier, and A.J. Tosser, J. Mater. Sci. 15, 2236 (1980).
13. M. Bedda, S. Messaadi, C.R. Pichard, and A.J. Tosser, J. Mater Sci. 21, 2643 (1986).

14. C.R. Tellier and A.J. Tosser, Size Effects in Thin Films (Elsevier, Amsterdam, New York, 1982) Chapt. 1.

15. M. Bedda, C.R. Pichard, and A.J. Tosser, J. Mater. Sci. 21, 1405 (1986).

16. Ajay Kumar and O.P.Katyal, J. Mater. Science (In press).

17. N. Garcia, Y.H. Kao, and M. Strongin, Phys. Rev. B5, 2029 (1972).

18. M. Inoue, Y. Tamaki, and H. Yagi, J. Appl. Phys. 45, 1562 (1974).

19. R.A. Hoffman and D.R. Frankl, Phys. Rev. B3, 1825 (1971).

20. Yu.F. Komnik, E.I. Bukhshtab, Yu.V. Nikitin, and V.V. Andrievskii, Sov. Phys. JETP 33, 364 (1971).

21. Yu.F. Komnik and V.V. Andrievsky, Thin Solid Films 42, 1 (1977).

22. H. Asahi and A. Kinbara, Thin Solid Films 66, 131 (1980).

23. Y. Sawatari, A. Kinbara, and T. Nakao, Oyo Butsuri 33. 461 (1964).

24. J. Buxo, M. Saleh, G. Sarrabayrouse, G. Dorville, J. Berty, and M. Brieu, Revue Phys. Appl. 15, 961 (1980).

25. S. Kochowski and A. Opilski, Thin Solid Films 48, 345 (1978).

26. S. Chaudhuri and A.K. Pal, J. Appl. Phys. 48, 3455 (1977).

27. B. Abeles and S. Meiboom, Phys. Rev. 101, 544 (1956).

28. W. Schnelle and U. Dillner, Phys. Status Solidi(a) 44, 197 (1977).

CHAPTER V

SUMMARY AND CONCLUSIONS

In general, a thin metal film has a higher resistivity than that of the bulk metal. This is due to the size effect and the high concentration of lattice defects in thin film. When film thickness is of the order of mean free path, the resistivity gets modified due to the geometrical limitations imposed by the film boundaries on the mean free path of charge carriers. The size effect theory of Fuchs and Sondheimer deals with the phenomena of isotropic background scattering and surface scattering of charge carriers. The electrical resistivity of a polycrystalline film is influenced not only by isotropic electron scattering due to phonons and point defects and by surface scattering, but also by grain boundary scattering effects. This grain boundary scattering effect (internal size effect) becomes significant when the mean grain width is of the order of mean free path of conduction electrons. Mayadas et al. developed a theory of electrical resistivity for polycrystalline film which takes into account the grain boundary scattering. They related the film resistivity with mean grain diameter. Another theory which considers the effect of grain boundary scattering on the resistivity was given by Pichard et al.

Using Matthiessen's rule, the grain boundary

resistivity has been calculated with p = 0 from the experimental data on resistivity of polycrystalline Sn and Pb films at 175 and 300 K. This grain boundary resistivity ρ_g arises when two types of electron scatterings (background and grain boundary scattering) are simultaneously operative. The experimental results show that ρ_g increases with the decreasing grain diameter. This behaviour of ρ_g can be explained very well by MS and PTT models. At 300 K, for Sn films in which ρ_o = 12.6 $\mu\Omega$ cm and ℓ_o = 8.3 nm, the MS equation (3.2) with R = 0.60 and PTT equation (3.4) with t = 0.15 reproduce the experimental results on ρ_g. While in case of Pb films for which ρ_o = 24.4 $\mu\Omega$ cm and ℓ_o = 4.3 nm, equation (3.2) with R = 0.72 and equation (3.4) with t = 0.005 reproduce the results on ρ_g at 300 K. Similarly at 175 K the results on ρ_g of polycrystalline Sn and Pb films are consistent with MS and PTT equations. Both MS and PTT grain boundary models give nearly the same results on ρ_g. It is also concluded that in Sn and Pb films scattering from external surface is not significant. The electron scattering at grain boundaries is large and contributes mainly to the film resistivity.

The grain boundary resistivity ρ_g of SnPb alloy film exhibits the size effect. In case of SnPb alloy film which is a mixture of two phases, the total resistivity is the weighted sum of resistivities of two components. Using the expression for the film resistivity given by Wissmann, an equation for the grain boundary resistivity (equation 3.11)

has been found in terms of resistivities of constituent films. This equation (3.11) reproduces the experimental results on ρ_g of SnPb alloy film with R = 0.945 at 300 K. Similarly, at 200 K, experimental values on ρ_g are in agreement with equation (3.11). Therefore, this equation describes the experimental results with good agreement. In case of SnPb alloy film also, the surface scattering is small and the grain boundary scattering is the main dominating factor in the film resistivity.

The TCR of Sn and Pb films increases with the increase of film thickness. This thickness dependence of TCR can be studied with the help of three dimensional model of Pichard et al. It is found that for p = 0.2 the results of TCR are consistent with the theoretical equation (3.18) of PTT model. As no marked discrepancy is observed in the value of p and thickness dependence is well described, therefore, it can be concluded that TCR model of Pichard et al. gives a suitable description of the TCR of polycrystalline Sn and Pb metal films.

The structural studies of Sb and Bi films show that these films are polycrystalline in nature. The average grain size of these films is found to increase with the film thickness. These films are highly textured.

The resistivity of Sb films increases with the temperature thus antimony films exhibit metallic behaviour. The resistivity and TCR of Sb films vary with the

thickness and exhibit the size effect. The values of ρ_o and $\ell_o(1-p)$ for Sb at 300 K are 49.0 $\mu\Omega$ cm and 241.8 nm respectively. Fuchs model is not appropriate to explain our results on the resistivity of Sb films. The grain boundary resistivity increases with the decreasing grain diameter. The experimental results on ρ_g at different temperatures are found to be consistent with the theoretical curves of MS and PTT equations. Both MS and PTT models give almost the same results on ρ_g and the degree of agreement of the experimental results with the theoretical curves i.e. MS and PTT, is satisfactory to the same extent. Therefore, behaviour of ρ_g vs D can be successfully explained with the help of MS and PTT models. To describe experimental results on resistivity of Sb films PTT equation (3.12) have been used. It is found that at 150, 225, and 300 K, the experimental results are consistent with the equation (3.12). The specularity parameter $p \simeq 0.49$ and is temperature independent.

The electrical resistivity of Bi films decreases with the increasing temperature and it also appears from ρ_F vs T curves of thicker samples that a minimum in resistivity exists at some temperature T_c. For thin samples, this minimum in resistivity shifts towards higher temperature. This behaviour arises due to the competition between the temperature dependences of carrier density and carrier mobility. The carrier mobility decreases with the increasing temperature but rather weakly. On the other

hand the carrier density unlike their mobilities increases noticeably faster and, therefore, ρ_F decreases with the increase of temperature. The thickness dependence of minimum in resistivity can be understood in terms of change of temperature variation of carrier mobility with changing film thickness. The charge carrier concentration increases with the decreasing film thickness. This increase in charge carrier concentrations of Bi films can be accounted for by using a model involving potential bending near the film surface. The variation of carrier concentration as a function of thickness can be estimated theoretically from the presence of surface states. Using a surface state model, the surface state density is found to be about 2×10^{12} cm^{-2}. To include this variation of carrier concentrations, the conductivity equations have been modified. These modified conductivity equations (4.8) to (4.10) have been used to explain the experimental results on resistivity of Bi films. The values of bulk resistivity and mean free path of Bi at 300 K are 2.25×10^{-4} Ωcm and 0.331 μm respectively. The specularity parameter p ($\simeq 0.43$) is independent of temperature. The experimental results on ρ_g at 77, 150, and 300 K are found to be consistent with the PTT equation (4.9). Similarly the results on total resistivity of Bi films at 77, 150, and 300 K agree well with the theoretical curves of PTT equation (4.10). Hence, we see that due to the presence of surface states, the electrical properties of bismuth films are drastically

altered. The thickness dependence of resistivity of polycrystalline Bi films in a temperature range 77 to 350 K can be successfully explained with the help of the modified Pichard et al. model which also includes the variation of carrier concentration with film thickness.

We see that PTT model explains completely the experimental results on resistivity of polycrystalline metal films. Therefore, it can be suggested that simple analytic equation (3.12) (Chapter III) of Pichard et al. model can be regarded as an alternative formulation for the complicated expression of total conductivity of polycrystalline film obtained in the Mayadas-Shatzkes model.